MULTIVALENT SELF-ASSEMBLY AT INTERFACES: FROM FUNDAMENTAL KINETIC ASPECTS TO APPLICATIONS IN NANOFABRICATION

MULTIVALENT SELF-ASSEMBLY AT INTERFACES: FROM FUNDAMENTAL KINETIC ASPECTS TO APPLICATIONS IN NANOFABRICATION

PROEFSCHRIFT

ter verkrijging van

de graad van doctor aan de Universiteit Twente,

op gezag van de rector magnificus,

prof. dr. H. Brinksma,

volgens besluit van het College voor Promoties

in het openbaar te verdedigen

op donderdag 8 januari 2009 om 15.00 uur

door

András Perl

geboren op 7 november 1977

te Marghita, Roemenië

Dit proefschrift is goedgekeurd door:

Promotoren: prof. dr. ir. J. Huskens

prof. dr. ir. D. N. Reinhoudt

To my family

Contents

Chapter 7   Self-assembled monolayers of α-cyclodextrin derivatives on gold and their host-guest behavior

General introduction

Nanotechnology is a multidisciplinary field of science and technology dealing with the understanding of governing principles of matter at the nanometer scale. Nanofabrication targets the design and fabrication of (multi)functional devices with nanometer dimensions. In contrast to 'top-down' nanofabrication techniques, by which small structures are shaped from bulk material, building devices from elemental components in the 'bottom-up' strategy requires deeper knowledge about the foundations which govern the interactions between these building blocks at the aimed length scale.

Self-assembly offers the simple and rapid creation of features at various length scales.[1] Supramolecular interactions[2] govern the assembly process of molecules and make the creation of functional nanostructure possible. Self-organization of molecules on solid surfaces constitutes the basis of a technology creating monomolecular thick self-assembled monolayers (SAMs).[3-5] The development of soft-lithographic techniques,[6] which combine the large-area surface patterning capabilities of 'top-down' techniques with the effectiveness and simplicity of self-assembly, has opened the way for easy and advanced nanotechnological schemes and for new experimental setups to investigate the underlying principles of the nanosized building blocks of interest.

Multivalency denotes the simultaneous interaction of multiple functionalities between two non-covalently interacting species resulting in strong and selective binding. Multivalent host-guest interactions are reversible, and they offer flexibility, controllable binding strength and dynamics for the controlled positioning of molecules, assemblies and particles on a substrate.[7] Profound understanding of multivalency is important for an advanced control in biological systems, where often

contacts between cells and viruses or bacteria are initiated by multivalent protein-carbohydrate interactions.[8]

This thesis deals with the investigation of various aspects of molecular and supramolecular structures on solid surfaces. Control over surface spreading, SAM formation capability of molecules and a detailed view over the spreading mechanism of multivalent guest molecules on a host-functionalized surface are the issues studied here, while SAMs, supramolecular self-assembly and multivalency are the linking themes.

Chapter 2 presents a general overview of the development of microcontact printing (μCP),[9] a soft lithographic technique with high potential in the field of nanopatterning and nanofabrication. This technique is generally used in this thesis to build nano- and microstructures on surfaces in order to investigate the used molecular systems.

In μCP, the ink is transferred to the surface to form a patterned SAM by bringing an inked stamp in conformal contact with a metal surface. This monomolecular thin pattern can be used to transfer the relief of the stamp into the metal surface, but the mobility of the inks causes a lateral spreading in the printing step which changes the dimensions of the transferred pattern. In Chapter 3, heavyweight dendritic molecules with thioether end-groups are employed as low diffusive inks, to faithfully transfer sub-micrometer features onto gold via positive μCP. The high molecular weight of dendrimers is combined with the affinity of sulfides for gold, and the development and properties of a class of poly(propylene imine) (PPI) dendrimer-based thioethers as positive inks for μCP on gold is described. Surface spreading of these dendritic inks is studied and compared to other inks, and the etching process of sub-micrometer features on gold is tailored to the behavior of these inks.

More control over the transferred amount of ink during microcontact printing is achieved by receptor-functionalized stamps, as described in Chapter 4. This chapter illustrates how supramolecular interactions can serve to achieve advanced control in the μCP process. The possibilities to selectively recognize ink molecules and to tune the amount of ink molecules transferred by μCP are realized by using β-cyclodextrin-functionalized stamps to which target ink molecules can be anchored through specific and directional supramolecular host-guest interactions. The influence of specific vs nonspecific interactions and the effect of multivalency on the selectivity of inking and

printing is discussed using the concept of molecular printboards which are SAMs of host molecules to which guest molecules bind according to their binding strength.[7,10]

In Chapters 5 and 6, the spreading of multivalent guest molecules on the β-cyclodextrin-based molecular printboard is studied in order to investigate the kinetics of multivalent interactions on surfaces. Fluorescent guest molecules are printed on the molecular printboard and the evolution of the fluorescent patterns in time is monitored in situ. This is performed at various β-cyclodextrin (β-CD) concentrations in aqueous solution in order to induce competition for the guest sites to interact with host sites at the surface and in solution. The dynamics of mono-, di- and trivalent host-guest interactions on the molecular printboard is analyzed, simulated and discussed with the help of various thermodynamic and kinetic parameters. Chapter 5 focuses on the implementation of the experiments and methodology together with the presentation of the main results, while in Chapter 6 the detailed discussion of the occurring mechanisms and related issues, like the directionality of the surface spreading, are presented.

Chapter 7 describes the monolayer formation ability of novel sulfur-modified α-cyclodextrin (α-CD) derivatives. The absence of long alkyl chains in the molecular structure render the SAMs of these compounds more suitable for electrochemical applications than the previously described sulfur-modified cyclodextrins.[11] The SAMs of α-CDs with different anchoring configurations have been characterized by means of water contact angle goniometry, electrochemistry, X-ray photoelectron spectroscopy (XPS) and atomic force microscopy (AFM). The host-guest affinity of the compounds on surfaces is studied by electrochemical measurements. The use of the α-CD derivatives in electrochemical detection and molecular electronics is foreshadowed by electrochemical capacitance measurements in the presence of aliphatic carboxylic acid salts with varying chain lengths. The binding strength of these guests to the surface-confined α-CD hosts have been determined.

1.1 References

1   G. M. Whitesides, B. Grzybowski, *Science* **2002**, *295*, 2418.

2   D. N. Reinhoudt, M. Crego-Calama, *Science* **2002**, *295*, 2403.

3   J. C. Love, L. A. Estroff, J. K. Kriebel, R. G. Nuzzo, G. M. Whitesides, *Chem. Rev.* **2005**, *105*, 1103.

4   F. Schreiber, *Prog. Surf. Sci.* **2000**, *65*, 151.

5   L. Yan, W. T. S. Huck, G. M. Whitesides, *J. Macromol. Sci., Polym. Rev.* **2004**, *C44*, 175.

6   B. D. Gates, Q. B. Xu, M. Stewart, D. Ryan, C. G. Willson, G. M. Whitesides, *Chem. Rev.* **2005**, *105*, 1171.

7   M. J. W. Ludden, D. N. Reinhoudt, J. Huskens, *Chem. Soc. Rev.* **2006**, *35*, 1122.

8   M. Mammen, S. K. Choi, G. M. Whitesides, *Angew. Chem. Int. Ed.* **1998**, *37*, 2755.

9   A. Kumar, G. M. Whitesides, *Appl. Phys. Lett.* **1993**, *63*, 2002.

10   T. Auletta, B. Dordi, A. Mulder, A. Sartori, S. Onclin, C. M. Bruinink, M. Péter, C. A. Nijhuis, H. Beijleveld, H. Schönherr, G. J. Vancso, A. Casnati, R. Ungaro, B. J. Ravoo, J. Huskens, D. N. Reinhoudt, *Angew. Chem., Int. Ed. Engl.* **2004**, *43*, 369.

11   M. W. J. Beulen, J. Bügler, M. R. de Jong, B. Lammerink, J. Huskens, H. Schönherr, G. J. Vancso, B. A. Boukamp, H. Wieder, A. Offenhauser, W. Knoll, F. C. J. M. van Veggel, D. N. Reinhoudt, *Chem. Eur. J.* **2000**, *6*, 1176.

Microcontact printing: limitations and achievements

Microcontact printing (μCP) offers a simple and low-cost surface patterning methodology with high versatility and sub-micrometer accuracy. This technology has undergone a spectacular evolution since its invention, improving its capability to form sub-100 nm SAM patterns of various polar and apolar materials and biomolecules over macroscopic areas. Several developments of μCP are discussed in this work detailing various printing strategies. New printing schemes with improved stamp materials render μCP a reproducible surface patterning technique with high pattern resolution. New stamp materials and PDMS surface treatment methods allow the use of polar molecules as inks. Flat elastomeric surfaces and low-diffusive inks push the feature sizes to the nanometer range. Chemical and supramolecular interactions between the ink and the substrate increase the applicability of the μCP process.

2.1 Introduction

Miniaturization of material features constitutes one of the main research and development trends in material sciences in the last few decades. Products of micro- and nanotechnology offer several advantages over conventional macroscopic functional structures: lower energy consumption, higher efficiency and many unexplored but possible benefits arriving from the properties of the materials at micro- and nanometer lengthscales. Two main lines of micro- and nanofabrication strategies have evolved: bottom-up and top-down methods.

Top-down fabrication methods shape structures from bulk material making new types of small structures based on miniaturization. Lithography is the most successful class of top-down techniques, which include photolithography and non-photolithographic methods.[1] Nowadays, for the fabrication of microelectronic devices photolithography is used exclusively. Despite the fact that it is an expensive technique with costly instruments, it has proven to be the most viable method in the microelectronic market, and no other fabrication method has been able to compete.

Bottom-up methods build highly ordered micro- and nanostructures from smaller elementary components. The most efficient and applied method is the self-assembly of molecules or (nano)particles. When self-assembly is applied to a solid surface, the vertical nanometer dimensions of structures are instantaneously achieved by creating self-assembled monolayers (SAMs).[2-4] Self-assembly has the potential of creating highly ordered and multifunctional micro- and nanostructures,[5] but until the invention of soft lithography, in particular microcontact printing (μCP) the possibility of area and volume pattern fabrication by bottom-up methods was very limited. The combination of self-assembly of SAMs with the large-area surface patterning capabilities of top-down techniques, initiated by Whitesides, has opened the way for cheap and easily accessible nanofabrication.[6-9] Despite its many advantages, μCP did not prove to be a competitive alternative for photolithography in the semiconductor industry. However, the continuous efforts to improve μCP bring forth a spectacular increase in applicability and versatility in other areas.

Here, we will review the emergence of different μCP methods and strategies which offer possibilities for new applications that make μCP a powerful surface patterning technique.

2.2 Microcontact printing: the principle and the main limitations

The original aim of Whitesides and coworkers when they introduced µCP was a fast and easy way to replicate patterns generated by photolithography. In photolithography (Figure 2.1) the surface of a silicon wafer is coated with a thin and uniform layer of organic polymer sensitive to ultraviolet light -a photoresist- which is then exposed to light through a metal photomask.
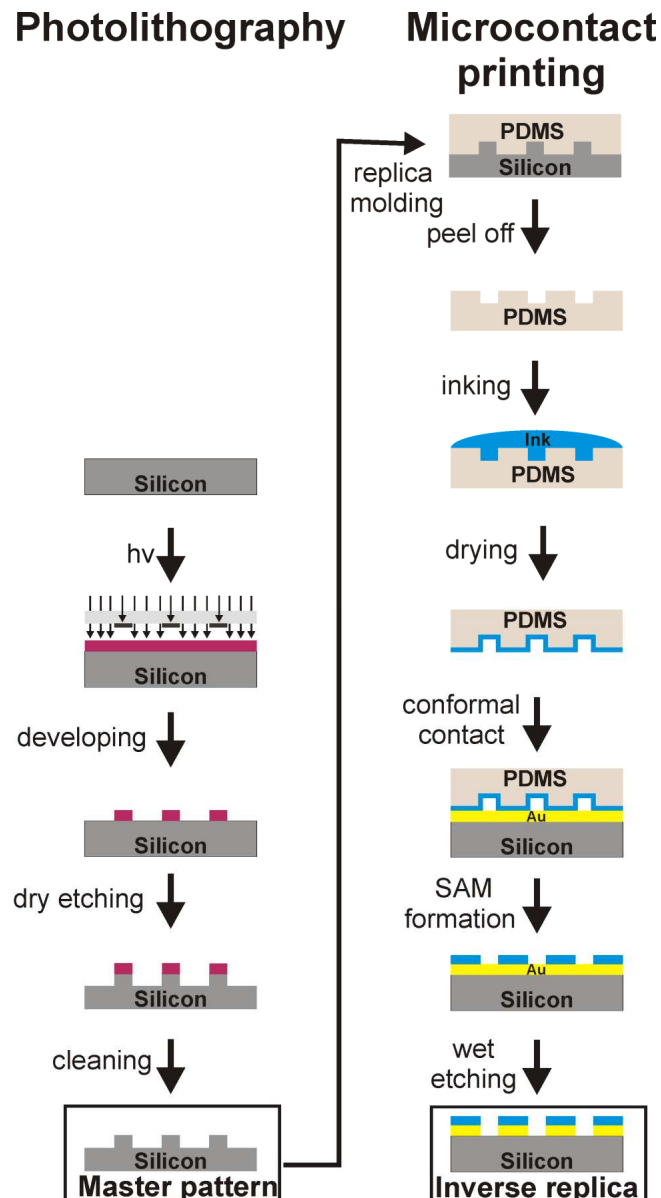

Figure 2.1 Schematic comparison of photolithography vs. µCP. The crucial step in both techniques is the accurate transfer of the patterned etch-resist layer.

The light passes the mask only through the non-metallized areas generating the area-selective polymerization (or degradation) of the photoresist according to the designed

pattern on the mask. After the uncured polymer is removed, the cross-linked photoresist is used as an etch resist in the subsequent etching step, yielding a patterned silicon surface.[1] Microcontact printing exploits the spontaneous adsorption of organic thiols to form SAMs on gold.[10] Similar to the photoresist in photolithography, SAMs of thiols with long alkyl chains act as an etch resist for gold when using alkaline cyanide as a wet etchant.[11] The novelty of µCP was the use of an elastomer, casted and cured from a master structure (Figure 2.1), as a tool to generate a patterned thiol SAM on the gold surface. [6-9]

Microcontact printing uses a hard silicon master or any solid patterned surface as a template (Figure 2.1). A poly(dimethylsiloxane) (PDMS) elastomer is typically used to transfer the pattern from the template to the substrate. In most of the µCP experiments, a commercially available two-component siloxane polymer (Sylgard 184, Dow Corning) is used. In the stamp preparation step, the liquid vinyl-terminated pre-polymer and the curing agent, which consists a short hydrosilane crosslinker containing a platinum complex as a catalyst, are mixed and the mixture is poured onto the patterned template.[12] The PDMS is cured at elevated temperatures (usually 60 $^{\circ}$C) and a solid but elastomeric polymer is formed. The PDMS product is a crosslinked polymer containing the $-Si(CH_3)_2-O-$ structural unit.[13]

After peeling off the PDMS, the stamp is cut to proper size and, in the inking step, saturated with a thiol. The highly hydrophobic PDMS material allows only the use of apolar inks. Wet inking is achieved either by immersion of the stamp in the ink solution or by placing a few droplets of the thiol solution on the patterned side of the stamp. Hydrophobic long-chain thiols reside not only on the stamp surface but diffuse into the bulk of the stamp material creating an ink reservoir.[14] After inking, the solvent (ethanol) is evaporated in a stream of nitrogen and the stamp surface is dried. By bringing the inked stamp in conformal contact with the gold surface, the thiol is transferred to the surface.[4,15] Due to the patterned structure of the stamp, only the areas with protrusions are able to contact the gold surface and the thiol is area-selectively transferred according to the pattern of the template. If the concentration of the used inking solution is higher than a few mM, the order and quality of the SAMs of long chain-thiols formed by printing are indistinguishable from those formed in solution.[4,16]

In the wet-etching step the patterned gold sample is immersed in an etching solution and the unprotected gold is etched away, while the areas covered by long-chain thiol

SAMs remain mostly intact. By this selective etching of the sample, the inverse replica of the surface relief from the original template is created in the gold substrate. Disorder and pinholes in the thiol SAM can lead to some etching in the protected areas too, but the etch rates of the protected and bare gold areas are usually sufficiently different. Methyl-terminated thiols with long alkyl chains provide a good protection from etching. Shorter alkanethiols and polar group-terminated thiols provide a less effective protection.[7]

Soon after the initial publications on μCP with alkanethiols on gold, other metals were successfully used as substrates to achieve pattern replication, such as Ag[17,18], Cu[19] and Pd.[20] The low costs and simplicity of the technique have inspired the interest in creating smaller patterns with higher edge resolution and in broadening the versatility of the technique. However, several limitations have hindered the reproducible creation of sub-micrometer features.

The stamp deformation during the stamp removal from the template and during the contacting of the substrate limits the resolution of the patterning.[21-24] The mechanical properties of the elastomeric PDMS stamps provide sufficient mechanical stability for the printing down to 500 nm.[13] The height of the features divided by their lateral dimensions defines the aspect ratio of a pattern.[21] When the aspect ratio is high, buckling and lateral collapse of the PDMS features can occur, while at low aspect ratios roof collapse is possible (Figure 2.2 A).[23,25] Any deformation of the stamp will affect the printed pattern and decrease the reproducibility.

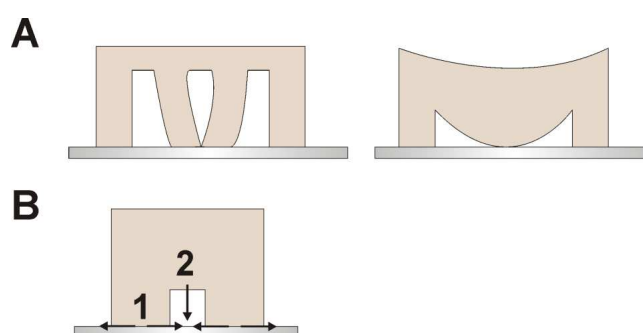**Figure 2.2** The pattern resolution and reproducibility of the μCP process is mainly limited by stamp deformation (A; buckling, left, and roof collapse, right) and diffusion phenomena of the ink (B) along the surface (1) and through the ambient (2).

The PDMS crosslinking process typically leaves some uncured and low-molecular-weight fragments, which may contaminate the substrate upon contacting, thus

decreasing the quality of the printed SAM.[26-28] The transfer of these impurities is enhanced when the ink molecules contain polar groups.[29]

Almost all organic solvents induce swelling of the PDMS stamp, changing the dimensions and shape of the protrusions.[30] Ethanol has a minimal swelling effect on the polymer, but many other solvents can not be used for wet inking of the stamp due to their pronounced swelling,[31] therefore the μCP process is limited to apolar inks that are soluble in ethanol.

Due to the hydrophobic surface properties of PDMS, water soluble inks do not wet the surface of the elastomer and do not permeate the bulk restricting the usage of, for example, inorganic complexes and biomolecules.[13] The oxidation of the PDMS surface (e.g. by oxygen plasma) allows the printing of such polar inks owing to the polar, thin silica-like surface layer formed upon oxidation.[32] However, this silica-like layer has mechanical properties different from PDMS, and cracks can be formed on the surface. These cracks allow the migration of low-molecular-weight PDMS fragments leading to the recovery of the hydrophobic character of the surface,[32,33] a process which occurs within a few hours after oxidation and which limits the applicability and reuse of an oxidized stamp. [34,35]

The formation of an ordered SAM on the substrate is typically achieved by ink diffusion from the PDMS bulk to the surface.[36,37] Mobility of the inks causes a lateral spreading from the edge of the contact region to the noncontacted areas (Figure 2.2 B, path 1).[38,39] When sub-micrometer features are transferred via μCP, this surface spreading can significantly influence the pattern as a function of the printing time and the ink concentration in the stamp.[39] Moreover as a function of the vapor pressure, temperature and humidity, the inks can diffuse through the ambient vapor phase reaching surface areas where no ink is desired (Figure 2.2 B, path 2).[40,41]

In Biebuyck's and Whitesides' approximation,[42] monolayers spread across a surface as a liquid precursor film consisting of unbound molecules. The binding and organization of the molecules to the substrate alters the surface energy of the substrate and influences the interaction of the surface with both the liquid precursor and the ambient. The altered surface energy could favor the expansion of the liquid precursor (reactive spreading) or inhibit the spreading (autophobic spreading and autophobic pinning).[42] They suggested that the lateral spreading of inks could be suppressed by a deliberate design of systems where the interfacial tension and the kinetics of organization of the SAMs limit the spreading of the precursor liquid. Later, Biebuyck

and coworkers stated that the role of autophobic pinning in lateral spreading during µCP is probably irrelevant as the surface-to-volume ratio of the ink source generated by the stamp is increased and a large percentage of the applied ink volume is consumed by the formation of the precursor film.[40] The total quantity of the available ink has a more pronounced effect on the spreading of the ink. The concentration of the ink solution used while inking, plays a crucial role in the spreading rate; at higher ink concentration, the surface spreading is faster.[39,40]

With the emerge of dip-pen nanolithography, in which an atomic force microscopy (AFM) tip coated with a molecular ink is used to transfer molecules to a substrate,[43] new studies and models that deal with the diffusion of thiols on gold have been developed. Sheehan and Whitman assumed that the lateral spreading of a SAM from an ink source obeys Fick's laws.[44] In this model the coverage of the surface is decreasing with the distance from the ink source. The boundary of a SAM detectable by AFM is determined by a critical surface concentration for which the standing orientation of the adsorbed thiols is obtained. The model faithfully describes the empirically found lateral spreading. However, the model also implies the dispersion of a dense monolayer pattern, which has not been observed experimentally. Ratner and coworkers introduced a diffusion model where spreading is possible only over SAM-covered regions.[45] Ink molecules coming from the source are immediately trapped and immobilized by available adsorption sites at the surface. When all nearby surface sites are occupied, new ink molecules migrate from the source across the covered region, thus continuously moving the boundary of the SAM-covered area.[45]

To overcome the limitations of the original µCP technique, several alternatives have been developed either by changing in the printing procedure itself or by varying the properties of the ink or the stamp. New ink materials have been introduced to control spreading and to enrich the variety of the applicable substrates and immobilized molecules. Parallel to the appearance of these new strategies and methods, the objective has slowly shifted from 3D pattern replication toward high resolution surface patterning of chemical templates in surface-related applications.

2.3 Alternative µCP strategies

2.3.1 High-speed µCP

By decreasing the stamp-substrate contact times to the range of ms, the uniformity and the reproducibility of the printed monolayer has been improved by Wolf and

coworkers.[46] This ms printing time is three orders of magnitude shorter than the usual contact time and it appeared to be sufficient to transfer uniform and etch-protective hexadecanethiol SAMs onto a gold surface. At these very low contact times, the surface spreading of the thiol and the diffusion via the ambient vapor phase did not occur. Positioning, printing and retraction of the 100 μm-thick PDMS stamp with 1 μm-wide features were realized with an automated piezoelectric actuator mounted on a motorized two-axis stage. A process window of high-speed μCP was defined (Figure 2.3), in which the recommended printing conditions are mapped by limits of the contact dynamics, the distortion of the stamp due to swelling and the conditions for complete SAM formation and surface spreading.[46]
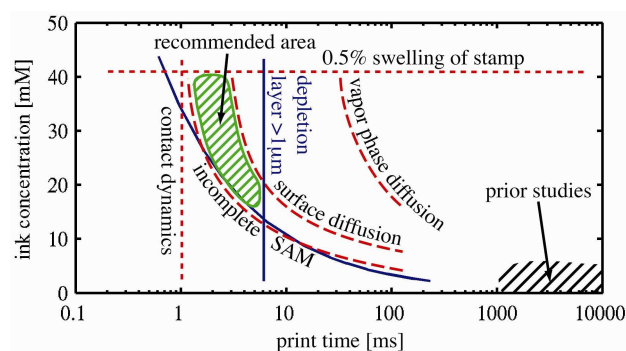
Figure 2.3 High-speed μCP process window as a function of ink concentration and contact time.[46]

2.3.2 Submerged μCP

The stamp stability was greatly improved by performing μCP in a liquid medium.[25,47,48] Xia and Whitesides showed that by printing hydrophobic long-chain thiols under water, the vapor transport of the ink is efficiently inhibited and by varying the printing time, a controlled surface spreading of the thiols was achieved to create sub-micrometer gold features.[48] The main advantages of performing μCP with long-chain thiols in liquid media come from the incompressibility of the fluid and the immiscibility of the ink molecules. μCP under submerged conditions allowed the use of 15:1 PDMS aspect ratio which was not possible with conventional printing in the work of Errachid and coworkers.[47] They suggested that some stamp designs would allow submerged transfer of features with 100:1 aspect ratio after a study of submerged printing using stamps with different aspect ratios.

2.3.3 Microdisplacement µCP

The surface spreading of thiol ink molecules can be suppressed by using a preassembled monolayer that has a sufficiently low Au-S interaction so they can be replaced by other molecules during the printing step. Weiss and coworkers used 1-decanethiol and 11-mercaptoundecanoic acid to replace 1-adamantanethiol from the gold surface during µCP with a PDMS stamp.[49,50] The extent of displacement during the printing of micrometer-wide features was controlled by tuning the ink concentration and contact time. The original 1-adamantanethiolate SAM hinders the lateral surface spreading of the ink molecules from the stamp. This competitive adsorption is also useful when patterned SAMs of different molecules have to be created on the surface.

2.3.4 Contact inking of stamps for µCP

Unlike wet inking, in which also solvent permeates the stamp, contact inking offers a solvent-free inking of the stamp.[51] It is based on the direct contact between a featured stamp and a flat PDMS substrate impregnated with the ink (ink pad). The ink molecules migrate only to the designated, protruding areas which will constitute the contact areas with the substrate in the subsequent printing step. The absence of ink molecules in the remainder of the stamp reduces the amount of ink transferred through the vapor phase that would otherwise compromise the pattern.[40] The patterns on the stamps are not exposed to mechanical damage from ink solution-induced capillary forces or pressure from a nitrogen stream used for drying. Delamarche and coworkers were using contact inked PDMS stamps to transfer sub-micrometer eicosanethiol patterns down to 100 nm-feature sizes.[51] Both the concentration of the thiol solution used for the impregnation of the inkpad and the contact time in the printing step affected the surface spreading of the thiol and influenced the etch-protective quality of the printed SAM. These counteracting process factors needed to be balanced when minimizing both the surface spreading and the occurrence of defects in the transferred SAM.[51]

2.3.5 Positive µCP

The term 'positive' in positive µCP[52] ((+)µCP) refers to the relation between the master and the obtained replica after etching. While in the original µCP a given master design leads to a 'negative' i.e. inverse replica, the (+)µCP process generates

an identical 'positive' replica of the original master, which is achieved by using two different inks in the process (Figure 2.4).[52]
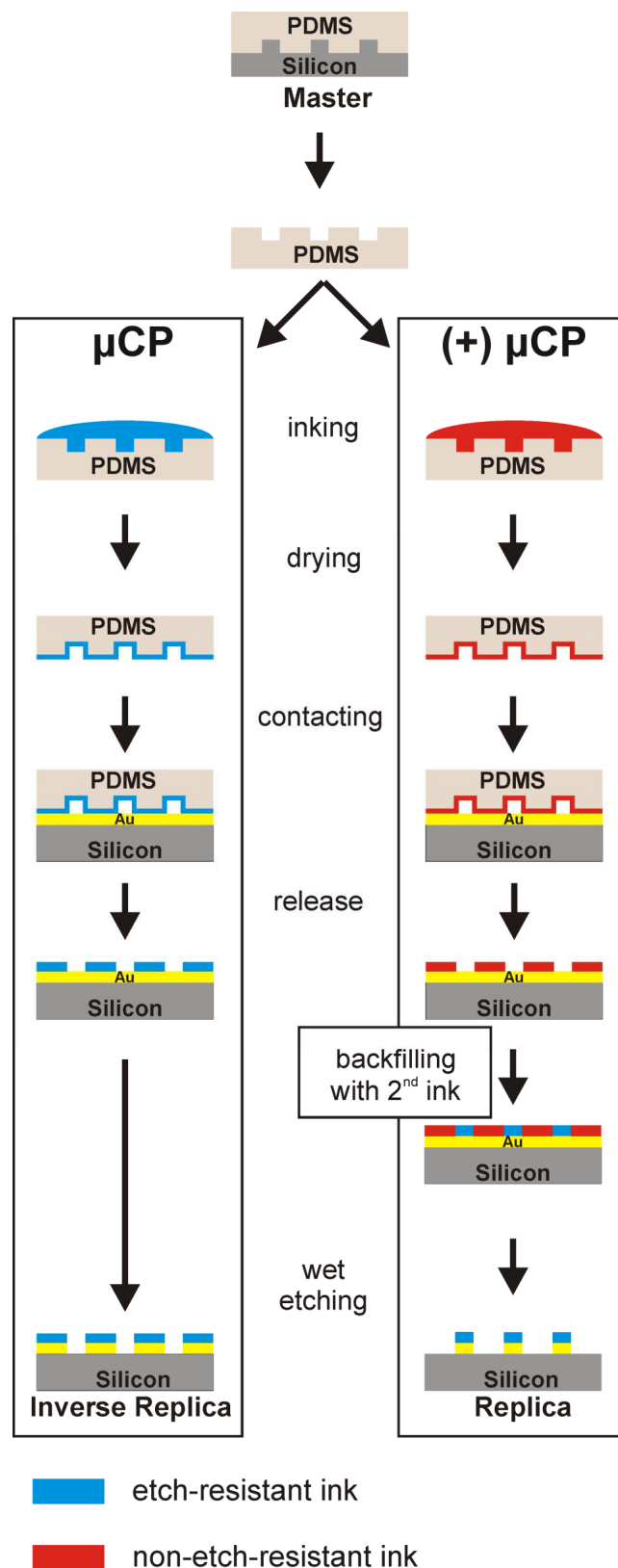

Figure 2.4 Schematic comparison of μCP and (+)μCP techniques.

While the first ink used for printing in (+)μCP does not form an ordered etch-protective SAM, a second ink is used to backfill the available gold surface from solution thus forming a patterned etch-resistant SAM. Pentaerythritol-tetrakis(3-mercaptopropionate) was used by Delamarche and coworkers as a positive ink, because it forms a stable SAM on gold and copper, which is not replaced by etch-resistant alkanethiols, and does not provide significant etch resistance.[52] High-resolution structures formed on Cu substrates indicated that the diffusion characteristics of PTMP are sufficiently low to create patterns at 200 nm length scales. (+)μCP allows the use of stamps with high fill factors to create inverse, low-fill factor patterns, overcoming the main stamp stability problems when creating such a features by common (-)μCP.

2.3.6 Edge transfer lithography

Edge transfer lithography uses a patterned elastomeric stamp inked with an ink solution prepared from solvents that dewet the patterned surface of the stamp.[53,54] A discontinuous dewetting confines the ink to the recessed areas of the stamp only. After evaporation of the solvent, the inks are selectively transferred from the edges of the recessed areas in the printing step, leading to ink adsorption on the substrate only along the edges of the contacted areas. Silanes, nanoparticles and thiols have been successfully transferred with 100-nm-scale resolution using stamps with micrometer-sized features.[53,54]

2.4 Modifications of the stamp

2.4.1 New stamp materials and composite stamps

For an accurate and uniform transfer of the ink to the substrate by a stamp, in general two conflicting stamp characteristics are needed: high mechanical stability of the micro- and nanostructures and good capability to form conformal contact down to the nanometer scale despite potential substrate roughness. A high mechanical stability requires a high Young's modulus while efficient conformal contact is facilitated by increased elasticity. The physical properties of PDMS are determined by the chemical formulation of the stamp, the number of monomer units between junctions and the functionalities of the junctions, and by the curing conditions.[13]

To improve the stamp stability, a composite stamp structure, a thin PDMS stamp built on a rigid back support, has been used to pattern proteins on solid substrates.[55] Sub-

micrometer accuracy over 1 cm^2 has been achieved using composite thin stamps. The thickness of the PDMS on the rigid substrate could be even in the sub-micrometer range, but any non-planarity of the substrate could preclude the use of such composite stamps.[56,57]

Schmid and Michel have developed a hard PDMS (h-PDMS) which is more suitable for sub-micrometer pattern transfer.[12] A stamp material composed of vinylmethyl copolymers and hydrosilane components (material A) and some additional glass fillers (material B) were found to be the best candidates for high resolution μCP after a systematic study of physical parameters of the stamps as a function of the chemical formulation.[12] Structures down to 80 nm were accurately replicated with this stamp material. h-PDMS is relatively brittle and, due to the hardness of the stamp material, manual pressure on the stamp is required to establish conformal contact with the substrate. This pressure can induce non-uniform distortions in the pattern. A composite stamp design, used by Whitesides and coworkers, where a thick and flexible PDMS supported a thin h-PDMS top layer improved the utility of h-PDMS.[58] During the thermal curing of h-PDMS, the pattern can alter due to thermal shrinking. To overcome these drawbacks, Choi and Rogers have developed a photo-curable h-PDMS chemistry.[59]

Other, entirely new stamp materials were also introduced to achieve better mechanical properties. An additional advantage of these new materials is the possible decrease of the transfer of uncured polymer impurities. Block-copolymer thermoplastic elastomers such as poly(styrene-b-butadiene-b-styrene) and poly(styrene-b-(ethylene-co-butylene)-b-styrene) were used as stamp materials for printing thiols by Bastiaansen and coworkers. Both have a high modulus and toughness in comparison to conventional PDMS.[60] A UV-curable stamp material based on a functionalized prepolymer with acrylate groups for cross-linking and different monomeric modulators was developed by Lee and coworkers and successfully used for printing sub-100-nm hexadecanethiol patterns on gold.[61] By changing the modulator, the mechanical properties of the poly(urethane acrylate) stamp could be tuned.

Greater ink compatibility was achieved by varying the hydrophobicity of the stamp material. Polyolefin plastomers as stamp materials showed identical printing performance compared with conventional PDMS when printing micrometer-sized protein features, and higher printing quality for sub-micrometer structures in the work of Spencer and coworkers.[62] Stamps made of poly(ether-ester) multiblock copolymers

consisting of poly(tetramethylene glycol) and poly(butylene terephthalate) segments were used for repetitive printing without re-inking of polar pentaerythritol-tetrakis(3-mercaptopropionate) (PTMP). The thermoplastic elastomer-printed PTMP SAM showed a higher etch-resistance than the PDMS-printed SAM.[63]

Other hydrophilic stamp materials were developed for printing of proteins and biomolecules. Hydrogel copolymers of 6-acryloyl-β-O-methylgalactopyranoside and ethylene glycol dimethacrylate on solid support were used as stamps for μCP.[64] Self-supporting hydrogel stamps consisting of 2-hydroxyethyl acrylate, poly(ethylene glycol) diacrylate as the cross-linker, and water had comparable physical and printing properties to those of PDMS.[65] However, these hydrogel-based stamps have the disadvantage that they require a high-humidity atmosphere during curing, inking and printing to avoid deformation of the stamp due to the loss of water. Composite stamps made from two UV-curable materials, Norland Optical Adhesives 63 and poly(ethylene glycol) diacrylate, were used to perform μCP of polar biomolecules.[66]

2.4.2 PDMS surface modification for the μCP of polar inks

As mentioned previously, native PDMS cannot be used for printing of polar inks due to the hydrophobic character of both the bulk and the surface of PDMS. In the previous section a variety of recently developed new stamp materials was discussed, however, PDMS is still the most widely used stamp material for μCP owing to its ease of preparation. A modification of the PDMS surface hydrophobicity appeared to be a reasonable and simple choice to print polar inks. The hydrophobic character of the native PDMS surface is conveyed by chemically inert methyl groups. Exposure to reactive oxygen species increases the hydrophilicity of the PDMS surface. Oxygen plasma and UV ozone treatment are most widely used.[32,33,67-69] A thin silica-like layer and a top region rich in $SiCH_2OH$ groups are formed when the PDMS surface is oxidized.[32] However, the silica-like layer easily cracks, which may allow the migration of low-molecular-weight PDMS fragments leading to hydrophobic recovery.[32,33] The oxidized PDMS layer generated by all plasma treatment methods significantly reduces the amount of transferred low-molecular-weight PDMS fragments during printing.[70]

To increase the stability and tune the hydrophilicity of surface-oxidized PDMS stamp, silanes were chemically attached to the reactive silica-like top layer followed by grafting of amino-terminated polyethylene glycol by the IBM group.[71] Poly(ethylene

oxide) silanes were also attached to the oxidized stamp surface.[72] Both methods provided hydrophilic PDMS surfaces that are stable for several days.

Polymer layers have been covalently bound onto the PDMS surface. They act as a stable (physical) barrier against hydrophobic recovery. Most of these methods have found applications in PDMS-based microfluidic systems rather than μCP.[73-78]

He and coworkers have developed a method using argon and hydrogen mixed gas microwave plasma pretreatment and acrylonitrile grafting to prepare stable hydrophilic PDMS surfaces for μCP applications.[79] In our group, we used PDMS stamps with plasma-polymerized allylamine thin films for printing of polar inks.[80] Plasma polymerization led to a homogeneous hydrophilic polymer layer on top of the stamp that remained stable for prolonged periods.

2.4.3 Catalytic μCP

The PDMS stamp surface can be made catalytically active in order to catalyze a chemical reaction at the substrate. In such a catalytic μCP scheme, no ink is needed and therefore the lateral resolution reducing effect of surface spreading is efficiently sidestepped. In our group, oxidized PDMS stamps were used to create patterns via covalent modification of preformed SAMs of bis(ω-trimethylsiloxyundecyl)disulfide or bis(ω-tert-butyldimethylsiloxy-undecyl)disulfide on gold.[81] Triallylsilyl ethers were easily hydrolyzed to free alcohols in the presence of an acid. The silicon oxide of oxidized PDMS stamps was sufficiently acidic to induce catalysis in the contacted areas.

Toone and coworkers used piperidine-functionalized polyurethane acrylate stamps to promote the catalytic cleavage of the 9-fluorenylmethoxycarbonyl amino-protecting group.[82] Sub-micrometer patterns were created with this inkless method by selective deprotection of (9H-fluoren-9-yl)methyl-11-mercaptoundecylcarbamate SAMs on gold. They extended catalytic μCP to biochemical substrates, by immobilizing exonuclease enzymes on biocompatible poly(acrylamide) stamps and created patterned DNA both on glass and gold surfaces.[83]

2.4.4 Printing with flat stamps

Patterned SAM formation with flat, featureless stamps in μCP offers an effective solution to avoid the typical mechanical stamp deformation and ink transport issues in the original μCP process. When the stamp is flat, no buckling or side and roof collapse can occur, and the undesired vapor transfer of the ink can be eliminated as

well. However, the main difficulty is the area-selective inking or creation of chemical barriers on the stamp's surface.

Flat stamps were inked in an area-selective manner by using a robotic spotting system and then used to fabricate a multi-probe array of amino-modified oligonucleotide spots.[84] The main disadvantage of this system is the pattern size limitation that is given by the resolution of the spotting system.

Sub-100-nm resolution in protein patterning was achieved in the work of Delamarche and coworkers by exploiting the differences in adhesion of proteins to PDMS and silicon.[85] A flat PDMS stamp with a homogeneous protein layer was placed on a patterned silicon nanotemplate. With the removal of the stamp, due to the less hydrophobic character of silicon compared to PDMS, proteins were removed ("subtracted") from the stamp leaving a patterned protein layer on the non-contacted areas. These protein patterns could be subsequently transferred onto another substrate.[85]

The hydrophobicity of PDMS was exploited by the IBM group by selectively oxidizing flat PDMS surfaces through a mask and grafting poly(ethylene oxide) silanes to stabilize the oxidized parts.[72] After wet inking of the stamp with proteins, which adhered to the oxidized parts, these were easily printed onto various substrates. Work in our lab showed that a perfluorinated silane layer could act as an ink barrier during μCP using regular thiol inks.[86] After the local modification of the stamp surface through a mask, the stamp was inked with thiols and the unmodified areas of the surface led to ink transfer (Figure 2.5).
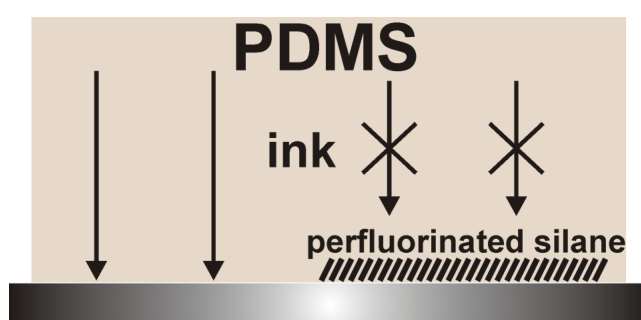

Figure 2.5 Schematic representation of printing thiols with flat stamps: the 1H,1H,2H,2H perfluorodecyltrichlorosilane-covered area acts as an ink barrier, while the non-covered PDMS transfers the thiol to the gold substrate.[86]

The 1H,1H,2H,2H-perfluorodecyltrichlorosilane-covered parts efficiently acted as an ink barrier, while the rest of the surface allowed the diffusion of ink molecules from the bulk of the PDMS to the gold substrate. The further development of this technique to the grafting of 3-aminopropyl-triethoxysilane in the non-fluorinated areas, allowed the efficient printing of polar inks with these chemically patterned flat stamps.[87] Sub-micrometer sized features were printed using chemically patterned flat stamps, and the pattern size depends on the mask used for the selective oxidation.

2.5 Alternative inks and substrates

2.5.1 Inks with low diffusion

Using inks with increased molecular weight or with multiple attachment points may reduce the surface spreading rate of the ink molecules, but possibly at the expense of order and etch resistance of the formed monolayer.[40,88] The etch-resistant properties of long-chain thiol SAMs on gold are determined by steric hindrance of the hydrophobic alkyl chains, which are densely packed and protect the underlying gold from reactive aqueous species. When the number of the carbon atoms was increased, the surface spreading rate of the ink was decreased in accordance to its increased molecular weight.[40] To further increase the molecular weight, new heavyweight ink molecules were designed with multiple thioether moieties, but the etch resistance of SAMs of these molecules was not sufficient.[89]

The extension of the μCP methodology to (+)μCP, (see Figure 2.3) has resulted in the possibility of pattern replication by printing a poorly etch-resistant ink followed by immersion of the sample in a second, etch resistant adsorbate solution, which fills the available areas and acts as a resist in the subsequent etching step.[52] Mercaptoalkyl-oligo(ethylene glycol)s were used as heavyweight inks for (+)μCP by Burdinski et al., but the relatively fast surface spreading inhibited the accurate replication of sub-micrometer features.[90]

2.5.2 Reactive μCP

In addition to patterning SAMs of sulfur compounds on gold, other adsorbate/substrate systems have been used for μCP, in which patterning is realized through covalent bonding. Soon after the development of conventional μCP, alkylsilanes were successfully printed on silicon oxide.[91-93] Monolayers of silanes on silicon oxide are less well-defined than SAMs of thiols on gold because the process

involves covalent bond formation, and thus error correction is limited.[13,94] Lateral spreading limited the pattern resolution in the work of Nuzzo and coworkers, when they printed octadecyltrichlorosilane onto silicon.[93,95]

An alternative for the direct patterned SAM formation of complex molecules is offered by the formation of a reactive SAM on a substrate, followed by μCP to locally transfer reagents to the reactive SAM leading to a chemical reaction.[96] Using this method, amines and poly(ethylene imines) were printed onto reactive anhydride or activated carboxylic acid-terminated SAMs on gold and silver.[69,97,98] This method was also successfully used by Huck et al. for reacting N-protected amino acids to surface-confined amino groups when a plasma-oxidized flat PDMS stamp inked with an N-Boc-L-amino acid was put into contact with an amino SAM.[99] Well-defined functional micro- and nanostructured biointerfaces were fabricated by reactive printing of trifluoroacetic acid onto reactive block-copolymer films by Schönherr et al.[100,101] The trifluoroacetic acid deprotects the tert-butyl acrylate side chains present in the skin layer of the block-copolymer films, making the films chemically reactive with any amino-terminating (bio)molecule. In an another study of the same group, amino end-functionalized poly(ethylene glycol) was printed onto spin-coated thin films of reactive poly(N-hydroxysuccinimidyl methacrylate) to serve as a blocking layer and prevent nonspecific adsorption of other molecules.[102]

Our group has demonstrated the reversible formation of imines through reactive printing of octadecylamine onto aldehyde-terminated SAMs.[103] The obtained imine pattern was stable in water but was completely removed after acid-catalyzed hydrolysis. We also printed acetylenes onto azido-terminated SAMs (Figure 2.6) by "click" chemistry in the contact area between the PDMS stamp and the reactive substrate without the need for using a catalyst.[104]
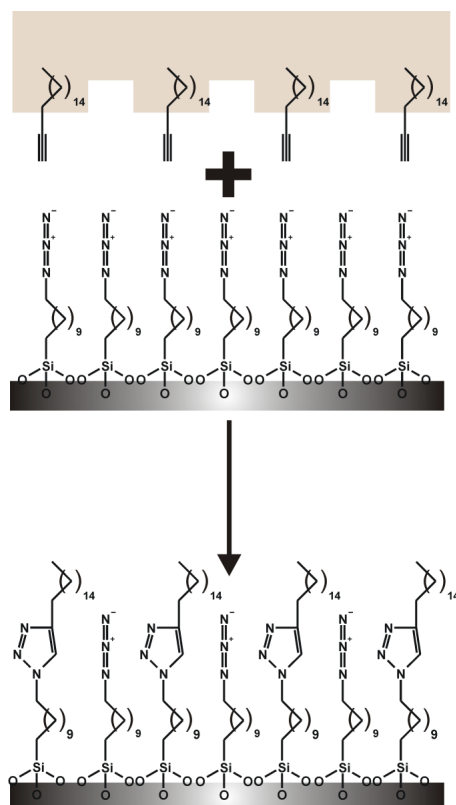
Figure 2.6 Schematic representation of click chemistry by reactive μCP: 1-octadecyne is printed onto an azido-terminated SAM forming a patterned triazole layer on the surface.[104]

2.5.3 Supramolecular μCP

Supramolecular interactions play a pivotal role in biology and are being extensively used for other, non-biological applications as well. The reversible nature of the supramolecular binding of complementary host/guest partners offers flexibility, controllable binding strength and dynamics for the controlled positioning of molecules, assemblies and particles on a substrate.[105]

The combination of μCP with supramolecular host-guest interactions led to various improvements in nano-patterning of (bio)molecules. Proteins were selectively picked up from crude biological solutions and then printed on substrates by the Delamarche et al.[106] Stamps functionalized with reactive groups bound the proteins from complex mixtures and aided the transfer of these biomolecules onto the chosen substrate. Other groups immobilized single-strand DNA on a stamp and immersed it in a solution containing the complementary DNA previously end-functionalized with chemical motifs able to interact with the targeted substrate. During printing, the preformed ds-DNA is dissociated and after the removal of the stamp the complementary copy of the master pattern is created.[107-111]

For some years, our group has been exploiting supramolecular interactions focusing mainly on multivalency on surfaces. Molecular printboards, which are self-assembled monolayers functionalized with receptor groups, were used as substrates to print various organic monovalent and multivalent molecules, in order to study the kinetic and thermodynamic characteristics of these surface-confined complex systems.[105] Suitable guest-functionalized dendrimers, fluorescently labeled molecules and polymers were used as inks for supramolecular µCP.[112-116]

2.5.4 Other inks for µCP

Since the discovery of µCP, various ink materials have been successfully used to pattern surfaces. Advances in printing of biomolecules on various substrates and in general microcontact processing for biology display the creation of high-performance, miniaturized bio-analytical systems.[117-119] PDMS contamination was used intentionally to pattern surfaces, and its effect on the assembly of biomolecules was investigated.[120,121]

A few nanometer thin metal layers evaporated on the stamp surface could be transferred onto substrates.[122,123] The process, described by Rogers and coworkers, is called nanotransfer printing (nTP) and uses an adhesive SAM on the substrate to stick to the metal layer and to promote the release of the layer from the stamp when the stamp is removed. The technique can generate complex patterns without the risk of surface diffusion and edge disorder.

Colloidal particles and nanoparticles have been printed on various substrates.[53,72,124-126] However, the stochastic printing of nanoparticles typically results in patterned, but randomly ordered particle arrangements. The combined printing and self-assembly of nanoparticles into larger structures was realized by pre-arrangement of the particles on the stamp surface prior to printing. Andres and Santhanam created a uniform nanoparticle layer on the water-air interface and then transferred the self-assembled particle layer onto a patterned PDMS stamp by bringing the stamp parallel to the water surface and touching the nanoparticle film.[127] Patterned and ordered particle arrays on the substrate were formed in the subsequent printing step. Wolf and coworkers moved the meniscus of a colloidal suspension over a patterned layer to self-assemble particles with high precision inside the features.[128] Subsequently, the assembly was printed onto the substrate with single-particle resolution. Lines, arrays and bitmap particle arrangements were created preserving the catalytic and optical properties of the individual nanoparticles.[128]

2.6 Outlook

Since Whitesides and coworkers developed the μCP technique, a spectacular evolution of the technique has followed. While the main concept of the technique remained the same, a pattern is transferred onto a surface via conformal contact between an elastomeric stamp and the substrate, the manner of effectuation and the material of the constituents showed a diverse development. The mechanical properties of the elastomeric stamp material were improved by developing new stamp materials and composite stamp designs. Some stamp materials allowed the use of polar inks increasing the applicability of the technique. Parallel to this, new printing concepts were introduced to use inverse stamp pattern designs or even flat stamps, the mechanical properties of which became irrelevant for resolution. Despite a wider variety of new stamp materials, PDMS remained the cheapest and easiest stamp material, causing the popularity of surface treating techniques to change the hydrophobicity of the PDMS stamp. Non-diffusive inks were developed making the sub-100 nm pattern resolution attainable, while catalytic printing techniques eliminated the limitations arriving from diffusion.

Parallel to the evolution of μCP, the huge potential of the technique in creating chemical, supramolecular, and biomolecular patterns on surfaces started to be appreciated. Often the main development efforts were motivated by possible applications in sensing, (bio)analysis, functional nanofabrication, and in basic research. Using the possibility of creating chemically distinct patterned SAMs, the elemental basics of chemical, supramolecular and biological interactions could be studied and understood. Today, a wide variety of strategies is available to create surface patterns of both polar and apolar (bio)molecules and nanoparticles on a microscopic scale, while the reproducible resolution is approaching the sub-100 nm range. Mechanical issues of the stamp were addressed in various ways and the loss in pattern resolution due to ink spreading was analyzed and reversed. Despite its original fundamental limits, μCP has proven to be a reliable and useful surface patterning technique and has the potential for further unexpected developments.

2.7 References

1   G. M. Wallraff, W. D. Hinsberg, *Chem. Rev.* **1999**, *99*, 1801.

2   F. Schreiber, *Prog. Surf. Sci.* **2000**, *65*, 151.

3   L. Yan, W. T. S. Huck, G. M. Whitesides, *J. Macromol. Sci., Polym. Rev.* **2004**, *C44*, 175.

4   J. C. Love, L. A. Estroff, J. K. Kriebel, R. G. Nuzzo, G. M. Whitesides, *Chem. Rev.* **2005**, *105*, 1103.

5   W. Lu, A. M. Sastry, *IEEE Trans. Semicond. Manuf.* **2007**, *20*, 421.

6   A. Kumar, G. M. Whitesides, *Appl. Phys. Lett.* **1993**, *63*, 2002.

7   A. Kumar, H. A. Biebuyck, G. M. Whitesides, *Langmuir* **1994**, *10*, 1498.

8   J. L. Wilbur, A. Kumar, H. A. Biebuyck, E. Kim, G. M. Whitesides, *Nanotechnology* **1996**, *7*, 452.

9   Y. Xia, X. M. Zhao, G. M. Whitesides, *Microelectron. Eng.* **1996**, *32*, 255.

10   C. D. Bain, E. B. Troughton, Y. T. Tao, J. Evall, G. M. Whitesides, R. G. Nuzzo, *J. Am. Chem. Soc.* **1989**, *111*, 321.

11   A. Kumar, H. A. Biebuyck, N. L. Abbott, G. M. Whitesides, *J. Am. Chem. Soc.* **1992**, *114*, 9188.

12   H. Schmid, B. Michel, *Macromolecules* **2000**, *33*, 3042.

13   C. M. Sotomayor Torres, *Alternative lithography : unleashing the potentials of nanotechnology*, Kluwer Academic/Plenum Publishers, New York **2003**.

14   T. E. Balmer, H. Schmid, R. Stutz, E. Delamarche, B. Michel, N. D. Spencer, H. Wolf, *Langmuir* **2005**, *21*, 622.

15   B. Michel, A. Bernard, A. Bietsch, E. Delamarche, M. Geissler, D. Juncker, H. Kind, J. P. Renault, H. Rothuizen, H. Schmid, P. Schmidt-Winkel, R. Stutz, H. Wolf, *Chimia* **2002**, *56*, 527.

16   N. B. Larsen, H. Biebuyck, E. Delamarche, B. Michel, *J. Am. Chem. Soc.* **1997**, *119*, 3017.

17   Y. Xia, E. Kim, G. M. Whitesides, *J. Electrochem. Soc.* **1996**, *143*, 1070.

18   Y. Xia, N. Venkateswaran, D. Qin, J. Tien, G. M. Whitesides, *Langmuir* **1998**, *14*, 363.

19   Y. Xia, E. Kim, M. Mrksich, G. M. Whitesides, *Chem. Mater.* **1996**, *8*, 601.

20   A. Carvalho, M. Geissler, H. Schmid, B. Michel, E. Delamarche, *Langmuir* **2002**, *18*, 2406.

21   A. Bietsch, B. Michel, *J. Appl. Phys.* **2000**, *88*, 4310.

22   C. Y. Hui, A. Jagota, Y. Y. Lin, E. J. Kramer, *Langmuir* **2002**, *18*, 1394.

23   K. G. Sharp, G. S. Blackman, N. J. Glassmaker, A. Jagota, C. Y. Hui, *Langmuir* **2004**, *20*, 6430.

24   E. Delamarche, H. Schmid, B. Michel, H. Biebuyck, *Adv. Mater.* **1997**, *9*, 741.

25   P. Roca-Cusachs, F. Rico, E. Martinez, J. Toset, R. Farre, D. Navajas, *Langmuir* **2005**, *21*, 5542.

26   I. Bohm, A. Lampert, M. Buck, F. Eisert, M. Grunze, *Appl. Surf. Sci.* **1999**, *141*, 237.

27   K. Glasmastar, J. Gold, A. S. Andersson, D. S. Sutherland, B. Kasemo, *Langmuir* **2003**, *19*, 5475.

28   D. J. Graham, D. D. Price, B. D. Ratner, *Langmuir* **2002**, *18*, 1518.

29   R. B. A. Sharpe, D. Burdinski, C. van der Marel, J. A. J. Jansen, J. Huskens, H. J. W. Zandvliet, D. N. Reinhoudt, B. Poelsema, *Langmuir* **2006**, *22*, 5945.

30   E. Favre, *Eur. Polym. J.* **1996**, *32*, 1183.

31   J. N. Lee, C. Park, G. M. Whitesides, *Anal. Chem.* **2003**, *75*, 6544.

32   M. J. Owen, P. J. Smith, *J. Adhes. Sci. Technol.* **1994**, *8*, 1063.

33   B. Olander, A. Wirsen, A. C. Albertsson, *J. Appl. Polym. Sci.* **2004**, *91*, 4098.

34   H. Hillborg, M. Sandelin, U. W. Gedde, *Polymer* **2001**, *42*, 7349.

35   H. Hillborg, N. Tomczak, A. Olah, H. Schönherr, G. J. Vancso, *Langmuir* **2004**, *20*, 785.

36   G. E. Poirier, M. J. Tarlov, H. E. Rushmeier, *Langmuir* **1994**, *10*, 3383.

37   S. J. Stranick, A. N. Parikh, D. L. Allara, P. S. Weiss, *J. Phys. Chem.* **1994**, *98*, 11136.

38   Y. Xia, G. M. Whitesides, *J. Am. Chem. Soc.* **1995**, *117*, 3274.

39   R. B. A. Sharpe, D. Burdinski, J. Huskens, H. J. W. Zandvliet, D. N. Reinhoudt, B. Poelsema, *Langmuir* **2004**, *20*, 8646.

40   E. Delamarche, H. Schmid, A. Bietsch, N. B. Larsen, H. Rothuizen, B. Michel, H. Biebuyck, *J. Phys. Chem. B* **1998**, *102*, 3324.

41   R. K. Workman, S. Manne, *Langmuir* **2004**, *20*, 805.

42   H. A. Biebuyck, G. M. Whitesides, *Langmuir* **1994**, *10*, 4581.

43   R. D. Piner, J. Zhu, F. Xu, S. H. Hong, C. A. Mirkin, *Science* **1999**, *283*, 661.

44   P. E. Sheehan, L. J. Whitman, *Phys. Rev. Lett.* **2002**, *88*.

45   J. Y. Jang, S. H. Hong, G. C. Schatz, M. A. Ratner, *J. Chem. Phys.* **2001**, *115*, 2721.

46   J. A. Helmuth, H. Schmid, R. Stutz, A. Stemmer, H. Wolf, *J. Am. Chem. Soc.* **2006**, *128*, 9296.

47   F. Bessueille, M. Pla-Roca, C. A. Mills, E. Martinez, J. Samitier, A. Errachid, *Langmuir* **2005**, *21*, 12060.

48   Y. Xia, G. M. Whitesides, *Langmuir* **1997**, *13*, 2059.

49   A. A. Dameron, J. R. Hampton, S. D. Gillmor, J. N. Hohman, P. S. Weiss, *J. Vac. Sci. Technol. B* **2005**, *23*, 2929.

50   A. A. Dameron, J. R. Hampton, R. K. Smith, T. J. Mullen, S. D. Gillmor, P. S. Weiss, *Nano Lett.* **2005**, *5*, 1834.

51   L. Libioulle, A. Bietsch, H. Schmid, B. Michel, E. Delamarche, *Langmuir* **1999**, *15*, 300.

| 52 | E. Delamarche, M. Geissler, H. Wolf, B. Michel, *J. Am. Chem. Soc.* **2002**, *124*, 3834. |

53   O. Cherniavskaya, A. Adzic, C. Knutson, B. J. Gross, L. Zang, R. Liu, D. M. Adams, *Langmuir* **2002**, *18*, 7029.

54   R. B. A. Sharpe, B. J. F. Titulaer, E. Peeters, D. Burdinski, J. Huskens, H. J. W. Zandvliet, D. N. Reinhoudt, B. Poelsema, *Nano Lett.* **2006**, *6*, 1235.

55   C. D. James, R. C. Davis, L. Kam, H. G. Craighead, M. Isaacson, J. N. Turner, W. Shain, *Langmuir* **1998**, *14*, 741.

56   M. Tormen, T. Borzenko, B. Steffen, G. Schmidt, L. W. Molenkamp, *Appl. Phys. Lett.* **2002**, *81*, 2094.

57   M. Tormen, T. Borzenko, B. Steffen, G. Schmidt, L. W. Molenkamp, *Microelectron. Eng.* **2002**, *61-2*, 469.

58   T. W. Odom, J. C. Love, D. B. Wolfe, K. E. Paul, G. M. Whitesides, *Langmuir* **2002**, *18*, 5314.

59   K. M. Choi, J. A. Rogers, *J. Am. Chem. Soc.* **2003**, *125*, 4060.

60   D. Trimbach, K. Feldman, N. D. Spencer, D. J. Broer, C. W. M. Bastiaansen, *Langmuir* **2003**, *19*, 10957.

61   P. J. Yoo, S. J. Choi, J. H. Kim, D. Suh, S. J. Baek, T. W. Kim, H. H. Lee, *Chem. Mater.* **2004**, *16*, 5000.

62   G. Csucs, T. Kunzler, K. Feldman, F. Robin, N. D. Spencer, *Langmuir* **2003**, *19*, 6104.

63   D. C. Trimbach, M. Al-Hussein, W. H. de Jeu, M. Decré, D. J. Broer, C. W. M. Bastiaansen, *Langmuir* **2004**, *20*, 4738.

64   B. D. Martin, S. L. Brandow, W. J. Dressick, T. L. Schull, *Langmuir* **2000**, *16*, 9944.

65   N. Coq, T. van Bommel, R. A. Hikmet, H. R. Stapert, W. U. Dittmer, *Langmuir* **2007**, *23*, 5154.

66   N. Y. Lee, J. R. Lim, M. J. Lee, J. B. Kim, S. J. Jo, H. K. Baik, Y. S. Kim, *Langmuir* **2006**, *22*, 9018.

67   K. Efimenko, W. E. Wallace, J. Genzer, *J. Colloid Interface Sci.* **2002**, *254*, 306.

68   J. R. Hollahan, G. L. Carlson, *J. Appl. Polym. Sci.* **1970**, *14*, 2499.

69   L. Yan, W. T. S. Huck, X. M. Zhao, G. M. Whitesides, *Langmuir* **1999**, *15*, 1208.

70   B. A. Langowski, K. E. Uhrich, *Langmuir* **2005**, *21*, 6366.

71   C. Donzel, M. Geissler, A. Bernard, H. Wolf, B. Michel, J. Hilborn, E. Delamarche, *Adv. Mater.* **2001**, *13*, 1164.

72   E. Delamarche, C. Donzel, F. S. Kamounah, H. Wolf, M. Geissler, R. Stutz, P. Schmidt-Winkel, B. Michel, H. J. Mathieu, K. Schaumburg, *Langmuir* **2003**, *19*, 8749.

73   V. Barbier, M. Tatoulian, H. Li, F. Arefi-Khonsari, A. Ajdari, P. Tabeling, *Langmuir* **2006**, *22*, 5230.

74   H. Makamba, J. H. Kim, K. Lim, N. Park, J. H. Hahn, *Electrophoresis* **2003**, *24*, 3607.

75   W. Hellmich, J. Regtmeier, T. T. Duong, R. Ros, D. Anselmetti, A. Ros, *Langmuir* **2005**, *21*, 7551.

76   J. Lahann, M. Balcells, H. Lu, T. Rodon, K. F. Jensen, R. Langer, *Anal. Chem.* **2003**, *75*, 2117.

77   S. W. Hu, X. Q. Ren, M. Bachman, C. E. Sims, G. P. Li, N. L. Allbritton, *Anal. Chem.* **2004**, *76*, 1865.

78   S. W. Hu, X. Q. Ren, M. Bachman, C. E. Sims, G. P. Li, N. Allbritton, *Electrophoresis* **2003**, *24*, 3679.

79   Q. G. He, Z. C. Liu, P. F. Xiao, R. Q. Liang, N. Y. He, Z. H. Lu, *Langmuir* **2003**, *19*, 6982.

80   V. B. Sadhu, A. Perl, M. Péter, D. I. Rozkiewicz, G. Engbers, B. J. Ravoo, D. N. Reinhoudt, J. Huskens, *Langmuir* **2007**, *23*, 6850.

81   X. M. Li, M. Peter, J. Huskens, D. N. Reinhoudt, *Nano Lett.* **2003**, *3*, 1449.

82   A. A. Shestopalov, R. L. Clark, E. J. Toone, *J. Am. Chem. Soc.* **2007**, *129*, 13818.

83   P. W. Snyder, M. S. Johannes, B. N. Vogen, R. L. Clark, E. J. Toone, *J. Org. Chem.* **2007**, *72*, 7459.

84   D. I. Rozkiewicz, W. Brugman, R. M. Kerkhoven, B. J. Ravoo, D. N. Reinhoudt, *J. Am. Chem. Soc.* **2007**, *129*, 11593.

85   S. R. Coyer, A. J. Garcia, E. Delamarche, *Angew. Chem., Int. Ed. Engl.* **2007**, *46*, 6837.

86   R. B. A. Sharpe, D. Burdinski, J. Huskens, H. J. W. Zandvliet, D. N. Reinhoudt, B. Poelsema, *J. Am. Chem. Soc.* **2005**, *127*, 10344.

87   X. Duan, V. B. Sadhu, A. Perl, M. Péter, D. N. Reinhoudt, J. Huskens, *Langmuir* **2008**, *24*, 3621.

88   M. Liebau, J. Huskens, D. N. Reinhoudt, *Adv. Funct. Mater.* **2001**, *11*, 147.

89   M. Liebau, H. M. Janssen, K. Inoue, S. Shinkai, J. Huskens, R. P. Sijbesma, E. W. Meijer, D. N. Reinhoudt, *Langmuir* **2002**, *18*, 674.

90   M. Saalmink, C. van der Marel, H. R. Stapert, D. Burdinski, *Langmuir* **2006**, *22*, 1016.

91   Y. Xia, M. Mrksich, E. Kim, G. M. Whitesides, *J. Am. Chem. Soc.* **1995**, *117*, 9576.

92   N. L. Jeon, P. G. Clem, D. A. Payne, R. G. Nuzzo, *Langmuir* **1996**, *12*, 5350.

93   N. L. Jeon, K. Finnie, K. Branshaw, R. G. Nuzzo, *Langmuir* **1997**, *13*, 3382.

94   S. Onclin, B. J. Ravoo, D. N. Reinhoudt, *Angew. Chem., Int. Ed. Engl.* **2005**, *44*, 6282.

95   K. R. Finnie, R. Haasch, R. G. Nuzzo, *Langmuir* **2000**, *16*, 6968.

96   X. M. Li, J. Huskens, D. N. Reinhoudt, *J. Mater. Chem.* **2004**, *14*, 2954.

97   J. Lahiri, E. Ostuni, G. M. Whitesides, *Langmuir* **1999**, *15*, 2055.

98   L. Yan, X. M. Zhao, G. M. Whitesides, *J. Am. Chem. Soc.* **1998**, *120*, 6179.

99   T. P. Sullivan, M. L. van Poll, P. Y. W. Dankers, W. T. S. Huck, *Angew. Chem., Int. Ed. Engl.* **2004**, *43*, 4190.

100   C. L. Feng, A. Embrechts, I. Bredebusch, J. Schnekenburger, W. Domschke, G. J. Vancso, H. Schönherr, *Adv. Mater.* **2007**, *19*, 286.

101   C. L. Feng, G. J. Vancso, H. Schönherr, *Langmuir* **2007**, *23*, 1131.

102   C. L. Feng, G. J. Vancso, H. Schönherr, *Adv. Funct. Mater.* **2006**, *16*, 1306.

103   D. I. Rozkiewicz, B. J. Ravoo, D. N. Reinhoudt, *Langmuir* **2005**, *21*, 6337.

104   D. I. Rozkiewicz, D. Janczewski, W. Verboom, B. J. Ravoo, D. N. Reinhoudt, *Angew. Chem., Int. Ed. Engl.* **2006**, *45*, 5292.

105   M. J. W. Ludden, D. N. Reinhoudt, J. Huskens, *Chem. Soc. Rev.* **2006**, *35*, 1122.

106   J. P. Renault, A. Bernard, D. Juncker, B. Michel, H. R. Bosshard, E. Delamarche, *Angew. Chem., Int. Ed. Engl.* **2002**, *41*, 2320.

107   A. A. Yu, T. Savas, S. Cabrini, E. diFabrizio, H. I. Smith, F. Stellacci, *J. Am. Chem. Soc.* **2005**, *127*, 16774.

108   A. A. Yu, T. A. Savas, G. S. Taylor, A. Guiseppe-Elie, H. I. Smith, F. Stellacci, *Nano Lett.* **2005**, *5*, 1061.

109   A. A. Yu, F. Stellacci, *J. Mater. Chem.* **2006**, *16*, 2868.

110   H. H. Lin, L. Sun, R. M. Crooks, *J. Am. Chem. Soc.* **2005**, *127*, 11210.

111   H. H. Lin, J. Kim, L. Sun, R. M. Crooks, *J. Am. Chem. Soc.* **2006**, *128*, 3268.

112   T. Auletta, B. Dordi, A. Mulder, A. Sartori, S. Onclin, C. M. Bruinink, M. Péter, C. A. Nijhuis, H. Beijleveld, H. Schönherr, G. J. Vancso, A. Casnati, R. Ungaro, B. J. Ravoo, J. Huskens, D. N. Reinhoudt, *Angew. Chem., Int. Ed. Engl.* **2004**, *43*, 369.

113   C. M. Bruinink, C. A. Nijhuis, M. Péter, B. Dordi, O. Crespo-Biel, T. Auletta, A. Mulder, H. Schönherr, G. J. Vancso, J. Huskens, D. N. Reinhoudt, *Chem. Eur. J.* **2005**, *11*, 3988.

114   A. Mulder, S. Onclin, M. Péter, J. P. Hoogenboom, H. Beijleveld, J. ter Maat, M. F. García-Parajó, B. J. Ravoo, J. Huskens, N. F. van Hulst, D. N. Reinhoudt, *Small* **2005**, *1*, 242.

115   S. Onclin, J. Huskens, B. J. Ravoo, D. N. Reinhoudt, *Small* **2005**, *1*, 852.

116   O. Crespo-Biel, M. Péter, C. M. Bruinink, B. J. Ravoo, D. N. Reinhoudt, J. Huskens, *Chem. Eur. J.* **2005**, *11*, 2426.

117   A. P. Quist, E. Pavlovic, S. Oscarsson, *Anal. Bioanal. Chem.* **2005**, *381*, 591.

118   S. A. Ruiz, C. S. Chen, *Soft Matter* **2007**, *3*, 168.

119   E. Delamarche, *Chimia* **2007**, *61*, 126.

120   X. J. Wang, M. Ostblom, T. Johansson, O. Inganäs, *Thin Solid Films* **2004**, *449*, 125.

121   C. Thibault, C. Severac, A. F. Mingotaud, C. Vieu, M. Mauzac, *Langmuir* **2007**, *23*, 10706.

122   Y. L. Loo, R. L. Willett, K. W. Baldwin, J. A. Rogers, *J. Am. Chem. Soc.* **2002**, *124*, 7654.

123   B. D. Gates, Q. B. Xu, M. Stewart, D. Ryan, C. G. Willson, G. M. Whitesides, *Chem. Rev.* **2005**, *105*, 1171.

124   P. C. Hidber, W. Helbig, E. Kim, G. M. Whitesides, *Langmuir* **1996**, *12*, 1375.

125   V. Santhanam, J. Liu, R. Agarwal, R. P. Andres, *Langmuir* **2003**, *19*, 7881.

126   H. S. Shin, H. J. Yang, Y. M. Jung, S. Bin Kim, *Vib. Spectrosc.* **2002**, *29*, 79.

127   V. Santhanam, R. P. Andres, *Nano Lett.* **2004**, *4*, 41.

128   T. Kraus, L. Malaquin, H. Schmid, W. Riess, N. D. Spencer, H. Wolf, *Nat. Nanotechnol.* **2007**, *2*, 570.

Chapter 3

Heavyweight dendritic inks for positive microcontact printing

Poly(propylene imine) dendrimers with dialkyl sulfide end-groups were prepared and developed as inks for positive microcontact printing ((+)μCP) on gold. Long (C_{10}-S-C_{10}-), medium (C_3-S-C_4-) and short (C_1-S-C_1-) dialkyl sulfide end-groups were attached to second and third generation PPI dendrimers to create a family of dendritic sulfides. The dendritic inks flatten upon adsorption and form thin monolayers on gold. (+)μCP was performed on gold using commercially available poly(dimethylsiloxane) as stamp material and n-octadecanethiol as etch resist. Using a $Fe(NO_3)_3$/thiourea acidic etching solution the gold beneath the dendrimers was selectively etched away to give the positive copy of the master pattern. The multivalent sulfide attachment and the relatively high molecular mass of these dendrimers ensured minimal lateral ink spreading and thus optimal feature reproducibility. Contact times were varied to analyze the spreading rates of the dendritic inks. The spreading rates of the dendritic inks were found to be much lower than that of pentaerythritol-tetrakis(3-mercapto-propionate). (+)μCP with the new inks was extended to submicrometer features. Optical microscopy, scanning electron microscopy, and atomic force microscopy were used to characterize the etched samples. 100 nm wide lines were faithfully replicated with the third generation dendrimers bearing medium (C_3-S-C_4-) end-groups.

3.1 Introduction

The transfer of molecules to surfaces by means of microcontact printing (μCP) allows simple and efficient formation of micrometer-sized patterns.[1,2] μCP consists of bringing a "molecularly inked" soft elastomeric stamp into conformal contact with a substrate in order to form self-assembled monolayers (SAMs) on the surface exclusively in the areas of contact between the stamp and the substrate. The SAM can pack and organize well enough to act as a wet etch resist, as was first shown for n-alkanethiol molecules on gold.[1,3] The pattern etched into the gold substrate is the negative replica of the original master (negative microcontact printing, (-)μCP). Although downsizing the features replicated by μCP would be very attractive, several difficulties have to be overcome to enter in the submicrometer range. The main limiting factors of downsizing the printed patterns are (i) the low mechanical stability of the elastomeric stamp which is prone to collapse and deformation,[4] and (ii) the lateral spreading of the ink molecules during printing, when conformal contact is achieved between the stamp and the surface.[5] Several ways have been proposed to increase the mechanical stability of the stamp, which range from improving the hardness of the PDMS[6] or the application of alternative stamp materials[7] to introducing new μCP techniques such as chemically patterned flat stamps.[8] Catalytically active stamps have been developed to prevent ink spreading.[9] Using inks with increased molecular weight or with multiple attachment points could reduce the spreading rate of the molecules but on the other hand that would be realized at the expense of order and etch resistance of the formed monolayer.[10]

The extension of the μCP methodology to positive μCP ((+)μCP) has resulted in the possibility of pattern replication by printing a poorly etch resistant ink[11,12] followed by immersion of the sample in a second, etch resistant adsorbate solution, which fills the available areas and acts as a resist in the subsequent etching step. It is an additional advantage of (+)μCP that one can use stamps with a high filling ratio to replicate master features with a low filling ratio. Originally, pentaerythritol-tetrakis(3-mercaptopropionate) (PTMP) was proposed as a positive ink, because it forms a stable SAM on gold and copper, which is not replaced by etch resistant n-alkanethiols (such as n-octadecanethiol (ODT)), and does not provide significant etch resistance.[11,13]
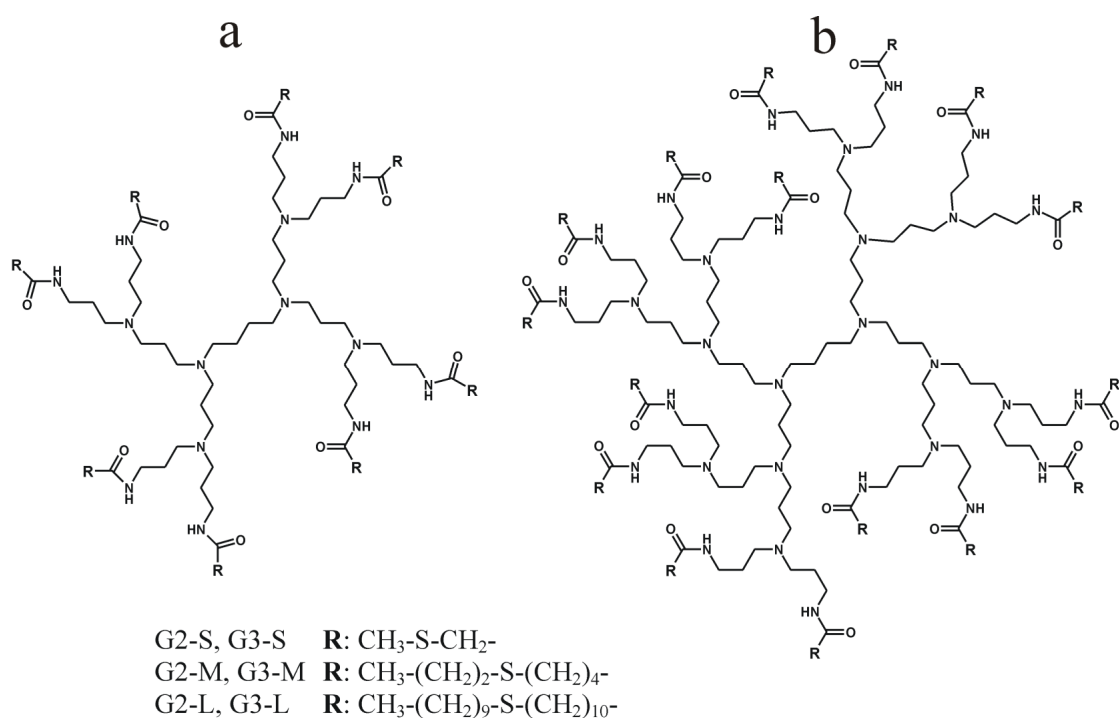
Dendrimers are highly branched, globular macromolecules that represent excellent building block candidates for nanostructured materials.[14] It was shown that amine- and hydroxyl-terminated poly(amidoamine) dendrimers form stable, densely packed SAMs on gold, which are porous toward electroactive species.[15] Dendrimers were also used as inks for μCP when amine-terminated dendrimer SAMs were patterned on silicon creating 140 nm wide dendrimer SAM lines with 70 nm interline spacing.[16]

In this chapter the high molecular weight of dendrimers is combined with the affinity of dialkyl sulfides for gold and a family of poly(propylene imine) (PPI) dendrimer-based dialkyl sulfides as positive inks for μCP on gold is described. Although the concept of "heavyweight" inks is not entirely new,[10,17] it is innovative to use them as positive inks. Dendrimers with tertiary amine and dialkyl sulfide functionalities adsorb to gold with both the sulfur atoms and the amine core.[17] Their high molecular mass and multiple sulfide attachment points to the gold surface should reduce the lateral spreading during printing and limit the exchange with molecules that form an etch resistant SAM. In addition, the open structure of the dendrimers should allow the access of electroactive species to the surface through the SAM and significantly decrease the etch resistance.

3.2 Results and discussion

3.2.1 Synthesis and monolayer characterization

Dialkyl sulfides with different chain length (L = long ($C_{10}H_{21}$-S-$C_{10}H_{20}$-), M = medium (C_3H_7-S-C_4H_8-) and S = short (CH_3-S-CH_2-)) were attached to second (G2) and third (G3) generation PPI dendrimers according to a method already published by our group.[17] First the n-alkylthiol was reacted with the ω-bromocarboxylic acid to form the thioether carboxylic acid. The acid was activated with pentafluorophenol and dicyclohexylcarbodiimide (DCC) and reacted with the amino-terminated PPI by overnight stirring in $CHCl_3$. Six dendritic dialkyl sulfides were synthesized as shown in Scheme 3.1. The three second generation dendrimers (G2) with 8 end-groups and the three third generation dendrimers (G3) with 16 end-groups have different polarities according to the carbon chain length in the dialkyl sulfide end-group. ^{1}H NMR, ^{13}C NMR, MALDI-TOF MS and elemental analysis data (see experimental section) are consistent with the expected molecular structures.

G2-S, G3-S   **R**: CH_3-S-CH_2-
G2-M, G3-M **R**: CH_3-$(CH_2)_2$-S-$(CH_2)_4$-
G2-L, G3-L   **R**: CH_3-$(CH_2)_9$-S-$(CH_2)_{10}$-

Scheme 3.1 The structure of the second (a) and third generation (b) poly(propylene imine) dendrimers with dialkyl sulfide end-groups.

Table 3.1 Properties of the prepared SAMs.

Compound	θ_a/θ_r immersion (H$_2$O, deg)[a]	θ_a/θ_r printing (H$_2$O, deg)[a]	XPS-S$_{2p}$ immersion (% S bound)[b]	C_{ml} immersion (F/m^2)[c]
G2-S	57/14	82/33	41	0.281
G3-S	52/19	81/30	42	0.325
G2-M	64/24	76/30	25	0.196
G3-M	63/31	79/29	27	0.174
G2-L	58/20	77/32	45	0.270
G3-L	60/19	77/32	51	0.241

[a] Advancing (θ_a) and receding (θ_r) contact angles of the monolayer with water. [b] Percentage of bound sulfurs of the dendrimer. [c] Capacitance of the monolayer determined by cyclic voltammetry at a scan rate of 0.1 V/s and -0.25 V.

SAMs of the dendritic dialkyl sulfides were prepared by two different methods: (i) by immersion of the gold sample for 12 h in a 10^{-5} M dendrimer solution in ethanol and (ii) by printing with an inked (c ≈ 10^{-5} M) featureless PDMS stamp for 1 min. In both

cases the samples were rinsed with clean solvent after SAM formation, to remove the excess of adsorbate. The variation in dialkyl sulfide chain length did not significantly affect the contact angle of the dendrimer SAMs. Dendrimer monolayers formed via printing showed higher contact angles than those formed in solution (Table 3.1). The higher contact angle of the printed monolayer suggests the transfer of low-molecular-weight PDMS fragments, in particular for the polar dendrimers G2-S and G3-S. The hysteresis between θ_a and θ_r of about 30-40° in all cases denotes a disordered monolayer.

The percentages of bound (to gold) and unbound sulfur have been determined based on the S_{2p} region of the X-ray photoelectron spectrum of the dendritic dialkyl sulfide SAMs (Table 3.1). The attachment to the gold surface is achieved, for example, with ~4 sulfur atoms in the case of G3-M, and ~6 atoms in the case of G3-S. Assuming that more attachment points within one molecule cause a flatter conformation, the XPS results are consistent with the ratio of the effective film thickness deduced from the electrochemical capacitance measurements. Higher capacitance values (C_{ml}) generally represent lower monolayer thicknesses.[18]
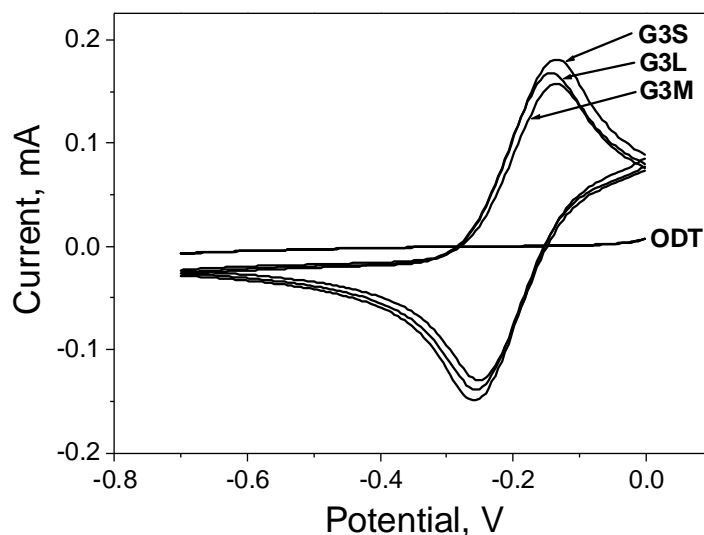

Figure 3.2 Heterogeneous electron transfer through third generation dialkyl sulfide dendrimer and ODT SAMs on gold electrodes. (Cyclic voltammetry in 1 mM $Fe(CN)_6^{3-}/Fe(CN)_6^{4-}$ and 0.1 M K_2SO_4. The scan rate was 0.1 V/s).

The dendritic dialkyl sulfide SAMs on gold had much lower blocking ability against electroactive species than ODT, as shown by heterogeneous electron transfer measurements. Figure 3.2 shows the cyclic voltammetric current-potential responses for ODT and dendrimer SAMs on gold in 1 mM $Fe(CN)_6^{3-}$/$Fe(CN)_6^{4-}$ and 0.1 M K_2SO_4. The well ordered ODT SAM blocked the surface efficiently. The voltammograms of the dendrimer SAMs are distinctly different: the currents were much higher showing electrochemical reactions between the ferro-/ferricyanide and gold. There were no significant differences between the intensities of electron transfer through different dendrimer SAMs. All dendrimer SAMs allowed electrochemical reaction between the electrode and electroactive species in the electrolyte solution.
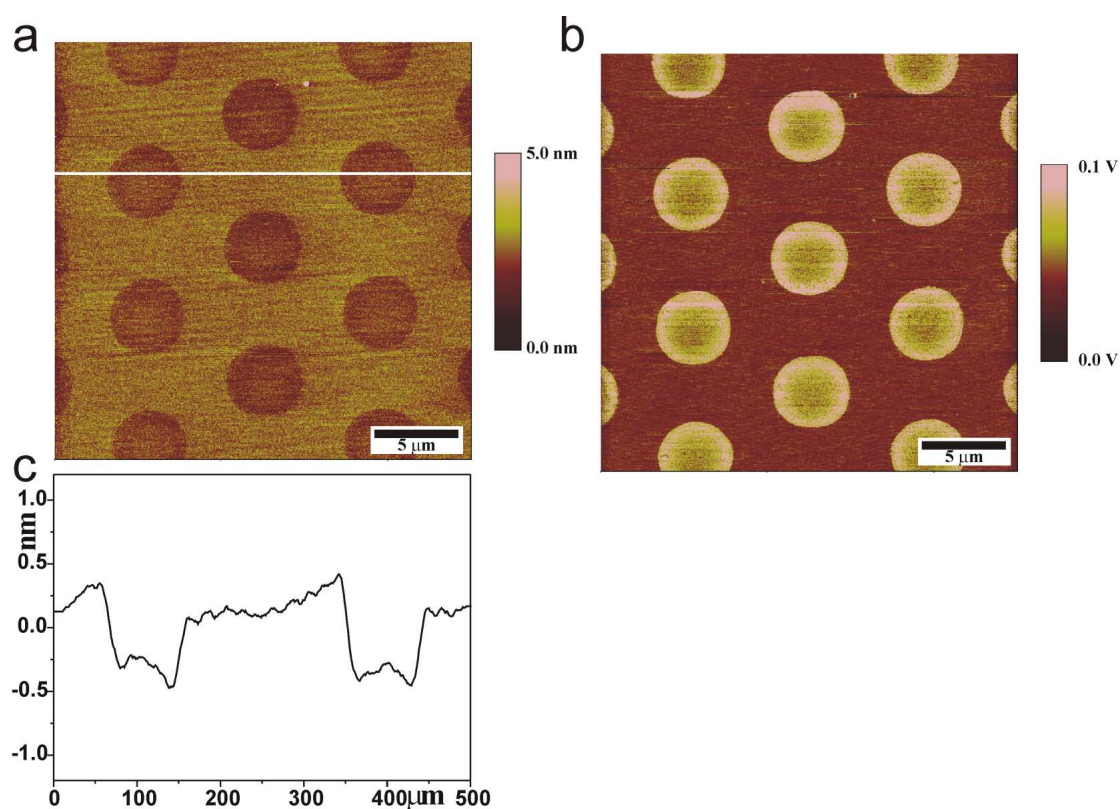
Figure 3.3 AFM height (a), friction (b) and cross section (c) images of a gold surface patterned by μCP (contact time 60 s) using G3-M (c = 5 × 10^{-5} M in ethanol) and subsequently immersed in ODT (c = 10^{-4} M in ethanol) for 5 s.

"Molecular ruler" experiments performed through AFM imaging confirmed that the dendritic dialkyl sulfides absorbed in a flattened conformation on the gold surface. The AFM height and friction images of a patterned gold surface with G3-M and ODT are presented in Figure 3.3. The G3-M SAM was formed in the dots, where the inked

36

PDMS stamp and the gold surface were contacted during μCP, and the ODT was assembled from solution on the uncovered areas surrounding the dots. The two monolayers can be clearly differentiated in the friction image (Figure 3.3b). The height image shows that the G3M SAM is appreciably thinner than the ODT SAM formed during 5 s dipping. The thickness of an ordered ODT SAM is about 2 nm,[19] but an ODT SAM assembled in only 5 s may be significantly thinner, which implies a nanometer or even sub-nanometer dendrimer SAM thickness at most.

The advancing contact angle of the G3-M SAM printed on gold and dipped in ODT solution in ethanol for 5 s increased significantly, from 79° to 103°, approaching the water contact angle of an ODT SAM: 113°.[19] This increase suggests that the voids present in the dendrimer monolayer are filled by ODT molecules and increase the hydrophobicity of the surface. However, the etch resistance of the dendrimer layer remained much lower than that of the ODT SAM.

3.2.2 Positive microcontact printing

The high molecular weight of dendrimers, the low etch resistance of their SAMs on gold, and the fact that they are not replaced by ODT during the dipping in the solution make them excellent inks for (+)μCP. The SEM and AFM images of a patterned and etched 20 nm thick gold film on a silicon wafer are presented in Figure 3.4. The dendritic ink was printed on a gold surface for 1 min with a PDMS stamp to form the dot-patterned dendrimer SAM. After that, the sample was immersed in ODT solution for 5 to 15 s. ODT formed an etch-protective SAM on the rest of the surface. The dendrimer SAM was not etch-resistant and the gold underneath was etched away to give the positive copy of the original master.

All dendrimers exhibited proper positive ink behavior, resulting in islands where the gold was completely etched away (black dots in Figure 3.4 and 3.5). The surrounding matrix was backfilled with ODT for 5 to 15 s. The packing and quality of the ODT SAM was high enough to act as an etch barrier. An acidic solution of 10 mM $Fe(NO_3)_3$, 15 mM thiourea and 1.2 % HCl at 45 °C was found to be optimal for the selective etching of this patterned monolayer.[2] The common alkaline etching solutions (1 M KOH, 0.1 M $Na_2S_2O_3$, 0.01 M $K_3Fe(CN)_6$ and 0.001 M $K_4Fe(CN)_6$) did not provide enough selectivity during the etching. The superiority of acidic over alkaline etching baths and the high selectivity of acidic etching system in the case of PPI based dendrimer SAMs is likely a consequence of the protonation of the amine groups

inside the dendrimer: the protonation 'swells' the dendrimers and makes the gold surface more accessible for electroactive species.
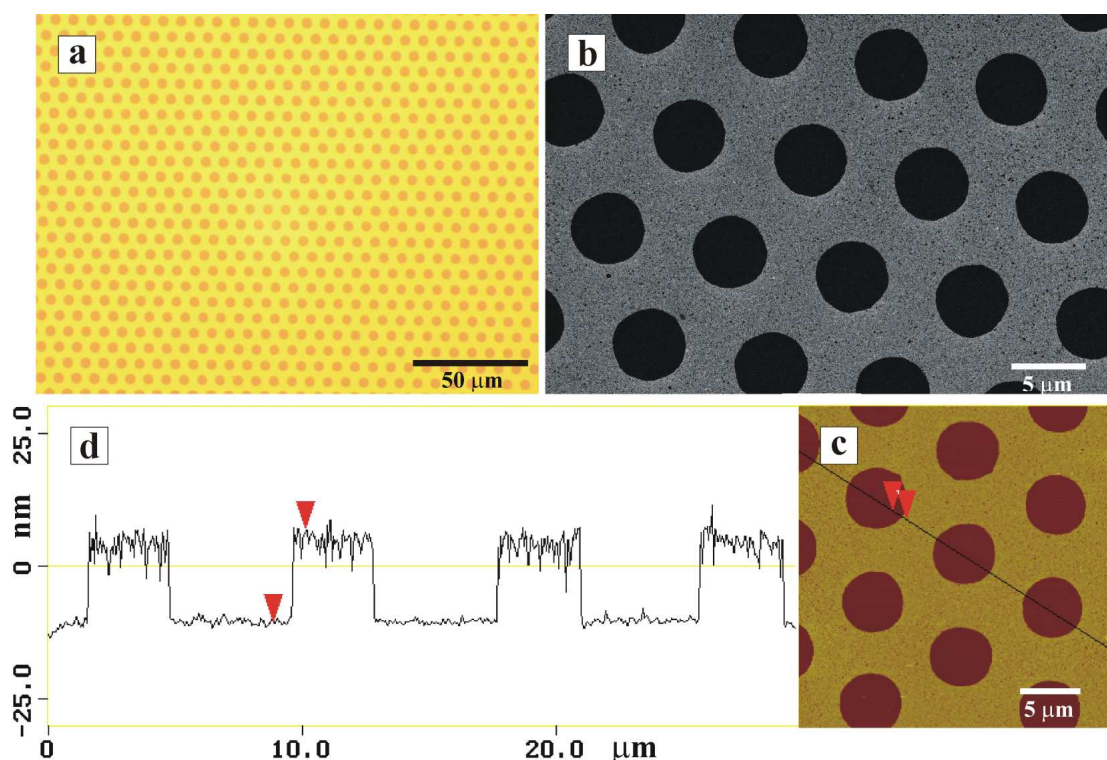

Figure 3.4 Images of etched gold patterns produced by (+)μCP using G3-L (6×10⁻⁶ M in ethanol) as ink and ODT (10⁻⁴ M in ethanol) as backfilling, followed by wet etching. The duration of printing was 1 min and the dipping time in ODT was 15 s. The sample was etched in a Fe(III)/thiourea etching bath[2] for 2.5 min at 45°C. (a) Optical microscopy; (b) Scanning electron microscopy (SEM); (c) AFM height; (d) AFM cross section image.

The (+)μCP experiments with the second and third generation dendrimers with short dialkyl sulfide end-groups (G2-S and G3-S) were carried out using oxidized PDMS stamps. These inks were very polar and therefore assisted the extraction of polar, low molecular weight PDMS impurities from the bulk of the stamps.[20] These impurities obscured the positive pattern formation because of their etch-resistance on the gold surface. It is known that all plasma treatment methods significantly reduce the amount of silicone related material transferred during printing as compared to untreated PDMS stamps.[21] Indeed, after oxidizing the PDMS stamp surface, G2-S and G3-S were successfully used as positive inks to replicate 5 μm-wide features (Figure 3.5c). Dendrimers G2-L and G3-L showed a low solubility in ethanol, while dendrimers G2-S and G3-S were too polar to use conventional PDMS stamps, therefore dendrimer

G3-M was chosen to test the lateral spreading during printing and SAM formation. This dendrimer has optimal solubility, medium polarity, and high molecular weight.
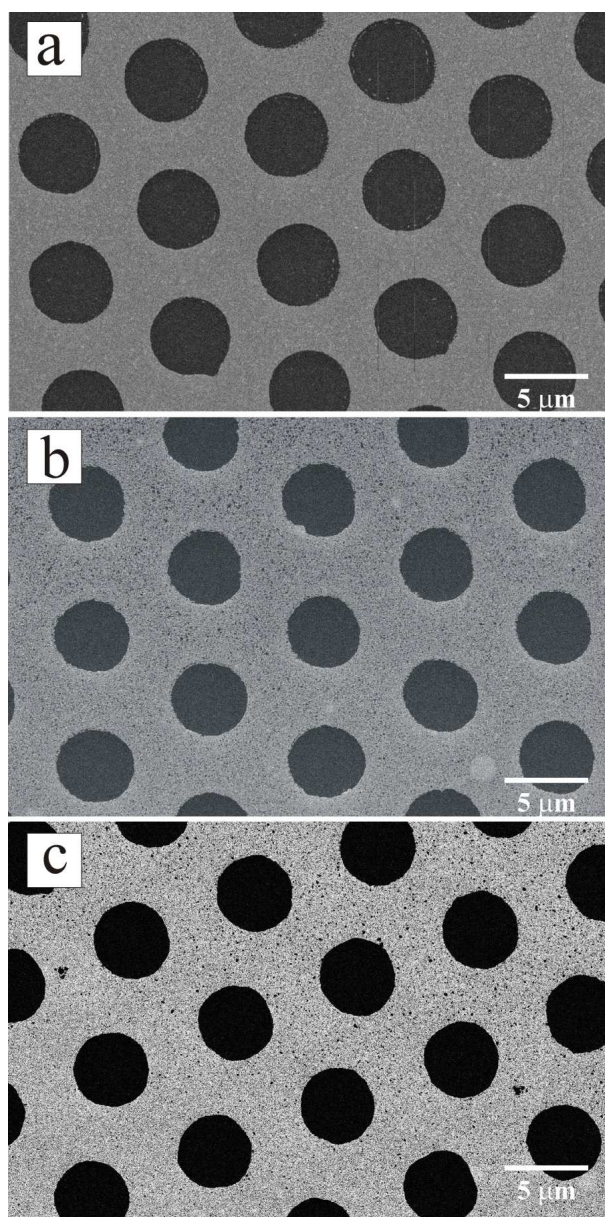

Figure 3.5 Scanning electron microscopy of etched gold patterns produced by (+)µCP using as ink (a) G2-M (1.6×10^{-4} M in ethanol), (b) G2-L (10^{-5} M in ethanol) and (c) G2-S (3.3×10^{-5} M in ethanol). The duration of printing in all cases was 1 min, samples were dipped in ODT for 15 s and etched in a Fe(III)/thiourea etching bath for 2.5 min at 45°C. G2-S was printed with an oxidized PDMS stamp.

To test the spreading tendency during conformal contact of the stamp with the surface of the dendritic inks, micrometer-sized line patterns of G3-M were printed on gold with increasing printing time. Subsequently the samples were immersed in ODT

solution and etched under identical conditions. SEM was used to characterize the etched surfaces and determine the width of the ODT-protected gold stripes. The results of the printing with G3-M were compared to the results of the same experiments carried out with PTMP as positive ink (Figure 3.6). Any lateral spreading on the surface during the printing step led to an increase of the ink covered area and, by necessity, to a decrease of the available bare gold area that would be covered by the ODT SAM. In case of line patterns, information about the lateral spreading could be obtained by measuring the line width. In Figure 3.6 the width of the ODT protected stripe area is plotted versus the printing time of G3-M and PTMP. The concentration in weight of the inks was the same in both cases: 0.6 g/l. While the G3-M/ODT system did not show a significant line width decrease with time, the PTMP covered the entire surface within 5 min printing by lateral spreading.
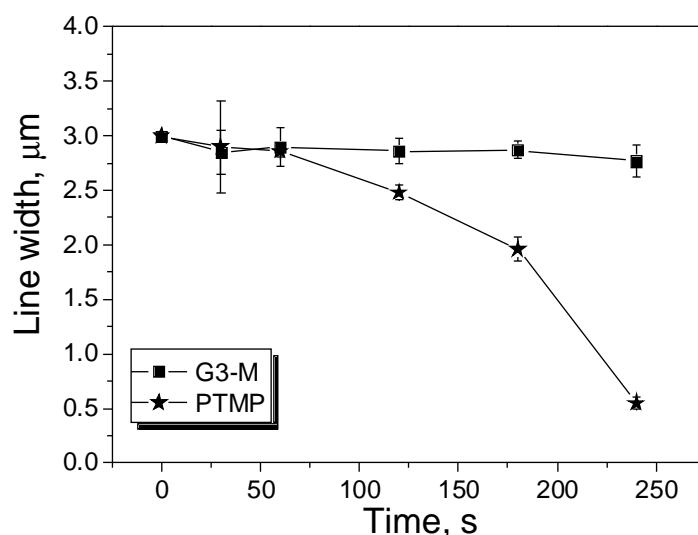

Figure 3.6 Plot of the width of the ODT-protected stripe area after (+)µCP with G3-M and PTMP vs the printing time. After printing the samples were immersed in ODT solution for 10 s, etched in a Fe(III)/thiourea etching bath for 2.5 min at 45°C and characterized by means of SEM imaging.

The spreading of G3-M on the surface was further investigated by (+)µCP with PDMS stamps made by the combination of capillary force lithography and replica molding.[22] Stamps with 300 nm wide trenches were prepared by this convenient and inexpensive method. Even for a dendrimer printing time of up to 5 min there was no

significant decrease in the width of the ODT-protected areas, which implies a sub-20 nm min^{-1} lateral spreading rate of the G3-M during conformal contact (Figure 3.7).
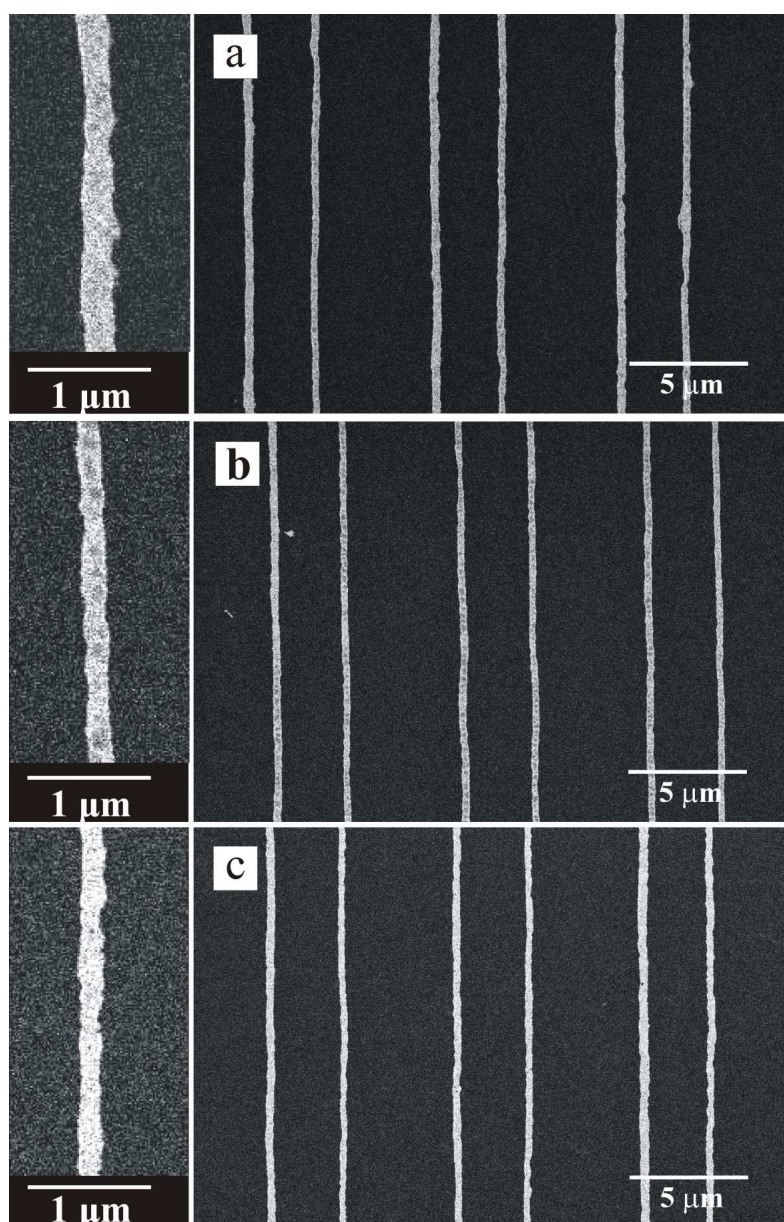

Figure 3.7 SEM images of etched submicrometer gold lines printed with second generation stamps prepared by capillary force lithography.[22] The stamp was inked with 5×10^{-5} M G3-M, printed for 1 min (a); 3 min (b) and 5 min (c); subsequently dipped in a 10^{-4} M ODT solution for 5 s and etched for 2.5 min in a Fe(III)/thiourea etching bath at 45 °C.

To achieve even higher resolution of the replicated patterns, a silicon master with 100 nm wide gratings (1 μm period) was used to prepare PDMS stamps for (+)μCP. Because (+)μCP provides inverse feature replication, a PMMA imprint of the original

silicon master was used as a master to prepare PDMS stamps. This feature inversion was necessary to provide the 100 nm-wide gold feature after the (+)μCP process. Figure 3.8 shows the result of (+)μCP experiments performed with G3-M as the ink and ODT as the etch resist. It is evident from Figure 3.8 that (+)μCP with this heavyweight dendritic ink results in faithful replication of features in the order of 100 nm.
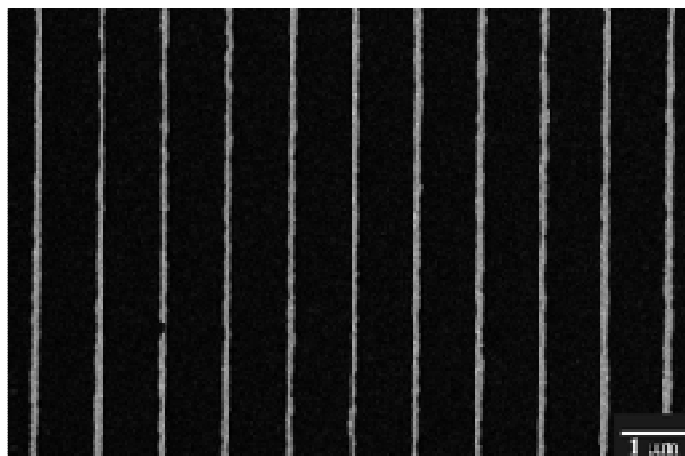

Figure 3.8 SEM image of 100-nm wide gold lines made by (+)μCP (4×10^{-5} M G3-M in ethanol, printing for 2 min, dipping in 10^{-4} M ODT in ethanol 6 s, etching in Fe(III)/thiourea at 45 °C for 2.5 min).

3.3 Conclusions

PPI dendrimer dialkyl sulfides were successfully applied as inks for positive microcontact printing and demonstrated their low spreading tendency on the surface during conformal contact between the stamp and the gold surface. Well-defined sub-micrometer gold wires on silicon were fabricated by positive microcontact printing using stamps made from commercially available PDMS and using acidic $Fe(NO_3)_3$ and thiourea based etching solutions. The new inks will be useful when sub-100 nm features should be replicated and fabricated by means of microcontact printing.

3.4 Experimental

Synthesis. All starting materials are commercially available and were used as received. The pentafluorophenylesters of methylthioacetic acid and propylthiovaleric acid were prepared in analogy to described procedures.[17] The synthesis of G2-L and

G3-L have been described elsewhere.[17] G2-S, G3-S, G2-M and G3-M were prepared in a similar way.

Modification of third generation poly(propylene imine) dendrimer with medium dialkyl sulfide chain (G3-M). The third generation amine terminated poly(propylene imine) dendrimer (206 mg, 0,15 mmol) was dissolved in dry $CHCl_3$ (4 ml) and a solution of the pentafluorophenylester of propylthiovaleric acid (1.05 g, 3 mmol) in 6 ml $CHCl_3$ was added to it. The solution was stirred at room temperature for two days under N_2 atmosphere. After the reaction the brownish mixture was washed twice with K_2CO_3 (0.05 M) and demineralized water (pH = 7). The organic phase was concentrated and was added dropwise to stirred isopropyl ether. The suspension was centrifuged and the solution above the oily and viscous precipitate was removed by decantation. Finally the collected product was dried in high vacuum. Yield: 561 mg (89 %) yellowish viscous liquid.

G3-M: ^{1}H NMR ($CDCl_3$, ppm): δ = 1.0 (48H, t, C$\underline{H}_3$), 2.5 (64H, t, S-C$\underline{H}_2$), 2.3 (32H, t, CH$_2$-C$\underline{H}_2$-CO), 3.3 (32H, m, CO-NH-C$\underline{H}_2$), 2.6 (84H, m, N-C$\underline{H}_2$), 1.8-1.5 (156H, m, -(CH$_2$)$_n$-), CO-NH not visible. ^{13}C NMR ($CDCl_3$, ppm): δ = 173.5 (NH-$\underline{C}$O), 51.9 (N-$\underline{C}$H$_2$-CH$_2$-CH$_2$-$\underline{C}$H$_2$-N), 51.4 (N-$\underline{C}$H$_2$-CH$_2$-$\underline{C}$H$_2$-N), 51.0 (N-$\underline{C}$H$_2$-CH$_2$-CH$_2$-NH), 37.3 (NH-$\underline{C}$H$_2$), 35.9 (CO-$\underline{C}$H$_2$), 34.2 ($\underline{C}$H$_2$-S-$\underline{C}$H$_2$), 31.7 (CH$_2$), 29.2 (N-CH$_2$-$\underline{C}$H$_2$-CH$_2$-N), 25.0 (CO-CH$_2$-$\underline{C}$H$_2$), 22.9 (CH$_3$-$\underline{C}$H$_2$) and 13.5 ($\underline{C}$H$_3$). $C_{216}H_{432}N_{30}O_{16}S_{16}$ (FW = 4219.0). Elemental analysis. Found: C = 60.53, H = 11.05, N = 10.07. Calcd: C = 61.49, H = 10.32, N = 9.95. MALDI-TOF MS: m/z = 4220 [M+H$^+$].

G2-M: Yield: 940 mg (91 %) yellowish viscous liquid. ^{1}H NMR ($CDCl_3$, ppm): δ = 1.0 (24H, t, C$\underline{H}_3$), 2.5 (32H, t, S-C$\underline{H}_2$), 2.3 (16H, t, CH$_2$-C$\underline{H}_2$-CO), 3.3 (16H, m, NH-C$\underline{H}_2$), 2.8 (36H, m, N-CH$_2$), 1.8-1.6 (76H, m, -(CH$_2$)$_n$-), CO-NH not visible. ^{13}C NMR ($CDCl_3$, ppm): δ = 173.4 (NH-$\underline{C}$O), 53.6 (N-$\underline{C}$H$_2$-CH$_2$-CH$_2$-$\underline{C}$H$_2$-N), 51.9 (N-$\underline{C}$H$_2$-CH$_2$-$\underline{C}$H$_2$-N), 51.6 (N-$\underline{C}$H$_2$-CH$_2$-CH$_2$-NH), 37.8 (NH-$\underline{C}$H$_2$), 36.3 (CO-$\underline{C}$H$_2$), 34.5 ($\underline{C}$H$_2$-S-$\underline{C}$H$_2$), 32.0 (S-CH$_2$-$\underline{C}$H$_2$), 29.6 (N-CH$_2$-$\underline{C}$H$_2$-CH$_2$-NH), 27.0 (N-CH$_2$-$\underline{C}$H$_2$-CH$_2$-N), 25.3 (CH$_2$), 23.2 ($\underline{C}$H$_2$), and 13.7 ($\underline{C}$H$_3$). $C_{104}H_{208}N_{14}O_8S_8$ (FW = 2039.4). Elemental analysis. Found: C = 59.99, H = 10.07, N = 9.17. Calcd: C = 61.25, H = 10.29, N = 9.61. MALDI-TOF MS: m/z = 2040 [M+H$^+$].

G2-S: Yield: 720 mg (78 %) yellowish viscous liquid. ^{1}H NMR (D_2O, ppm): δ = 2.0 (24H, s, C$\underline{H}_3$), 3.1 (16H, s, S-C$\underline{H}_2$-CO), 3.5 (16H, m, NH-C$\underline{H}_2$), 2.5-2.3 (36H, m, N-CH$_2$), 1.6-1.4 (28H, m, -(CH$_2$)$_n$-), CO-NH not visible. ^{13}C NMR (D_2O, ppm): δ =

172.5 (NH-$\underline{C}$O), 53.0 (N-$\underline{CH_2}$-CH$_2$-CH$_2$-CH$_2$-N), 51.3 (N-$\underline{CH_2}$-CH$_2$-$\underline{CH_2}$-N), 50.6 (N-$\underline{CH_2}$-CH$_2$-CH$_2$-NH), 38.0 (NH-$\underline{CH_2}$), 37.1 (CO-$\underline{CH_2}$), 25.3 (N-CH$_2$-$\underline{CH_2}$-CH$_2$-NH), 23.6 (N-CH$_2$-$\underline{CH_2}$-CH$_2$-N), 21.7 ($\underline{CH_2}$), and 15.3 ($\underline{CH_3}$). C$_{64}$H$_{128}$N$_{14}$O$_8$S$_8$ (FW = 1478.3). Elemental analysis. Found: C = 51.87, H = 8.62, N = 13.39. Calcd: C = 51.99, H = 8.72, N = 13.26. MALDI-TOF MS: m/z = 1479 [M+H$^+$].

G3-S: Yield: 298 mg (78 %) yellowish viscous liquid. ^{1}H NMR (D$_2$O, ppm): δ = 2.0 (48H, s, CH_3), 3.1 (32H, s, S-CH_2-CO), 3.4 (32H, m, NH-CH_2), 2.8-2.6 (84H, m, N-CH$_2$), 1.7-1.5 (60H, m, -(CH$_2$)$_n$-), CO-NH not visible. ^{13}C NMR (D$_2$O, ppm): δ = 172.5 (NH-$\underline{C}$O), 53.3 (N-$\underline{CH_2}$-CH$_2$-CH$_2$-$\underline{CH_2}$-N), 51.3 (N-$\underline{CH_2}$-CH$_2$-$\underline{CH_2}$-N), 50.6 (N-$\underline{CH_2}$-CH$_2$-CH$_2$-NH), 38.1 (NH-$\underline{CH_2}$), 37.2 (CO-$\underline{CH_2}$), 25.3 (N-CH$_2$-$\underline{CH_2}$-CH$_2$-NH), 23.5 (N-CH$_2$-$\underline{CH_2}$-CH$_2$-N), 21.8 ($\underline{CH_2}$), and 15.4 ($\underline{CH_3}$). C$_{136}$H$_{272}$N$_{30}$O$_{16}$S$_{16}$ (FW = 3096.9). Elemental analysis. Found: C = 51.18, H = 7.77, N = 12.10. Calcd: C = 52.74, H = 8.85, N = 13.57. MALDI-TOF MS: m/z = 3098 [M+H$^+$].

Microcontact printing. Stamps were prepared from commercially available, Sylgard-184 poly(dimethyl siloxane) (Dow Corning). The curing agent and the prepolymer were manually mixed in 1:10 volume ratio and cured overnight at 60 ^{o}C against the master. The cured stamp was pealed off from the master at the curing temperature. Silicon masters with micrometer sized features were fabricated by photolithography. The silicon master with submicrometer lines was obtained from our NaPa partner AMO GmbH.

Gold substrates were obtained from Ssens BV (Hengelo, The Netherlands) as a layer of 20 nm gold on titanium (2 nm) on silicon. Before use, the substrates were treated with oxygen plasma, immersed in ethanol for 1 hour, rinsed with water (Millipore) and ethanol and dried with nitrogen.

All glassware was cleaned with Hellmanex$^®$II (Helma GmbH & CoKG) (sonicated in a 2 % aqueous solution)

Before printing, the stamps were rinsed with pure ethanol and dried in a filtered steam of nitrogen. The stamps were inked with a few drops of solution of the dendrimer in ethanol ($\approx 10^{-5}$ M). After drying the surface of the stamps with nitrogen, conformal contact was achieved manually. In case of micrometer sized features the stamps were weakly pressed against the gold surface at the initial stage of the printing to induce the

formation of conformal contact. No external pressure was applied during the printing of submicrometer features.

The etching solution consisted of 10 mM $Fe(NO_3)_3$, 15 mM thiourea and 1,2 % HCl. Before every µCP experiment the freshly prepared etching solution was kept at 45 °C in a warm bath for 10 minutes before the samples were etched.

Monolayer characterization. Contact angles were measured on a Krüsss G10 contact angle setup equipped with a CCD camera. Advancing and receding contact angles were determined automatically during growth and reduction of a clean water droplet by the droplet shape analysis routine.

XPS measurements were performed on a Quantera Scanning X-ray Multiprobe instrument from Physical Electronics, equipped with a monochromatic Al Kα X-ray source producing approximatly 25 W of X-ray power. Spectra were referenced to the main C 1s peak set at 284.0 eV. A surface area of 1000 µm × 300 µm was scanned with an X-ray beam about 10 µm wide.

Electrochemical measurements were performed in a three-electrode setup using the SAM covered gold plate as working electrode, a platinum disc as counter electrode and a $Hg/HgSO_4$ (MSE) as reference electrode. ($E^o_{Hg/HgSO4}$ = 0.62 V *vs.* normal hydrogen electrode (NHE)). An AUTOLAB PGSTAT10 equipped with a frequency response analysis (FRA) module for electrochemical impedance spectroscopy was used for the measurements. 0.1 M K_2SO_4, 1 mM $K_3Fe(CN)_6$ / $K_4Fe(CN)_6$ in water was used for cyclic voltammetry.

AFM analyses were carried out with a NanoScope III (Veeco/Digital Instruments, Santa Barbara, CA, USA) Multimode Atomic Force Microscope equipped with a J-scanner, in contact mode by using Si_3N_4 cantilevers (Nanoprobes, Veeco/Digital Instruments) with a nominal spring constant of about 0.32 N m^{-1}. To ensure maximum sensitivity for lateral forces in the friction-force images, the sample was scanned at 90° with respect to the long axis of the cantilever. AFM imaging was performed at ambient conditions.

3.5 References

1   Kumar, A.; Whitesides, G. M. *Appl. Phys. Lett.* **1993**, *63*, 2002.

2 Geissler, M.; Wolf, H.; Stutz, R.; Delamarche, E.; Grummt, U. –W.; Michel, B.; Bietsch, A. *Langmuir* **2003**, 19, 6301.

3 a) Xia, Y.; Zhao, X.-M.; Whitesides, G. M. *Microelectronic Engineering* **1996**, 32, 255; b) Kumar, A.; Biebuyck, H. A.; Whitesides, G. M. *Langmuir* **1994**, 10, 1498; c) Larsen, N. B.; Biebuyck, H.; Delamarche, E.; Michel, B. *J. Am. Chem. Soc.* **1997**, 119, 3017.

4 a) Bietsch, A.; Michel, B. *J. Appl. Phys.* **2000**, 88, 4310; b) Michel, B. Bernard, A.; Bietsch, A.; Delamarche, E.; Geissler, M.; Juncker, D.; Kind, H.; Renault, J.-P.; Rothuizen, H.; Schmid, H.; Schmidt-Winkel, P.; Stutz, R.; Wolf, H. *IBM J. Res. Dev.* **2001**, 45, 697; c) Sharp, K. G.; Blackman, G. S.; Glassmaker, N. J.; Jagota, A.; Hui, C.-Y. *Langmuir* **2004**, 20, 6430.

5 a) Libioulle, L.; Bietsch, A.; Schmid, H.; Michel, B.; Delamarche, E. *Langmuir* **1999**, 15, 300; b) Delamarche, E.; Hoole, A. C. F.; Michel, B.; Wilkes, S.; Despont, M.; Welland, M. E.; Biebuyck, H. *J. Phys. Chem. B* **1997**, 101, 9263; c) Rogers, J. A.; Nuzzo, R. G. *Materials Today* **2005**, 8, 50; d) Quist, A. P.; Pavlovic, E.; Oscarson, S. *Anal. Bioanal. Chem.* **2005**, 381, 591.

6 a) Choi, K. M. Rogers, J. A. *J. Am. Chem. Soc.* **2003**, 125, 4060; b) Schmid, H.; Michel, B. *Macromolecules* **2000**, 33, 3042.

7 a) Csucs, G.; Künzler, T.; Feldman, K.; Robin, F.; Spencer, N. D. *Langmuir* **2003**, 19, 6104; b) Trimbach, D. C.; Feldman, K.; Spencer, N. D.; Broer, D. J.; Bastiaansen, C. W. M. *Langmuir* **2003**, 19, 10957.

8 Sharpe, R. B. A.; Burdinski, D.; Huskens, J.; Zandvliet, H. J. W.; Reinhoudt, D. N.; Poelsema, B. *J. Am. Chem. Soc.* **2005,** 127, 10344.

9 Li, X.-M.; Péter, M.; Huskens, J.; Reinhoudt, D. N. *Nano. Lett.* **2003**, 10, 1449.

10 Liebau, M.; Huskens, J.; Reinhoudt, D. N. *Adv. Funct. Mater.* **2001**, 11, 147.

11 Delamarche, E.; Geissler, M.; Wolf, H.; Michel, B. *J. Am. Chem. Soc.* **2002**, *124*, 3834.

12 Saalmink, M.; van der Marel, C.; Stapert, H. R.; Burdinski, D. *Langmuir* **2006**, 22, 1016.

13 a) Trimbach, D. C.; Al-Hussein, M.; de Jeu, W. H.; Decré, M.; Broer, D. J.; Bastiaansen, C. W. M. *Langmuir* **2004**, 20, 4738; b) Lee, M. –S.; Hong, S. –C.: Kim, D. *Jpn. J. Appl. Phys.* **2004**, 43, 8347.

14 Kriesel, J. W.; Tilley, T. D. *Chem. Mater.* **1999**, 11, 1190.

15 Tokuhisa, H.; Zhao, M.; Baker, L. A.; Phan, V. T.; Dermody, D. L.; Garcia, M. E.; Peez, R. F.; Crooks, R. M.; Mayer, T. M. *J. Am. Chem. Soc.* **1998**, 120, 4492.

16 Li, H.; Kang, D. J.; Blamire, M. G.; Huck, W. T. S. *Nano Lett.* **2002,** 4, 347.

17   Liebau, M.; Janssen, H. M.; Inoue, K.; Shinkai, S.; Huskens, J.; Sijbesma, R. P.; Meijer, E. W.; Reinhoudt, D. N. *Langmuir* **2002**, *18,* 674.

18   Porter, M. D.; Bright, T. B.; Allara, D. L.; Chidsey, C. E. D. *J. Am. Chem. Soc.* **1987**, 109, 3559.

19   Bain, C. D.; Troughton, E. B.; Tao, Y.-T.; Evall, J.; Whitesides, G. M.; Nuzzo, R. G. *J. Am. Chem. Soc.* **1989**, 111, 321.

20   Graham, D. J.; Price, D. D.; Ratner, B. D. *Langmuir* **2002**, 18, 1518.

21   Langowski, B. A.; Uhrich, K. E. *Langmuir* **2005,** 21, 6366.

22   Bruinink, C. M.: Péter, M.; de Boer, M.; Kuipers, L.; Huskens, J.; Reinhoudt, D. N. *Adv. Mater.* **2004**, 16, 1086.

Supramolecular microcontact printing with receptor-functionalized PDMS stamps

Poly(dimethylsiloxane) (PDMS) stamps have been functionalized with β-cyclodextrin (β-CD) receptors to achieve control over inking and transfer of specific molecules by supramolecular microcontact printing (SµCP). Through molecular recognition the surface-confined β-CD host cavities picked up and transferred monovalent adamantyl ink molecules (lissamine-Ad) from solutions containing other, nonbinding molecules with a selectivity of at least 4000. The adsorption of inks from a mixture of mono- and divalent guests was dominated by the divalent molecules owing to their higher binding strength. A host-functionalized silicon dioxide surface covered with host-guest-bound ink monolayer was used as a supramolecular inkpad to ink a β-CD-functionalized stamp, which offered an increased control over the amount of applied ink molecules.

4.1 Introduction

Microcontact printing (μCP) allows the creation of patterned self-assembled monolayers (SAMs) on solid surfaces with arbitrary pattern design.[1] It is an easy and versatile patterning technique which uses an inked elastomeric stamp to transfer a pattern onto a surface by conformal contact between the stamp and the substrate. Ink molecules migrate to the stamp-substrate interface during contact and form the patterned SAM.[2] Originally, μCP was used to create etch-resistant SAM patterns on various substrates in order to replicate the stamp design in a metal by etching. The original μCP technique lacks the possibility to selectively capture and transfer an ink from a mixture and to efficiently avoid over-inking. Creation of surface-confined chemical templates requires a more accurate control over the amount of the transferred molecules.

Supramolecular interactions are reversible and are based on highly specific molecular recognition.[3] The combination of μCP with supramolecular interactions has led to an improved control over the selective and coverage-controlled transfer of stable patterns. Delamarche and coworkers have used the specific binding between biomolecules from complex biological samples and receptor sites on a stamp to perform affinity μCP.[4,5] They selectively extracted proteins from mixtures, and then transferred the patterned protein assemblies onto glass substrates. Similarly, single-strand DNA was immobilized on a stamp and subsequently interacted with chemically functionalized complementary DNA to achieve specific inking.[6-10] The chemical motifs on the complementary DNA strands reacted with the substrate in the printing step. Heating[8-10] or mechanical force[6,7] facilitated DNA dehybridization, which resulted in a complementary copy of the master pattern on the substrate after stamp removal.

For some years, our group has been exploiting supramolecular interactions in printing molecules onto surfaces. Molecular printboards, which are SAMs functionalized with β-cyclodextrin (β-CD) cavities as receptor groups, have been used in μCP-directed assembly of various guest molecules.[11] Stable and densely packed β-CD-based molecular printboards have been prepared on both gold[12-14] and silicon[15] surfaces.

When multiple host or guest sites are present in a molecule or assembly, multivalency governs and strengthens the involved supramolecular interactions on surfaces.[11,16] Molecules containing one or multiple guest moieties have been successfully printed onto β-CD printboards.[13,14,17-20] The inking of the stamps was achieved through

traditional wet-inking, without specific interactions between the stamp and guest moiety-containing ink molecules. Stable patterns of fluorescent divalent molecules have been created on β-CD printboards which could be removed only by rinsing with a competing aqueous β-CD solution.[19]

In this chapter, the possibilities to selectively recognize ink molecules and to tune the amount of ink molecules transferred by μCP are reported. β-CD-functionalized stamps were used to which target ink molecules can be anchored through specific and directional supramolecular (host-guest) interactions. The influence of specific vs nonspecific interactions and of the valency of the ink on the selectivity of the pick-up and transfer of ink molecules were studied by using ink mixtures. A supramolecular inkpad strategy was developed to improve the control over the inking of the β-CD-functionalized stamps.

4.2 Results and discussion

4.2.1 Preparation of β-CD-functionalized stamps

Elastomeric poly(dimethylsiloxane) (PDMS) covalently functionalized with β-CD was used as the stamp material for supramolecular microcontact printing (SμCP). The β-CD monolayer on the stamp was prepared in three steps. First the stamp surface was functionalized with an amino-terminated layer by plasma polymerization of allylamine (PPAA).[21] Subsequently, the stamp was reacted with p-phenylene diisothiocyanate and amino-functionalized β-CD to give a β-CD monolayer (Scheme 4.1), analogous to the preparation of β-CD printboards on silicon.[15]
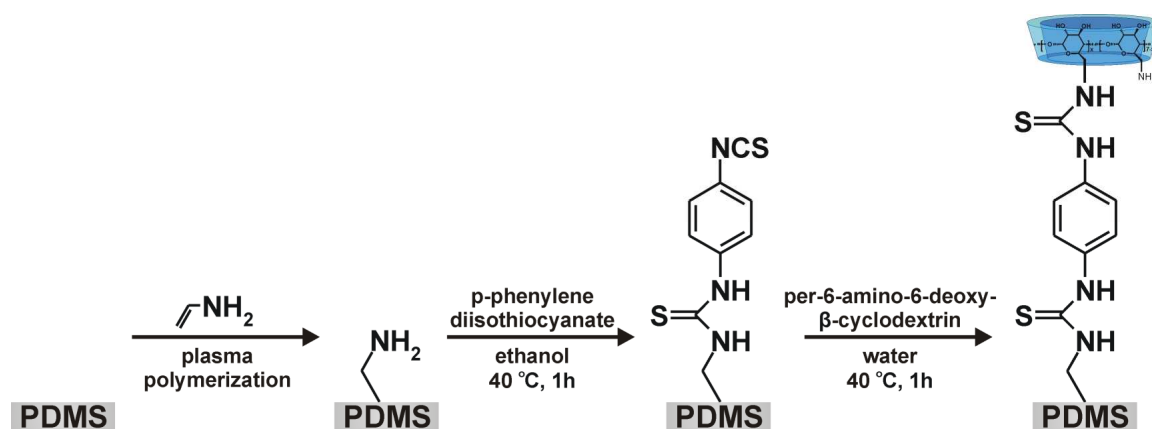
Scheme 4.1 The preparation of β-CD monolayers on PDMS stamp surfaces.

The surface reactions were monitored with a variety of techniques including water contact angle goniometry, ellipsometry and X-ray photoelectron spectroscopy (XPS) (see Table 4.1). A clear change in the polarity of the surface was observed after the isothiocyanate derivatization of the amino layer. The increase of the water contact angle from 53° to 73° is consistent with earlier observations.[15,22] Ellipsometry (performed on isothiocyanate monolayers on silicon) showed no significant thickness increase. Moreover the presence of sulfur detected by XPS as well as an increase of the C/N ratio are both indicative of the formation of an isothiocyanate layer. Due to the interference of the S_{2p} XPS signal with the Si_{2p} signal, the atomic concentration of sulfur (Table 4.1) was calculated based on the S_{2s} signal.

Table 4.1 Advancing water contact angles (θ_a), ellipsometric thicknesses on silicon and selected XPS data of layers on PDMS stamps shown in Scheme 4.1.

terminal functionality	θ_a (°)	ell. thickness (nm)	C/N (XPS)	Atomic conc. (S_{2s}, XPS)
NH_2	53±1	4.8	4.4 ± 0.7	0
SCN	73±1	4.8	9.2 ± 1.8	0.79
β-CD	62±1	5.6	15.1 ± 2.4	0.51

Reaction of the isothiocyanate-terminated layer with amino-functionalized β-CD to give the surface-confined host layer on PDMS was accompanied by an increase in the ellipsometric thickness of ~0.8 nm, which is in good agreement with the dimension of the β-CD molecules.[23] Due to the presence of a several nm thick polyallylamine layer rich in amino groups, XPS showed an increase of the C/N ratio after the introduction of the β-CD SAM to the isothiocyanate layer, while the atomic concentration of sulfur did not change significantly. As experienced with β-CD functionalization on silicon,[15] a decrease of the advancing contact angle was observed.

**4.2.2 Supramolecular printing of fluorescent ink molecules with β-CD-functionalized stamps**

Lissamine-labeled water-soluble molecules equipped with one (lissamine-Ad) or two (lissamine-Ad$_2$) adamantyl (Ad) moieties linked via flexible tetra(ethylene glycol) spacers, native fluorescein and a fluorescein dye bearing two adamantyl moieties

(fluorescein-Ad$_2$) were used as ink molecules to create supramolecular patterns on a β-CD printboard by SμCP using β-CD-functionalized PDMS stamps (Scheme 4.2).
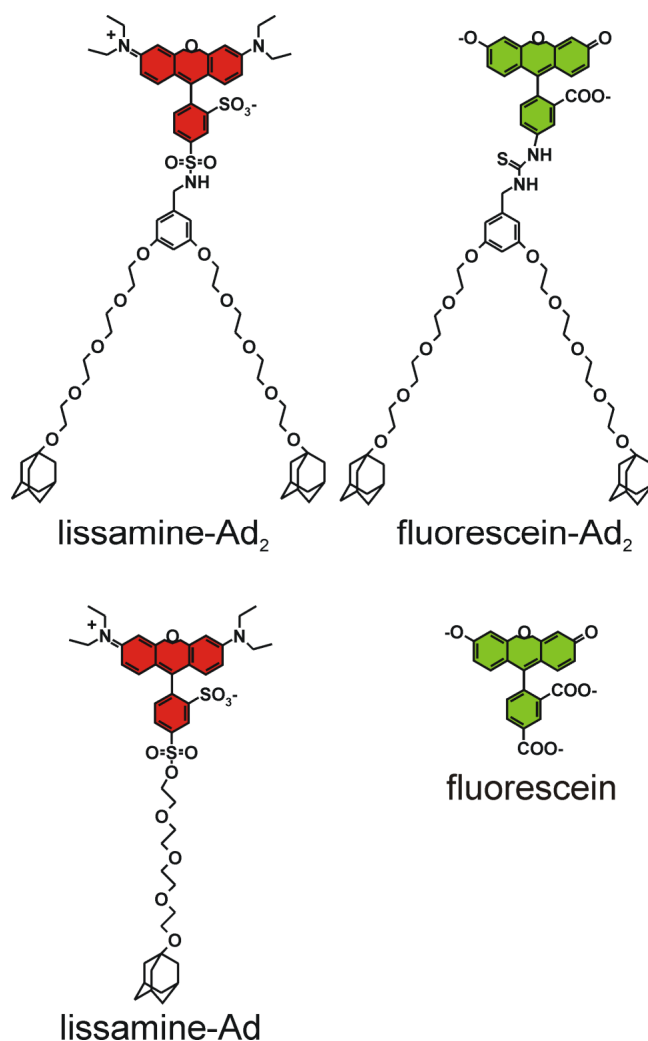
Scheme 4.2 Mono- and divalent adamantyl-functionalized fluorescent guest molecules and a fluorescent dye without any guest moieties used for SμCP with β-CD-functionalized PDMS stamps.

SμCP of multivalent molecules implies an equilibrium-based distribution of ink molecules between the β-CD receptor sites at the stamp and at the substrate in the contact area (Scheme 4.3). The chance to bind to a β-CD site at the stamp or substrate depends on the β-CD coverage on both surfaces and on the effective molarity[16] (EM) of the bound guests. A higher β-CD coverage and a higher EM induce an increased affinity for multivalent (here: divalent) guest molecules. After the equilibration, a uniform guest coverage is expected on both surfaces.
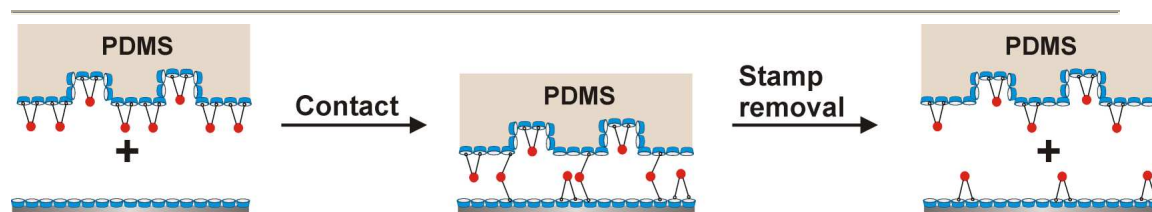
Scheme 4.3 SµCP of divalent guest molecules from a β-CD-functionalized PDMS stamp onto a β-CD SAM-covered substrate.

After wet-inking and rinsing the stamp with clean water, SµCP of lissamine-Ad$_2$ onto the β-CD-based printboard on glass yielded a distinct and homogeneous pattern (Figure 4.1a). The same procedure using a native PDMS stamp treated with oxygen plasma gave only a low fluorescence intensity (Figure 4.1b). In this case the lack of specific interactions between the ink and the stamp apparently caused the removal of the ink molecules from the stamp upon rinsing.
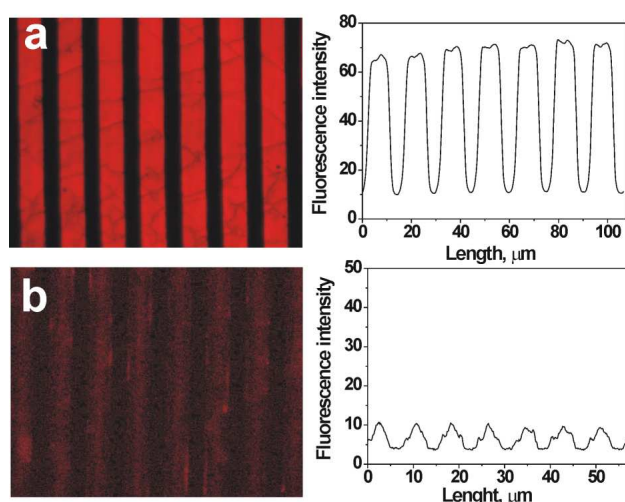
Figure 4.1 Fluorescence microscopy images and intensity profiles of β-CD-functionalized glass substrates after SµCP of lissamine-Ad$_2$ using a β-CD-functionalized PDMS stamp (a) and a native, oxygen treated PDMS stamp (b). Wet-inking was achieved in both cases with a 10 µM aqueous ink solution.

Stamps inked with a 1:1 mixture of lissamine-Ad$_2$ and fluorescein-Ad$_2$ gave fluorescent patterns with 50 % decreased fluorescence intensity for the lissamine rhodamine B-functionalized divalent dye (Figure 4.2a). As to be expected, the affinity of the two dyes for the substrate is the same independently of the β-CD coverage on the stamp and the substrate.
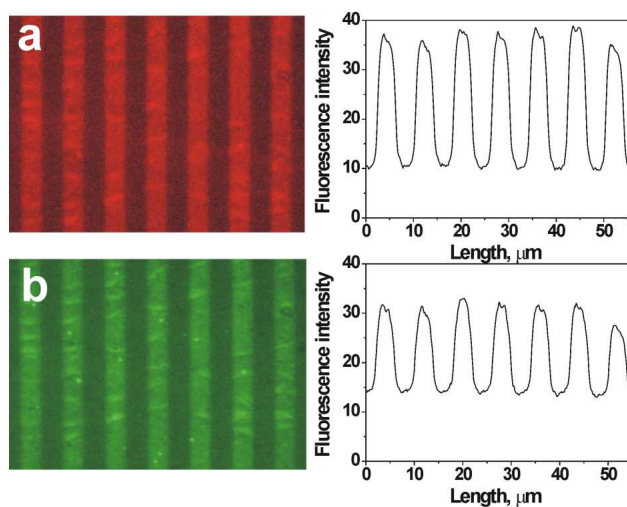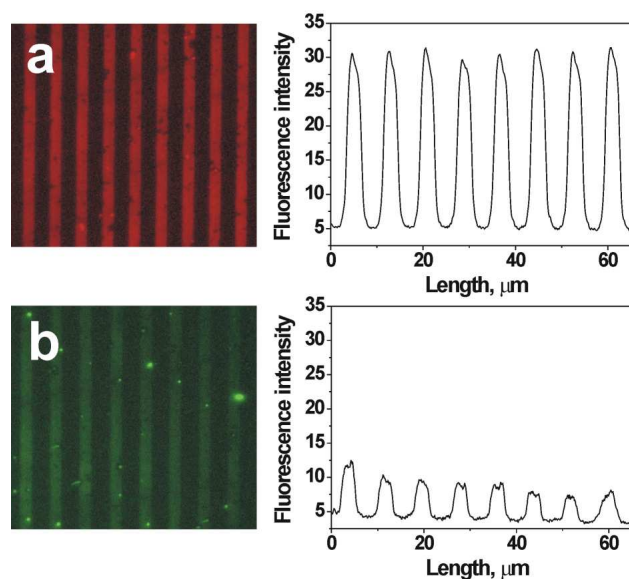
Figure 4.2 Fluorescence microscopy images taken at different emission wavelengths and intensity profiles of β-CD-functionalized glass substrates after SμCP of a 1:1 mixture of lissamine-Ad$_2$ (a) and fluorescein-Ad$_2$ (b). Images were recorded by measuring the red emission light of lissamine-Ad$_2$ and green emission light of fluorescein-Ad$_2$. Wet-inking was achieved with a 10 μM aqueous ink solution.

The effect of the specificity of the supramolecular host-guest interactions on SμCP was investigated by experiments involving ink mixtures of fluorescein and lissamine-Ad$_2$. The printing results presented in Figure 4.3 clearly indicate the high specificity of the host-guest interactions. Even at a 1000-fold excess of fluorescein, SμCP experiments yielded clearly visible red fluorescence patterns owing to the specific inking and subsequent transfer of divalent lissamine-Ad$_2$ (Figure 4.3a). Only traces of green patterns corresponding to the non-specific physisorption of fluorescein were observed (Figure 4.3b). The apparent intensity difference (4-fold higher intensity for lissamine-Ad$_2$), achieved at a 1000-fold excess of the nonspecific ink, suggests a selectivity of at least 4000.
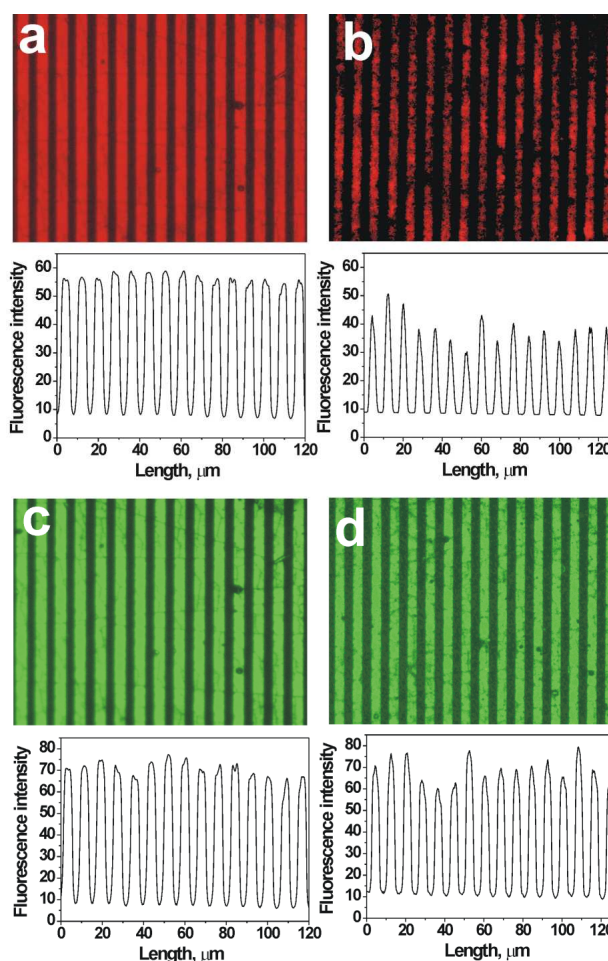
Figure 4.3 Fluorescence microscopy images taken at different emission wavelengths and intensity profiles of β-CD-functionalized glass substrates after SμCP of a mixture of red lissamine-Ad$_2$ (0.9 μM) (a) and green fluorescein (0.9 mM) (b).

SμCP of a 1:1 mixture of lissamine-Ad and fluorescein-Ad$_2$ was carried out to investigate the effect of the valency of the ink on the supramolecular transfer. After wet-inking, the stamps were in this case not rinsed in order not to influence the thermodynamic equilibrium achieved during inking of the stamp. The experiment resulted in the fluorescent patterns presented in Figure 4.4. Since the monovalent lissamine-Ad occupies only one β-CD site while fluorescence-Ad$_2$ occupies two, the relative intensities of Figure 4.4a and Figure 4.4c suggest that directly after printing ~75 % of the occupied β-CD cavities of the substrate are filled by the divalent fluorescein-Ad$_2$ molecules, and only about 25 % by the monovalent lissamine-Ad.

When the coverage of β-CD SAMs on the stamp and the substrate are the same, the transfer from the β-CD-functionalized stamp to the β-CD printboard is independent of the valency of the molecules and is equally possible for both the monovalent and divalent dyes. This means that the printing results reflect the ink ratio achieved on the stamp during inking.

Figure 4.4 Fluorescence microscopy images taken at red and green emission wavelengths and intensity profiles of β-CD-functionalized glass substrates after SμCP of a 1:1 mixture of lissamine-Ad (a before, b after rinsing) and fluorescein-Ad₂ (c before and d after rinsing). Wet-inking was achieved in both cases with a 10 μM aqueous 1:1 mixture of the dyes.

The decrease of the valency of 1-Ad-Lissamine induces a lower binding affinity to the β-CD stamp in the wet-inking step. In such a mixture of mono- and divalent guest molecules the thermodynamic equilibrium favors the adsorption of the guests with higher valency. The binding constant of a single adamantyl unit to a surface-confined β-CD is around $4.6 \times 10^4 \, M^{-1}$, orders of magnitudes lower than the binding strength of a molecule bearing two adamantyl moieties ($\sim 10^8 \, M^{-1}$).[13-15] With such an affinity difference, a better selection and a higher percentage of the divalent guest could have been expected. The lower selectivity observed here can most likely be attributed to physisorption or to a non-equilibrium distribution. As observed above for a mixture of fluorescein and lissamine-Ad₂, rinsing of the stamp after inking will probably improve this selectivity considerably.

Rinsing of the patterned substrate after SµCP with water mostly caused desorption of the monovalent lissamine-Ad from the surface (Figure 4.4b) while the pattern of the divalent fluorescein-Ad$_2$ remained mostly intact (Figure 4.4d). This is clearly the result of the stronger multivalent interaction of the divalent ink.

4.2.3 Supramolecular inkpad strategy to ink β-CD-functionalized stamps

To achieve control over the amount of ink applied for inking of the β-CD-functionalized stamp, contact inking of the stamps was carried out. Contact inking of a stamp for µCP is based on the direct contact between a featured stamp and a flat PDMS substrate impregnated with the ink (inkpad).[24] The technique does not involve any solvent in the actual inking of the stamp, and the stamp is inked only in the contacted areas. β-CD-based printboards were used as inkpads to transfer divalent fluorescent guest molecules onto the β-CD-functionalized stamps (see Scheme 4.4). The β-CD SAM on the hard glass substrate delivers a controlled amount of ink onto the stamp, e.g. a fraction of a monolayer, and thus, potentially, provides a better control over the amount of ink than fully impregnated flat PDMS. The inking of the solid inkpad was achieved by immersion in an ink solution, and the excess and physisorbed ink molecules are easily washed away by a subsequent rinsing step with water or a competitive β-CD solution.[13,14]
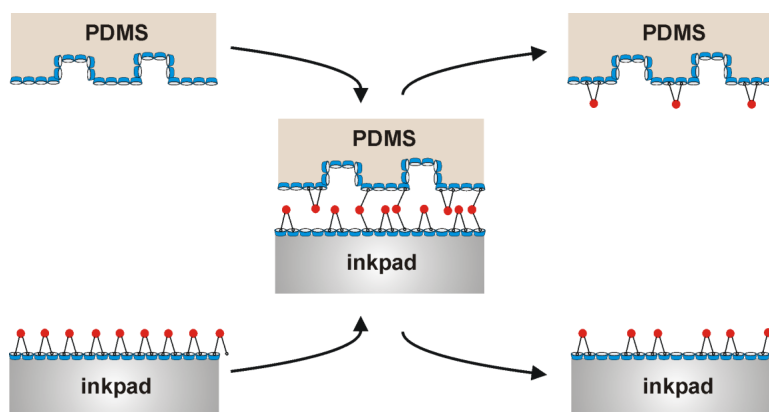
Scheme 4.4 Contact inking with a controlled amount of ink is achieved by contacting the β-CD-modified PDMS stamp with a flat β-CD printboard on glass (inkpad) with a preadsorbed ink monolayer.

SµCP with such an inked stamp resulted in a clearly visible fluorescent pattern (Figure 4.5). In the contact inking step, the β-CD-functionalized stamps efficiently picked up guest molecules from the inkpad according to the equilibrium between the

two receptor surfaces. Upon transfer to a bare β-CD substrate, a second equilibrium distributed the amount of the involved lissamine-Ad$_2$ molecules causing a somewhat lower fluorescence intensity than the one observed with the wet-inking method (Figure 4.1a). The decreased uniformity of the transferred pattern is probably a consequence of the insufficient rinsing of the inkpad after impregnation or an inhomogeneous β-CD coverage on the inkpad, stamp, or substrate. Nevertheless, these results show the feasibility of the inkpad method, and therefore the possibility to control the amount of ink picked up by a stamp by tuning the ink concentration with which the inkpad is inked while relying on the quantitatively known concentration-coverage relationship.
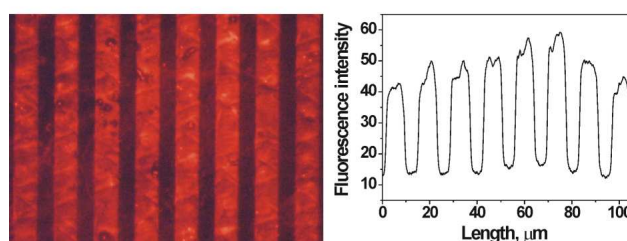
Figure 4.5 Fluorescence microscopy image and intensity profile of a β-CD substrate after SμCP with a β-CD-functionalized stamp inked by the supramolecular inkpad strategy.

4.3 Conclusions

The preparation of β-CD-functionalized PDMS stamps and their successful use in SμCP of specific guest molecules onto β-CD printboards were demonstrated in this chapter. The receptor-covered stamps showed a highly selective recognition ability when guest-functionalized molecules were captured from ink mixtures. Uniform, equilibrium-controlled host-guest ink transfer was achieved upon conformal contact between two β-CD-covered surfaces. A higher valency of the ink favored the adsorption from ink mixtures to the β-CD-functionalized PDMS stamp. A supramolecular inkpad method was introduced, where a solid β-CD printboard, onto which an ink monolayer was preadsorbed specifically, served as an inkpad. Control over the amount of transferred ink molecules can be exerted by tuning the coverage of the ink monolayer on the inkpad.

Selective attachment of compounds to functional surfaces avoiding nonspecific interactions is crucial for the development of (bio)analytical surfaces. SμCP with

receptor-functionalized stamps is a versatile technique which allows reversible patterning of controlled amounts of specific guest molecules.

4.4 Experimental

Materials. Lissamine-Ad$_2$,[19] fluorescein-Ad$_2$,[19] tetraethylene glycol mono-adamantyl ether[19] and per-6-amino-β-cyclodextrin[25] were prepared according to previously published procedures.

Lissamine-Ad. A solution of tetraethylene glycol mono-adamantyl ether (328 mg, 1 mmol) and 2 ml triethylamine in 40 ml acetonitrile was cooled down to 0-5 °C. Then lissamine sulfonyl chloride (866 mg, 1.5 mmol) was added and the mixture was stirred for 3 h. The solvent was evaporated at reduced pressure and the residue was partitioned between diethyl ether (50 ml) and water (30 ml). The organic layer was washed with water (2 × 20 ml) and brine (20 ml). The solvent was removed under reduced pressure and a monovalent guest labeled with lissamine rhodamine dye was obtained as a purple oil (201 mg, 0.231 mmol; 23 % yield). The compound was used without further purification. ^{1}H-NMR (d_6-DMSO, ppm): δ = 8.46 (s, 1H; ArH), 8.14 (d, 2H; ArH), 7.04 (d, 2H; ArH), 6.91 (d, 2H; ArH), 6.71 (s, 2H; ArH), 4.64 (t, 2H; SOCH_2), 3.56-3.36 (m, 14H; OCH_2CH_2O, NCH_2CH$_3$), 2.12 (m, 3H; CH$_2$CHCH$_2$[Ad]), 1.70 (m, 6H; CHCH_2C[Ad]), 1.65-1.55 (m, 6H; CHCH_2CH[Ad]), 1.27 ppm (t, 12H; NCH$_2$CH_3); ^{13}C NMR (d_6-DMSO, ppm): δ = 158.88, 150.04, 135.55, 132.04, 114.97, 110.30, 104.57, 95.37, 89.26, 72.06, 70.04, 60.86, 59.47, 53.58, 41.70, 34.31, 30.55 ppm. MALDI-TOF MS: m/z = 869.1, calcd. for [M+H]$^+$: 868.5.

General procedures. Contact angles were measured on a Krüss G10 contact angle setup equipped with a CCD camera. Advancing and receding contact angles were determined automatically during growth and reduction of a clean water droplet by the droplet shape analysis routine.

XPS measurements were performed on a Quantera Scanning X-ray Multiprobe instrument from Physical Electronics, equipped with a monochromatic Al Kα X-ray source producing approximately 25 W of X-ray power. XPS data were collected from a surface area of 1000 μm × 300 μm with pass energy of 224 eV and step energy of

0.8 eV for survey scans and 0.25 eV for element scans with equal numbers of sweeps for all elements. Spectra were referenced to the main C 1s peak set at 284.0 eV.

^{1}H NMR and ^{13}C NMR spectra were recorded using a Varian Inova 300 spectrometer operating at 300 MHz.

Ellipsometry measurements of the PPAA films were performed on silicon wafers by a Plasmon ellipsometer (λ = 632.8 nm) assuming a refractive index of 1.5 for polymer films and 1.457 for the underlying native oxide. The thickness of the SiO_2 layer was measured separately on an unmodified silicon wafer and subtracted from the total layer thickness determined for the polymer thin film deposited by plasma polymerization. Raster scans were taken at different points of the substrate and their values were averaged.

Fluorescence microscopy was performed using an Olympus inverted research microscope IX71 equipped with a mercury burner U-RFL-T as light source and a digital camera Olympus DP70 (12.5 million-pixel cooled digital color camera) for image acquisition. Green excitation light ($510 \leq \lambda \leq 550$ nm) and red emission light ($\lambda < 590$ nm) was filtered using a U-MWG Olympus filter cube. Blue excitation light ($450 \leq \lambda \leq 480$ nm) and green emission light ($\lambda < 515$ nm) was filtered using a U-MWB Olympus filter cube.

PDMS stamp preparation. Silicon masters with micrometer-sized features were fabricated by photolithography. PDMS stamps were prepared from commercially available Sylgard-184 poly(dimethyl siloxane) (Dow Corning). The curing agent and the prepolymer were manually mixed in 1:10 volume ratio and cured overnight at 60 ^{o}C against the master. The cured stamp was peeled off from the master at the curing temperature.

Monolayer preparation on glass and PDMS surfaces. β-CD-functionalized glass substrates (β-CD printboards) were fabricated as described previously.[15]

Surface coating of PDMS stamps through plasma polymerization of allylamine[21] was achieved using a CCR plasma coating system (Rheinbreitbach, Germany) by Ssens BV (Hengelo, The Netherlands). After cleaning of the deposition chamber with an air plasma (30 min, 300 W), the samples were positioned on the base plate, all at the same distance from the center of the reactor. After deposition of allylamine (1 min, 300 W), the chamber was brought to atmospheric pressure with argon and the samples

were transferred to their storage container, sealed in an aluminum foil pouch under a nitrogen atmosphere at reduced (30 %) pressure and stored at -20 °C.

Transformation of the amino-terminated layer to an isothiocyanate-bearing layer was accomplished by exposure to a 0.1 M solution of 1,4-phenylene diisothiocyanate in ethanol at 40 °C for 1 h, followed by rinsing with copious amounts of ethanol and drying in a stream of nitrogen. The surface-confined β-CD layer was obtained by immersion of the isothiocyanate-covered PDMS samples in 5 mM aqueous solution of per-6-amino-β-cyclodextrin at 40 °C for 1 h. After reaction the samples were sonicated in Millipore water for 5 min and rinsed with additional water to remove physisorbed material and dried in a stream of nitrogen. The prepared β-CD-functionalized PDMS stamps were stored at -20 °C in order to obtain long-term stability.

SμCP with β-CD-functionalized PDMS stamps. Wet inking of the stamps was achieved in all cases by immersion of the stamp in a 10 μM ink solution. After inking, the stamps were rinsed with Millipore water and dried in a stream of nitrogen. Exception was the printing of the mono- and divalent ink mixture, when the stamp was directly dried after inking without any additional rinsing.

Contact inking using an inkpad was achieved as follows. The inkpad, a fresh β-CD-functionalized glass substrate, was immersed in a 10 μM aqueous ink solution for 5 min. Thereafter, the inkpad was rinsed with copious amounts of water and dried in a stream of nitrogen. A fresh β-CD-functionalized PDMS stamp was placed on the inkpad and conformal contact was achieved for 1 min. A vessel with boiling water was kept nearby the experiment to keep the humidity at an elevated level in order to facilitate the formation of the host-guest interactions.

After inking of the stamp by either method, conformal contact between the stamp and the substrate was achieved manually by placing carefully the stamp on the substrate and aiding the formation of the uniform contact by slight manual pressure on the stamp. In all cases the contact time was 1 min.

4.5 References

1   A. Kumar, G. M. Whitesides, *Appl. Phys. Lett.* **1993**, *63*, 2002.

2   E. Delamarche, H. Schmid, A. Bietsch, N. B. Larsen, H. Rothuizen, B. Michel, H. Biebuyck, *J. Phys. Chem. B* **1998**, *102*, 3324.

3   D. N. Reinhoudt, M. Crego-Calama, *Science* **2002**, *295*, 2403.

4   A. Bernard, D. Fitzli, P. Sonderegger, E. Delamarche, B. Michel, H. R. Bosshard, H. Biebuyck, *Nat. Biotechnol.* **2001**, *19*, 866.

5   J. P. Renault, A. Bernard, D. Juncker, B. Michel, H. R. Bosshard, E. Delamarche, *Angew. Chem., Int. Ed. Engl.* **2002**, *41*, 2320.

6   H. H. Lin, J. Kim, L. Sun, R. M. Crooks, *J. Am. Chem. Soc.* **2006**, *128*, 3268.

7   H. H. Lin, L. Sun, R. M. Crooks, *J. Am. Chem. Soc.* **2005**, *127*, 11210.

8   A. A. Yu, T. Savas, S. Cabrini, E. diFabrizio, H. I. Smith, F. Stellacci, *J. Am. Chem. Soc.* **2005**, *127*, 16774.

9   A. A. Yu, T. A. Savas, G. S. Taylor, A. Guiseppe-Elie, H. I. Smith, F. Stellacci, *Nano Lett.* **2005**, *5*, 1061.

10   A. A. Yu, F. Stellacci, *J. Mater. Chem.* **2006**, *16*, 2868.

11   M. J. W. Ludden, D. N. Reinhoudt, J. Huskens, *Chem. Soc. Rev.* **2006**, *35*, 1122.

12   M. W. J. Beulen, J. Bügler, M. R. de Jong, B. Lammerink, J. Huskens, H. Schönherr, G. J. Vancso, B. A. Boukamp, H. Wieder, A. Offenhauser, W. Knoll, F. C. J. M. van Veggel, D. N. Reinhoudt, *Chem. Eur. J.* **2000**, *6*, 1176.

13   J. Huskens, A. Mulder, T. Auletta, C. A. Nijhuis, M. J. W. Ludden, D. N. Reinhoudt, *J. Am. Chem. Soc.* **2004**, *126*, 6784.

14   T. Auletta, B. Dordi, A. Mulder, A. Sartori, S. Onclin, C. M. Bruinink, M. Péter, C. A. Nijhuis, H. Beijleveld, H. Schönherr, G. J. Vancso, A. Casnati, R. Ungaro, B. J. Ravoo, J. Huskens, D. N. Reinhoudt, *Angew. Chem., Int. Ed. Engl.* **2004**, *43*, 369.

15   S. Onclin, A. Mulder, J. Huskens, B. J. Ravoo, D. N. Reinhoudt, *Langmuir* **2004**, *20*, 5460.

16   J. Huskens, *Curr. Opin. Chem. Biol.* **2006**, *10*, 537.

17   O. Crespo-Biel, M. Péter, C. M. Bruinink, B. J. Ravoo, D. N. Reinhoudt, J. Huskens, *Chem. Eur. J.* **2005**, *11*, 2426.

18   C. M. Bruinink, C. A. Nijhuis, M. Péter, B. Dordi, O. Crespo-Biel, T. Auletta, A. Mulder, H. Schönherr, G. J. Vancso, J. Huskens, D. N. Reinhoudt, *Chem. Eur. J.* **2005**, *11*, 3988.

19   A. Mulder, S. Onclin, M. Péter, J. P. Hoogenboom, H. Beijleveld, J. ter Maat, M. F. García-Parajó, B. J. Ravoo, J. Huskens, N. F. van Hulst, D. N. Reinhoudt, *Small* **2005**, *1*, 242.

20   S. Onclin, J. Huskens, B. J. Ravoo, D. N. Reinhoudt, *Small* **2005**, *1*, 852.

21   V. B. Sadhu, A. Perl, M. Péter, D. I. Rozkiewicz, G. Engbers, B. J. Ravoo, D. N. Reinhoudt, J. Huskens, *Langmuir* **2007**, *23*, 6850.

22   P. Maury, M. Péter, O. Crespo-Biel, X. Y. Ling, D. N. Reinhoudt, J. Huskens, *Nanotechnology* **2007**, *18*, 044007.

23   M. R. de Jong, J. Huskens, D. N. Reinhoudt, *Chem. Eur. J.* **2001**, *7*, 4164.

24   L. Libioulle, A. Bietsch, H. Schmid, B. Michel, E. Delamarche, *Langmuir* **1999**, *15*, 300.

25   P. R. Ashton, R. Koniger, J. F. Stoddart, D. Alker, V. D. Harding, *J. Org. Chem.* **1996**, *61*, 903.

Spreading of multivalent inks on a molecular printboard

Mono-, di- and trivalent fluorescent guest molecules were microcontact printed on the β-CD-based molecular printboard and the kinetic stability of the patterned SAMs was studied. In the presence of native host sites in the surrounding aqueous solution competition-induced surface spreading of the fluorescent molecules was observed. Line patterns of the monovalent guest showed a spreading rate of 0.9 nm/s in the presence of water and a continuous increase when the native β-CD concentration was increased in the solution. Experiments with the divalent guest indicated a lower spreading rate in water (0.02 nm/s) according to its higher affinity to the surface and a rate maximum at 0.8 mM β-CD in the solution. Patterned SAMs of the trivalent guest showed low spreading rates on the order of 10^{-3} nm/s.

5.1 Introduction

Multivalent noncovalent interactions at interfaces play an important role in many biological phenomena.[1-3] Multivalency controls the adhesion of a virus, bacterium, antibody or a macrophage to the surface of a cell via specific protein-carbohydrate interactions, and binding of transcription factors to multiple sites on DNA.[1] The main advantage of a multivalent interaction for a biological system arises from its enhancement effect on the overall binding strength and specificity. In addition, multivalency on surfaces is a powerful tool for molecular nanostructure fabrication.[4-6] The strength of the binding of multivalent molecules can be accurately tuned by varying the supramolecular chemistry of the host-guest system and by varying the number of noncovalent interactions. The reversible nature of the host-guest interactions offers the possibility of self-correction and tunability by changing the conditions. A surface serving as a multivalent receptor for multivalent ligands permits the supramolecular positioning of reversible self-assembled patterns. Reversible positioning can be superior to commonly used covalent immobilization techniques and it broadens the versatility of any nanofabrication scheme on surfaces. Profound understanding of the governing principles behind surface-confined multivalent interactions is crucial for a successful design and application of such systems in both biological and technological areas.

Several systems were used to obtain quantitative thermodynamic data from multivalent interactions on interfaces,[5,7] however a detailed kinetic analysis is lacking. Whitesides and coworkers, in the only quantitative kinetic study to date, characterized the binding of a trivalent derivative of vancomycin ($Host_3$) to a trivalent peptide ($Ligand_3$) in solution. The dissociation rate of the $Host_3$-$Ligand_3$ aggregate increased in the presence of a monovalent peptide (Ligand), which competed effectively with $Ligand_3$ for host sites of the trivalent derivative of vancomycin.[8,9] Two possible dissociation mechanisms were discussed. The first mechanism involved the complete dissociation of the $Host_3$-$Ligand_3$ aggregate followed by association of free $Host_3$ with three equivalents of Ligand. The rate of this process would be independent of the concentration of Ligand, which was in contrast with the experimental observations. The enhanced dissociation rate of the $Host_3$-$Ligand_3$ aggregate in the presence of Ligand was explained by a sequence of successive dissociation steps of one binding site in the $Host_3$-$Ligand_3$ aggregate and association of the empty binding site with a Ligand.[8,9]

This chapter describes a kinetic study of patterned mono-, di- and trivalent guest molecules on the surface of a β-CD-based molecular printboard. The concept of molecular printboards, which are self-assembled monolayers functionalized with receptor groups, is suited for studying the dynamics of host-guest binding of multivalent guests on liquid-solid interfaces, because the immobilized host SAM allows the variation of environmental conditions, such as competition by a host in solution or change of the polarity of the solution.[6,10] In this work fluorescent guest molecules were printed on the molecular printboard and the evolution of the fluorescent pattern in time was monitored in situ. This was performed at various β-cyclodextrin (β-CD) concentrations in aqueous solution in order to induce competition for the guest sites to interact with host sites at the surface and in solution. Methodology and experimental details are the focus of this chapter together with the presentation of the main results, while a theoretical discussion follows in the next chapter.

5.2 Results and discussion

5.2.1 Design of the system

In order to study the dynamics of multivalent supramolecular interactions on surfaces mono-, di- and trivalent fluorescent guest molecules were microcontact printed on β-CD-based molecular printboards. All guest molecules contained long, flexible tetraethylene glycol spacers to connect the guest moieties with the fluorescent label (see Chart 5.1). These spacers enhanced the solubility of the molecules in water and ensured enough flexibility and spacing between the guest moieties to allow multiple host-guest interactions without steric problems.
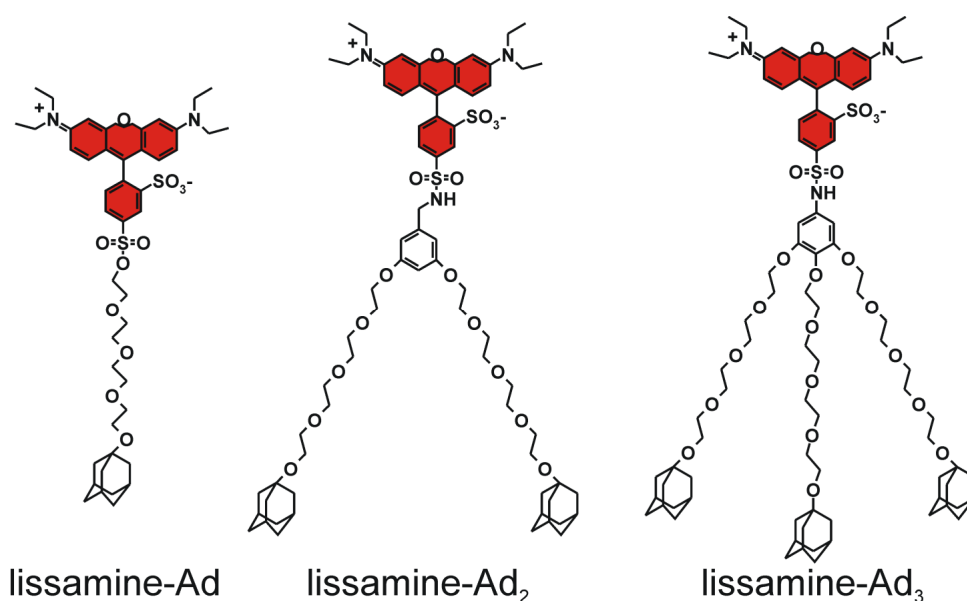
Chart 5.1 Guest molecules used in this study.

Lissamine Rhodamine B fluorescent dyes functionalized with one (lissamine-Ad), two (lissamine-Ad$_2$) and three (lissamine-Ad$_3$) adamantyl moieties were used to study the effect of valency on the kinetics of the surface-confined host-guest binding. µCP was used to pattern SAMs of these molecules on the molecular printboard, where they formed stable supramolecular patterns (Figure 5.1). Printing was achieved with oxygen plasma-treated PDMS stamps soaked in an aqueous solution of a fluorescent dye and dried prior to printing. After printing, the patterned substrates were rinsed with water to remove any physisorbed material. The evolution of the supramolecular patterns in time was monitored at various native β-CD concentrations in solution. These mobile hosts induced competition for the guest sites to interact with host sites at the surface and in solution (Figure 5.1b). Lines of 5 µm with 30 µm period were used in all experiments to facilitate the transformation of the fluorescence images, taken at frequent intervals, to quantitative data. The fluorescence intensity cross-section quantitatively represents the surface concentration of the fluorescent guest molecules. Using the known periodicity of the pattern and the average cross-section taken perpendicular to the direction of the lines, the profile of one average line pattern was generated, a single peak which characterizes the entire image (Figure 5.1d). The maximum peak intensity (I_{max}), the minimum peak intensity (I_{min}) and the peak width at half maximum (w) were used to describe the changes of the supramolecular patterns in time.
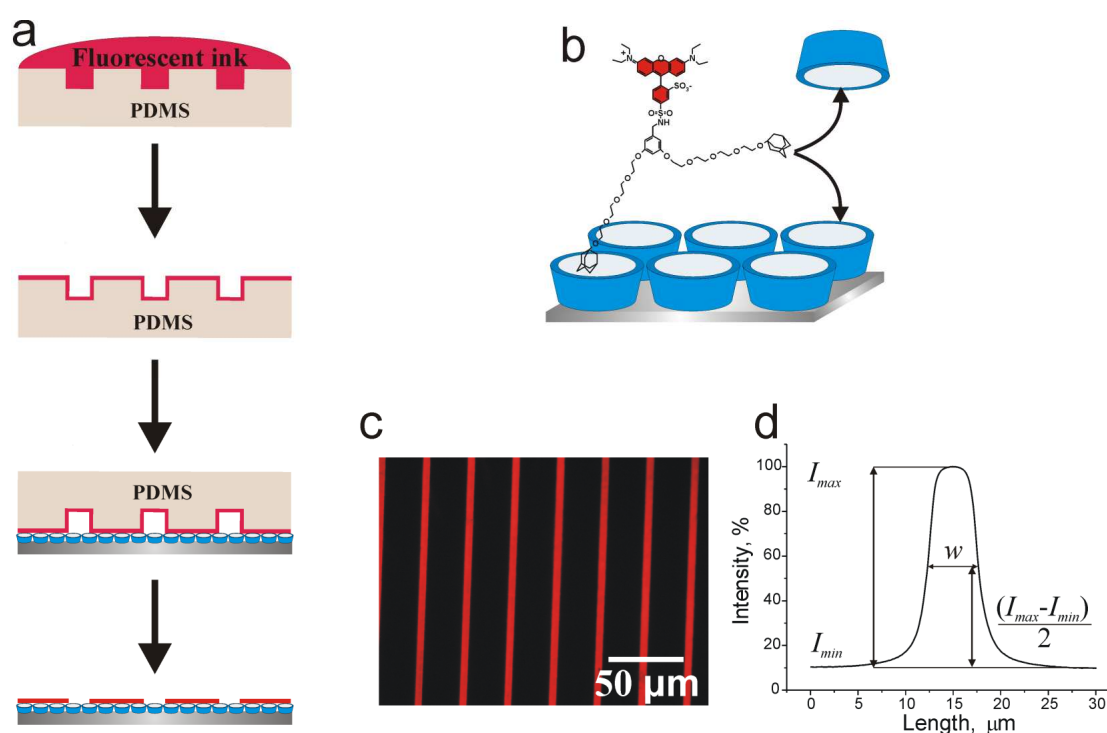
Figure 5.1 (a) Schematic representation of μCP of fluorescent guest molecules onto a β-CD SAM-covered substrate. (b) Native β-CD molecules in the solution induce competition for the guest sites to interact with hosts at the surface and in solution. (c) Fluorescence microscopy image of a β-CD substrate after μCP of lissamine-Ad$_2$. (d) The average surface profile perpendicular to the pattern is transformed into a single peak representing the profile of an average pattern period from the surface.

5.2.2 Coverage gradient-driven surface spreading

It was shown previously that patterns of SAMs of divalent inks on the molecular printboard are stable.[10] In dry conditions no spreading of lissamine-Ad, lissamine-Ad$_2$ or lissamine-Ad$_3$ was observed. However, in the presence of an aqueous solution with or without native β-CD, changes to the fluorescent patterns could be observed.

The lissamine-Ad pattern on the printboard showed a decreasing I_{max} and increasing w when water or native β-CD solution was placed on the patterned substrate (Figure 5.2). The spreading of the monovalent lissamine-Ad was studied in a 0-0.2 mM β-CD concentration range. Due to the relatively low binding strength and the consequently high desorption rate of lissamine-Ad at and from the molecular printboard, the fluorescent lissamine-Ad desorbed completely and instantaneously after adding a ≥ 1 mM β-cyclodextrin solution, making any data acquisition impossible under these conditions.
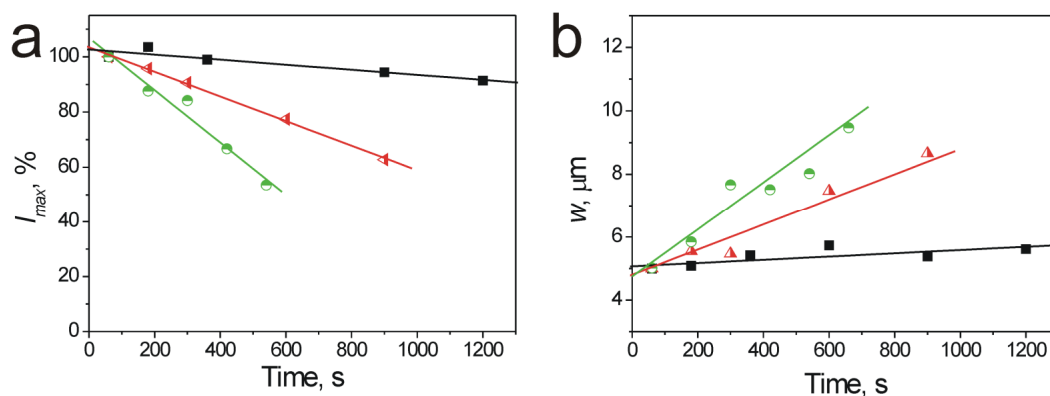
Figure 5.2 Spreading of lissamine-Ad on the molecular printboard: (a) The plot and the linear fit of I_{max} as a function of time; (b) The plot and the linear fit of the peak width at half maximum w as a function of time at different β-CD concentrations: (■) water, (▲) 0.1 mM β-CD and (⬭) 0.2 mM β-CD.

In all cases the plot of w as a function of time showed a linear increase (Figure 5.2b). Therefore the spreading rate of the guest molecules on the molecular printboard (r) was defined as the slope of the width increase in time ($r=\Delta w/\Delta t$), where t represents time.
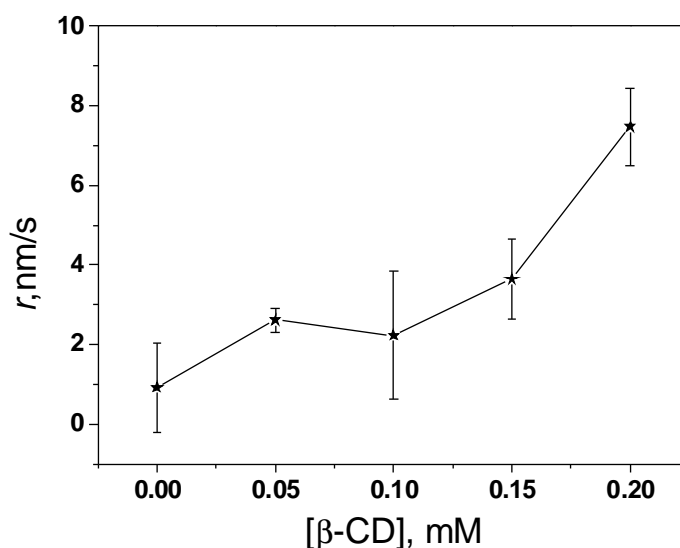
Figure 5.3 Spreading rate of lissamine-Ad on the molecular printboard as a function of the β-CD concentration in the surrounding solution. Error bars show the error of the linear fit of w as a function of time (Figure 5.2b).

The spreading rate of lissamine-Ad showed a continuous increase when the β-CD concentration was increased (Figure 5.3). A spreading rate of 0.9 nm/s was measured in water, going up to about 8 nm/s at 0.2 mM β-CD.

Due to the monovalent nature of lissamine-Ad, spreading is possible in this system only by complete desorption followed by re-adsorption. The desorbed monovalent guest diffuses in the solution, either as the free guest (G^I) or as the host-guest complex formed with a native β-CD from the solution (G^IH_l) (Scheme 5.1), and rebinds to the surface at a different location. The direction of the diffusion is governed by the guest concentration gradient experimentally created between the patterned and empty printboard areas. While G^I can rebind when it meets any available host at the surface, G^IH_l is forced to diffuse in the solution until it dissociates to give G^I again. The higher diffusion time of G^IH_l which is governed by the average lissamine-Ad/β-CD binding time causes longer travelled distances, therefore with an increasing concentration of native β-CD and a concomitantly increased G^IH_l concentration the spreading rate also increases.
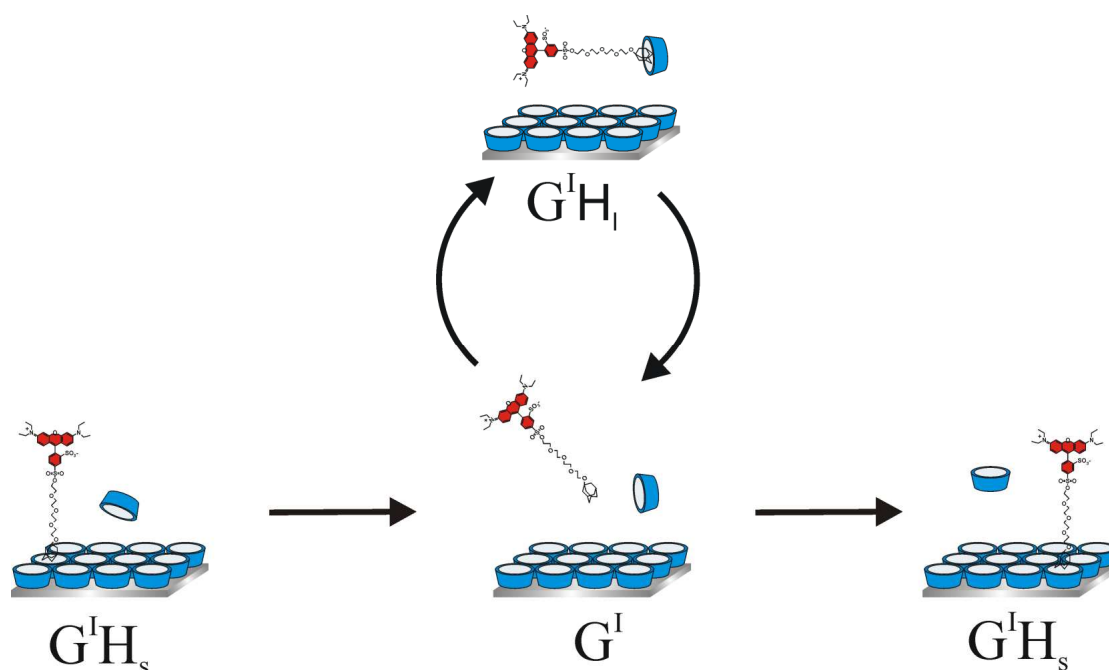
Scheme 5.1 Proposed spreading mechanism of lissamine-Ad on the molecular printboard (G^IH_s = guest bound to a β-CD at the surface; G^IH_l = guest bound to a β-CD from the solution; G^I = unbound guest).

The increased valency of lissamine-Ad$_2$ presents the simplest case of multivalency, a divalent system where both adamantyl moieties bind independently to any available host. The evolution in time of the fluorescent patterns of lissamine-Ad$_2$ on a β-CD-

based molecular printboard at different β-CD concentrations in solution is presented in Figure 5.4 together with the corresponding average line profiles.
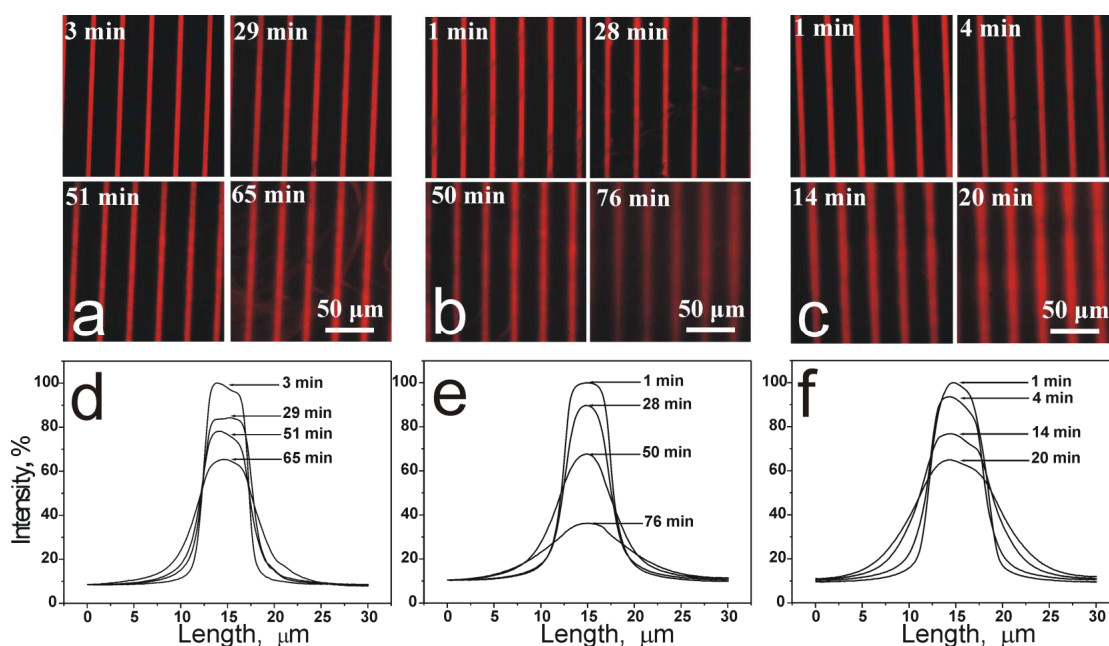

Figure 5.4 Spreading of lissamine-Ad$_2$ on the molecular printboard: fluorescence micrographs and the average line profiles when the guest-printed substrates were immersed in 0.6 mM (a and d), 2 mM (b and e) and 4 mM (c and f) β-CD solutions.

At all β-CD concentrations a decrease of I_{max} and an increase of w were observed (Figure 5.5). The maximum peak intensity decreased faster when the β-CD concentration was increased. The decrease of I_{max} was caused both by spreading on the surface and by complete desorption of lissamine-Ad$_2$ from the β-CD SAM followed by diffusion into the bulk of the surrounding solution. Similarly to the observed trend in the monovalent system, a linear increase in time of w was observed in all cases as a result of the spreading of lissamine-Ad$_2$ on the surface of the molecular printboard. However, the slope of this linear increase, defined as the spreading rates, did not increase continuously with the β-CD concentration in the solution, as is shown in Figure 5.6. In pure water the spreading rate of lissamine-Ad$_2$ was close to zero (0.02 nm/s). When the β-CD concentration was increased, a maximum in the spreading rate (~1.3 nm/s) was observed at 0.8 mM β-CD concentration. This complex and unexpected trend (Figure 5.6) suggests the occurrence of multiple spreading mechanisms.
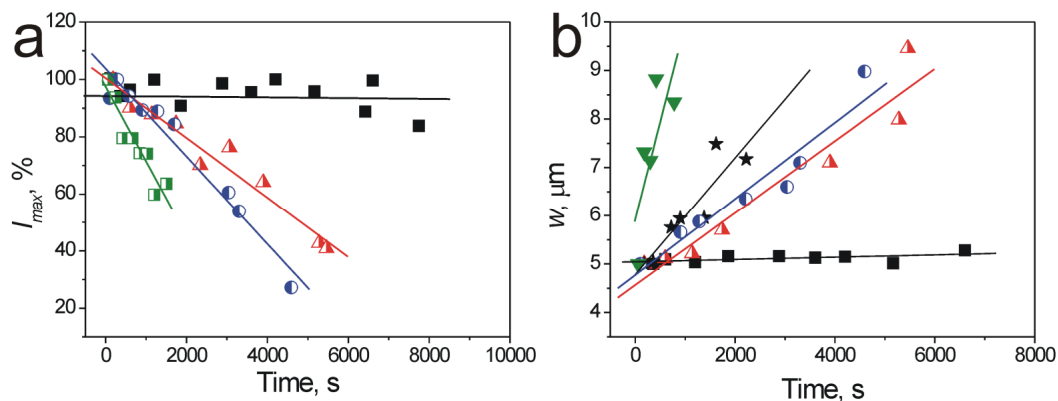
Figure 5.5 Spreading of lissamine-Ad$_2$ on the molecular printboard: (a) The plot and the linear fit of I_{max} as a function of time; (b) The plot and the linear fit of the peak width at half maximum w as function of time at different β-CD concentrations: (■) water, (▲) 0.6 mM β-CD, (★) 0.8 mM β-CD, (◑) 2 mM β-CD, (▨) 4 mM β-CD and (▼) 7 mM β-CD.
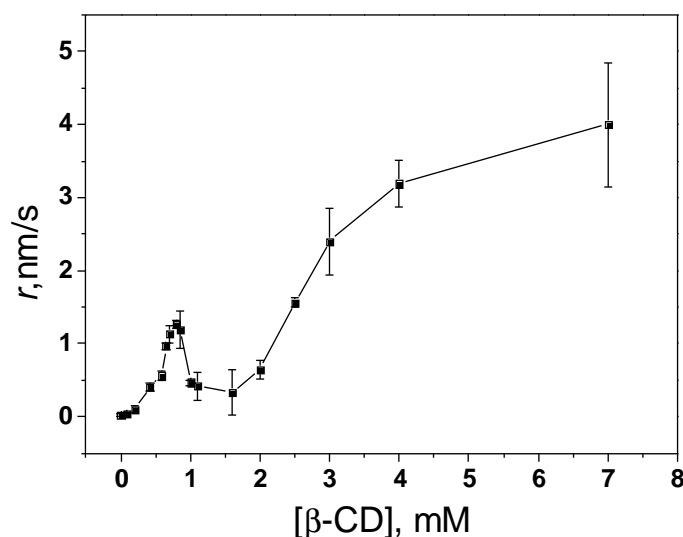

Figure 5.6 Spreading rate of lissamine-Ad$_2$ on the molecular printboard as a function of the β-CD concentration in the surrounding solution. Error bars show the error of the linear fit of w as a function of time (Figure 5.5b).

Three plausible mechanisms can control the spreading of the divalent guest (Scheme 5.2). In water, when no competitive β-CD is present in the solution, a 'walking' mechanism (Scheme 5.2a) governs the spreading. While the complete desorption is negligible, the high effective concentration[11] difference at the boundary of the printed SAM of lissamine-Ad$_2$ and the guest-free molecular printboard in the non-contacted

areas provides a significant driving force for the unbound adamantyl moieties to bind to new, free, surface-confined β-CD cavities.
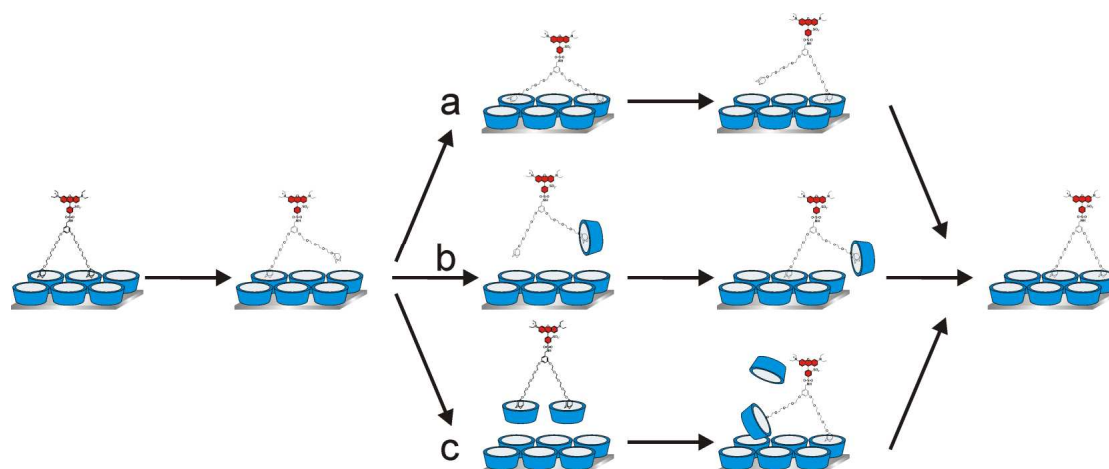
Scheme 5.2 Proposed spreading mechanisms of lissamine-Ad$_2$ on the molecular printboard (not all elementary steps shown), based on 'walking' (a), 'hopping' (b), and complete dissociation, diffusion and re-adsorption (c).

In the presence of β-CD molecules in the solution the walking events become less frequent due to the binding of the free guest moieties to the competitive β-CD cavities from the solution. The high spreading rate of lissamine-Ad$_2$ coupled with a low desorption rate observed at relatively low β-CD concentrations suggests a 'hopping' mechanism (Scheme 5.2b), where after a dissociation of one adamantyl moiety binding occurs immediately with an empty host from the solution. After the dissociation from the surface of the second adamantyl group, due to the low number of the available β-CD hosts from the solution no binding event happens. The monovalently bound complex diffuses in the solution and binds to the first available host from the surface. It stays close to the surface because its lifetime is very short owing to the unbound nature of the second adamantyl group (see Chapter 6). Spreading in low β-CD concentrations up to 1.5 mM is governed by 'hopping' mechanism. When the aqueous β-CD concentration is increased, the desorption rate of lissamine-Ad$_2$ and the formation of the divalent complex ($G^{II}(H_l)_2$, Chapter 6) in the solution is enhanced. This species (molecular mass 3569, $D \approx 10^{-10}$ m^2/s) diffuses into the bulk with an average rate of 20 µm/s. The complete desorption and re-adsorption mechanism (Scheme 5.2c) becomes rate determining (from 1.5 mM up to the measured β-CD concentrations), where the spreading rate intensely increases (Figure 5.6). The guest molecules are continuously desorbing from the patterned areas

creating a high local solution concentration of the divalent complex close to the printboard surface. The increased guest concentration above the guest-free molecular printboard in the non-contacted areas facilitates the rebinding of lissamine-Ad_2 to the molecular printboard.

Similar experiments were carried out using the trivalent lissamine-Ad_3 as the ink. A trivalent guest binds with a significantly higher overall binding strength to the β-CD printboard than the divalent one. According to this increased affinity to the host surface, I_{max} of the patterned lissamine-Ad_3 SAM remained constant even at higher concentrations of native β-CD in the solution (Figure 5.7). A measurable increase in time of w was only observed at a native β-CD concentrations between 1 and 2 mM.
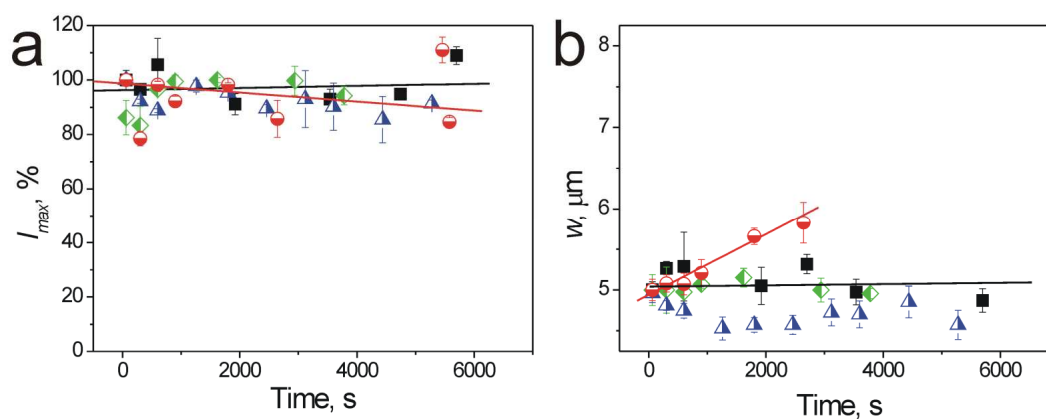
Figure 5.7 Spreading of lissamine-Ad_3 on the molecular printboard: (a) The plot and the linear fit of I_{max} as a function of time; (b) The plot of the peak width at half maximum w as a function of time at different β-CD concentrations: (■) water, (⬤) 1.25 mM β-CD, (◆) 9 mM β-CD and. (▲) 12 mM β-CD.

The spreading rate in water showed the lowest measured values of all studied systems. The spreading rate in water was only on the order of 10^{-3} nm/s. A moderate maximum of the spreading rate was observed between 1 and 2 mM aqueous β-CD concentrations (Figure 5.8). Unlike the divalent guest, in the case of lissamine-Ad_3 no rate increase was observed at higher β-CD concentrations, indicating the absence of desorption.
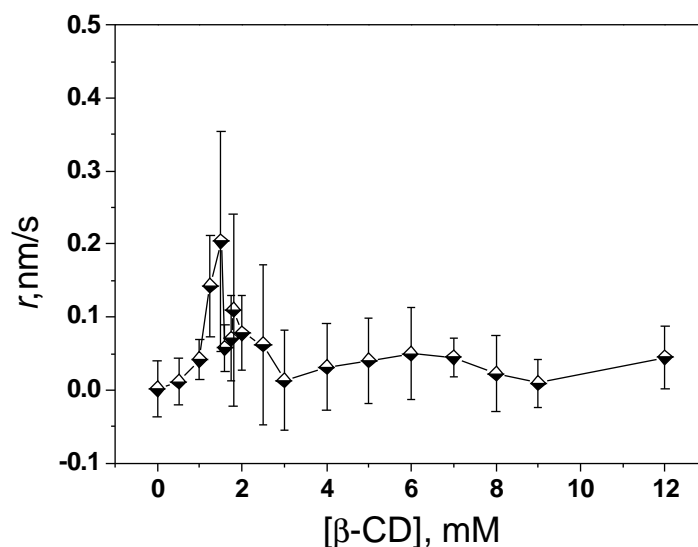
Figure 5.8 Spreading rate of the fluorescent dye lissamine-Ad_3 on the molecular printboard as a function of the β-CD concentration in the surrounding solution. Error bars show the error of the linear fit of *w* as a function of time.

Similar to the divalent system, spreading of lissamine-Ad_3 is potentially controlled by three main spreading mechanisms. In pure water, 'walking' occurs involving guest molecules bound to the surface with one or two adamantyl moieties. At low β-CD concentrations the 'hopping' of the guests bound to two β-CDs from the solution is mainly responsible for spreading. At higher β-CD concentration lissamine-Ad_3 molecules bound to three equivalent hosts from the solution are present and possibly contribute to the surface spreading. Although all spreading mechanisms can occur in the trivalent system, only 'hopping' is observed. Due to the high affinity of the trivalent guest to the printboard surface, no significant change in *r* was observed at higher β-CD concentrations, where the spreading rate showed similar values to the one measured in pure water. The low solubility of native β-CD in water prevented further spreading rate measurements at higher concentrations.

5.3 Conclusions

In this chapter the kinetic stability of patterned SAMs of mono-, di- and trivalent fluorescent guests on the β-CD-based molecular printboard is described. A surface spreading of the fluorescent SAMs in the presence of native β-CD in the surrounding solution was observed. Increasing the host concentration in solution induced a

continuous increase of the spreading rate of patterned SAMs of the monovalent guest. The divalent system exhibited a local spreading rate maximum followed by a renewed increase in the studied β-CD concentration range. The high binding strength of the trivalent guest to the surface reduces the surface spreading and only a moderate spreading rate maximum was observed, in this case followed by a region with negligible spreading. Qualitatively, these results indicate that the following mechanisms occur: (i) Monovalent guests spread in both pure water and β-CD solutions by complete desorption followed by re-adsorption; (ii) divalent molecules spread by 'walking' in pure water, by a 'hopping' mechanism in the 0-1.5 mM β-CD concentration range and by complete desorption and re-adsorption at higher β-CD concentrations; (iii) trivalent molecules follow spreading mechanisms similar to the divalent system generally with significantly lower spreading rates.

5.4 Experimental

Synthesis of the fluorescent dyes. All moisture-sensitive reactions were carried out under an argon atmosphere. All solvents and reagents were obtained from commercial sources and used without further purification. Solvents were dried according to standard procedures and stored over molecular sieves. The synthesis of lissamine-Ad is presented in Chapter 4. Lissamine-Ad$_2$ was synthesized according to literature procedures.[10] Lissamine-Ad$_3$ was synthesized by Henk Dam (Scheme 5.3). Compound **4**[10] was synthesized according to literature procedures. ^{1}H NMR chemical shift values (300 MHz) are reported as δ using the residual solvent signal as an internal standard (CDCl$_3$, δ 7.257). ^{13}C NMR chemical shift values (100 MHz) are reported as δ using the residual solvent signal as an internal standard (CDCl$_3$, δ 77.0).

1,2,3-tris[2-(2-{2-[2-(adamantan-1-yloxy)ethoxy]ethoxy}ethoxy)-ethoxy]benzene (6). A suspension of pyrogallol (3.00 g, 8.64 mmol), **4** (0.363 g, 2.88 mmol) and K$_2$CO$_3$ (1.20 g, 8.64 mmol) was refluxed in 30 ml acetone for 24h. After the volatiles were removed under vacuum and the crude product was extracted from the residue with 40 ml of Et$_2$O, the Et$_2$O layer was washed with H$_2$O (3 × 30 ml) and dried with MgSO$_4$. Evaporation of the volatiles gave **6** as a slightly colored oil (2.5 g, 82%) which was pure enough to be used in the subsequent reactions. ^{1}H NMR (ppm): δ = 6.91 (1 H, t, *J* 8.4, PhH), 6.58 (2 H, d, *J* 8.4, PhH), 4.23 (2 H, t, *J* 4.2, PhOC*H$_2$*CH$_2$-),

4.19-4.10 (4 H, m, PhOCH_2CH_2-), 2.13 (9 H, s, CH_2CHCH_2[Ad]), 1.74 (18 H, s, CHCH_2C[Ad]), 1.65-1.55 (18 H, t, CHCH_2CH[Ad]). ^{13}C NMR (ppm): δ = 152.8, 138.5, 123.5, 107.9, 72.3, 71.2-68.7, 59.2, 41.4, 36.4, 30.4. ESP-MS m/z = 1079.5 [M+Na]$^+$, calcd. 1079.7. MALDI-TOF-MS *m/z* = 1079.2 [M+Na]$^+$, calcd. 1079.7.
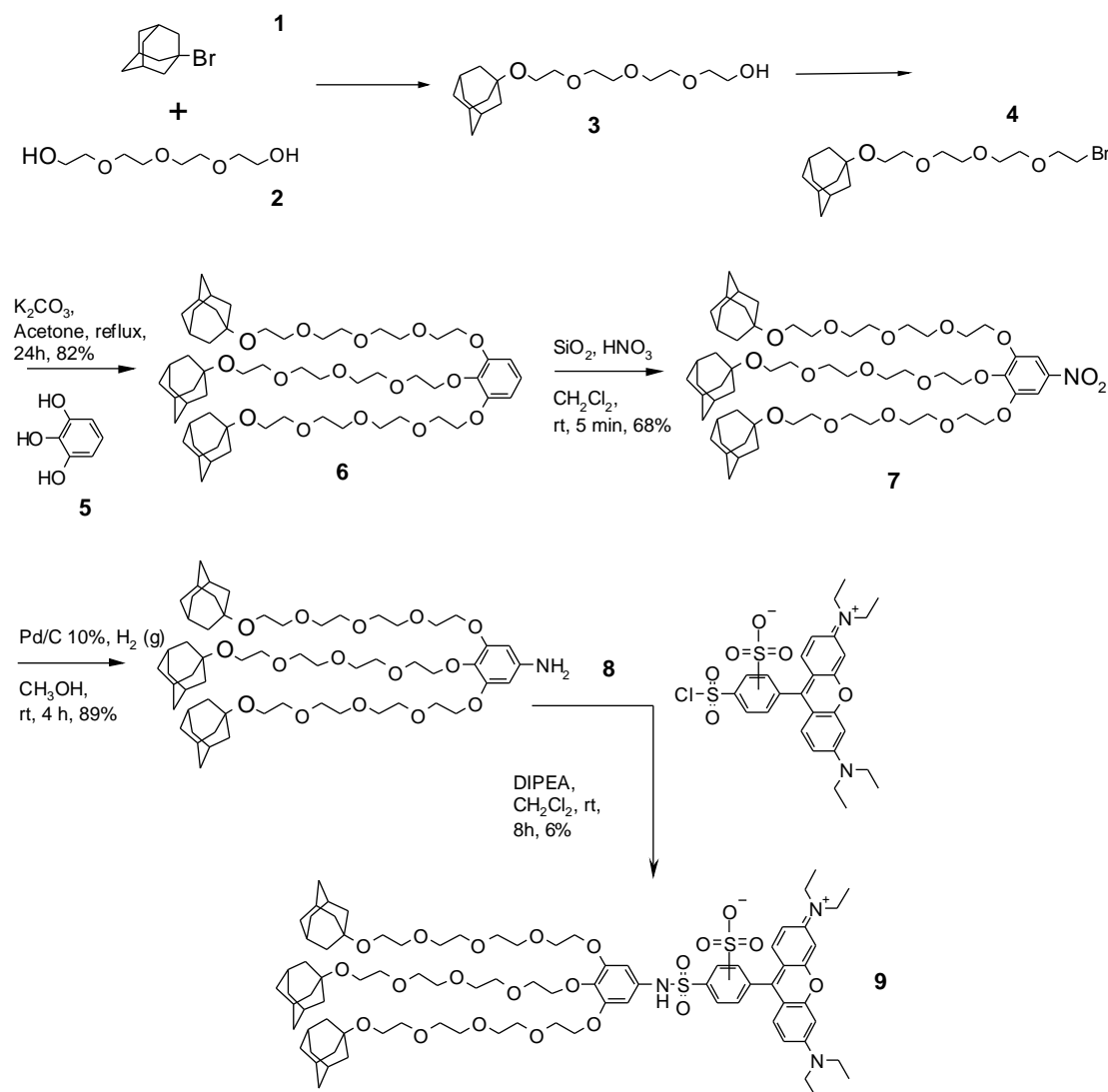
Scheme 5.3 The schematic representation of the synthetis of lissamine-Ad$_3$.

3,4,5-tris[2-(2-{2-[2-(adamantan-1-yloxy)ethoxy]ethoxy}ethoxy)-ethoxy]phenylnitrate (7). A solution of **6** (0.400 g, 0.38 mmol) in 3 ml CH$_2$Cl$_2$ was added at once to a well stirred suspension of 0.400 g of SiO$_2$ and HNO$_3$ (0.08 ml, 1.89 mmol) in 1 ml CH$_2$Cl$_2$. The resulting suspension was stirred for 5 min up on which it was quenched with 3 ml saturated K$_2$CO$_3$. The solids were filtered off and the filtrate was diluted with 10 ml CH$_2$Cl$_2$. The organic layer was washed with H$_2$O (3 × 10 ml)

and dried with MgSO$_4$. Evaporation of the volatiles gave **7** as an oil which was subjected to column chromatography (eluent CH$_2$Cl$_2$/MeOH, 9/1) yielding **7** (0.284 g, 68%) as a colorless oil. ^{1}H NMR (ppm): δ = 7.54 (2 H, s, PhH), 4.27 (2 H, t, *J* 5.1, PhOC*H*$_2$CH$_2$-), 4.22 (4 H, t, *J* 4.8, PhOC*H*$_2$CH$_2$), 3.88 (4 H, t, *J* 4.2, PhOCH$_2$C*H*$_2$), 3.79 (2 H, t, *J* 2.4, PhOCH$_2$C*H*$_2$), 3.72-3.58 (36 H, m, -OC*H*$_2$C*H*$_2$O-), 2,13 (9 H, s, CH$_2$C*H*CH$_2$[Ad]), 1.73 (18 H, s, CHC*H*$_2$C[Ad]), 1.66-1.55 (18 H, m, CHC*H*$_2$CH[Ad]). ^{13}C NMR (ppm): δ = 152.4, 144.3, 143.2, 103.4, 72.9-69.3, 59.6-59.2, 41.6, 36.6, 30.6. ESP-MS m/z = 1102.5 [M]$^+$, calcd. 1102.4. MALDI-TOF MS *m/z* = 1124.6 [M+Na]$^+$, calcd. 1125.4.

3,4,5-tris[2-(2-{2-[2-(adamantan-1-yloxy)ethoxy]ethoxy}ethoxy)-ethoxy]phenylamine (8). A suspension of **7** (0.220 g, 0.20 mmol) and a catalytical amount of Pd/C (10%) was stirred under 1 bar H$_2$(g) atmosphere in 3 ml methanol for 4 h. The suspension was filtered over celite and the volatiles were evaporated giving the product as a colorless oil (0.19 g, 89%). The product was pure enough to be used in the subsequent reaction. ^{1}H NMR (ppm): δ = 6.32 (2 H, s, PhH), 4.12-4.02 (6 H, m, PhOC*H*$_2$CH$_2$-), 3.84-3.73 (6 H, PhOCH$_2$C*H*$_2$), 3.69-3.56 (36 H, m, -OC*H*$_2$C*H*$_2$O-), 2,12 (9 H, s, CH$_2$C*H*CH$_2$[Ad]), 1.72 (18 H, s, CHC*H*$_2$C[Ad]), 1.64-1.54 (18 H, m, CHC*H*$_2$CH[Ad]). ^{13}C NMR (ppm): δ = 153.2, 136.2, 108.0, 99.6, 72.8-69.1, 59.4, 41.6, 36.6, 30.6. MALDI-TOF MS *m/z* = 1072.7 [M+H]$^+$, calcd. 1072.7.

Lissamine-Ad$_3$ (3,4,5-tris[2-(2-{2-[2-(adamantan-1-yloxy)ethoxy]ethoxy}ethoxy)-ethoxy]phenyllissamide) (9). A solution of **8** (0.120 g, 0.11 mmol), lissamine sulfonyl chloride (0.065 g, 0.11 mmol) and an excess of DIPEA was stirred for 8 h at rt in 3 ml CH$_2$Cl$_2$. Hereafter the volatiles were evaporated and the crude product was subjected to column chromatography (eluent gradient CH$_2$Cl$_2$/MeOH, 10/3, 9/1 and 7/1 subsequently) yielding one isomer of lissamine-Ad$_3$ (0.011 g, 6%) as a purple oil. MALDI-TOF MS m/z = 1614.3 [M+H]$^+$, calcd. 1614.1.

The starting lissamine sulfonyl chloride consists of several isomers which complicates the purification of the crude product of **9**. Column chromatography yielded a fraction of 11 mg of a pure isomer of **9** which was used in the spreading experiments. During the coupling between **8** and lissamine, the reactants did not completely react since a

fraction of lissamine (30 mg) and a fraction containing the starting amine **8** were collected after the column. No optimization of this reaction was attempted.

Substrate preparation. SAMs of β-cyclodextrin on glass were prepared in four steps, by a method developed by our group previously:[12] after the formation in solution of the SAM of 1-cyano-11-trichlorosilylundecane, the cyano-terminated SAM was reduced to amine, followed by the transformation to isothiocyanate-bearing layers which were finally reacted with per-6-amino-β-cyclodextrin.

Microcontact printing. Patterning on the molecular printboard with the fluorescent dyes was achieved by microcontact printing. Stamps were prepared from commercially available Sylgard-184 poly(dimethyl siloxane) (Dow Corning). The curing agent and the prepolymer were manually mixed in a 1:10 volume ratio and cured overnight at 60 ^{o}C against the master. The cured stamp was peeled off from the master at the curing temperature. Silicon masters with 5 μm wide line features separated by 25 μm spacing were fabricated by photolithography. This high spacing / feature ratio was necessary to ensure a large enough free spreading space for the guest molecules during the measurements, and for easy data transformation.

The stamps were mildly oxidized in an oxygen plasma reactor before use. Before printing, the stamps were inked by soaking them into an aqueous solution of the fluorescent dye (≈ 10 μM). After drying the surface of the stamps with nitrogen, conformal contact was achieved manually. The stamps were weakly pressed against the printboard surface at the initial stage of the printing to induce the formation of conformal contact. The printing time in all cases was 1 min. The samples with the patterned SAMs of the guest were rinsed right after the printing with a continuous flow of pure water (lissamine-Ad: 10 s; lissamine-Ad$_2$ and lissamine-Ad$_3$: 30 s) to remove the physisorbed molecules and dried in a stream of nitrogen.

Spreading experiments. 280 μL aqueous solutions with 0-12 mM β-CD were applied on top of the patterned surface confined by a rubber ring with a diameter of 11.6 mm. The printboard surface / rubber ring / liquid system was immediately covered with a clean glass slide to close the volume and to avoid any evaporation. A thin layer of vacuum grease on the rubber ring was used to stick together the solid components.

Fluorescence microscopy images were frequently taken. To avoid the effect of photobleaching, new areas were selected after each shot. The focusing time before taking the micrographs was in all cases 20 s. In case of a faster focusing, the analyzed spot was further irradiated, until the 20 s time period was reached.

Fluorescent images were taken using an Olympus inverted research microscope IX71 equipped with a mercury burner U-RFL-T as a light source and a digital camera Olympus DP70 (12.5 million-pixel cooled digital colour camera) for image acquisition. Green excitation light (510 nm $\leq \lambda \leq$ 550 nm) and red emission light ($\lambda <$ 590 nm) was filtered using a U-MWG Olympus filter cube.

5.5 References

1   M. Mammen, S. K. Choi, G. M. Whitesides, *Angew. Chem. Int. Ed.* **1998**, *37*, 2755.

2   T. K. Lindhorst, in *Host-Guest Chemistry*, 218, **2002**, 201.

3   L. L. Kiessling, J. E. Gestwicki, L. E. Strong, *Angew. Chem. Int. Ed.* **2006**, *45*, 2348.

4   A. Mulder, J. Huskens, D. N. Reinhoudt, *Org. Biomol. Chem.* **2004**, *2*, 3409.

5   J. Huskens, *Curr. Opin. Chem. Biol.* **2006**, *10*, 537.

6   M. J. W. Ludden, D. N. Reinhoudt, J. Huskens, *Chem. Soc. Rev.* **2006**, *35*, 1122.

7   B. T. Houseman, M. Mrksich, in *Host-Guest Chemistry*, 218, **2002**, 1.

8   J. H. Rao, J. Lahiri, L. Isaacs, R. M. Weis, G. M. Whitesides, *Science* **1998**, *280*, 708.

9   J. H. Rao, J. Lahiri, R. M. Weis, G. M. Whitesides, *J. Am. Chem. Soc.* **2000**, *122*, 2698.

10   A. Mulder, S. Onclin, M. Péter, J. P. Hoogenboom, H. Beijleveld, J. ter Maat, M. F. García-Parajó, B. J. Ravoo, J. Huskens, N. F. van Hulst, D. N. Reinhoudt, *Small* **2005**, *1*, 242.

11   J. Huskens, A. Mulder, T. Auletta, C. A. Nijhuis, M. J. W. Ludden, D. N. Reinhoudt, *J. Am. Chem. Soc.* **2004**, *126*, 6784.

12   S. Onclin, A. Mulder, J. Huskens, B. J. Ravoo, D. N. Reinhoudt, *Langmuir* **2004**, *20*, 5460.

The kinetics of multivalent spreading at interfaces

The spreading dynamics of mono-, di- and trivalent guests on a molecular printboard is discussed in this chapter. Spreading experiments with the divalent guest on a fully and uniformly covered printboard, in the presence of native host sites in the surrounding aqueous solution, show that the spreading of the guests is directional and is driven by the effective concentration gradient between neighboring areas. Increase of the spreading rate is observed when the coverage gradient-driven surface spreading of di- and trivalent guests is studied with weaker binding guest moieties. Multivalent binding and spreading are considered as consecutive events of sequential binding and unbinding steps, which are expressed in terms of intrinsic rate constants and effective concentration. Numerical calculations disclose the effect of the β-cyclodextrin concentration in the solution on the spreading rate and mechanisms. The calculated equilibrium concentrations can explain the rate increase but not the decrease for multivalent spreading rates. Additional factors, such as the lifetime of unsaturated species and the relative chances of successful and unsuccessful rebinding events, are incorporated to explain the experimentally observed spreading rate maximum. Molecular dynamics calculations support the 'walking' and 'hopping' mechanisms of the multivalent guests on the molecular printboard.

6.1 Introduction

The kinetics of multivalent interactions at interfaces is poorly understood despite its fundamental importance in the biology of cell membranes and in the design and application of multivalent ligands in nanofabrication at self-assembled monolayers (SAMs).[1-3] In contrast, the thermodynamics of such multivalent systems has been extensively studied and is well understood.[1,4]

Two parameters, effective molarity (*EM*) and effective concentration (C_{eff}), have been used to describe the thermodynamics of multivalent interactions at a molecular level.[2] In an interaction between a multivalent host and a multivalent guest the first intermolecular binding event is followed by intramolecular steps. *EM* represents in such a system the ratio of association rates or stability constants for intra- and intermolecular processes, and C_{eff} represents the real physical concentration of the uncomplexed host site experienced by the uncomplexed guest site.[1,5] The two terms have been shown conceptually close or equal in several systems,[6] and therefore C_{eff}, which is based on the probability with which two interacting sites meet depending on the linker length, conformational possibilities and other possible factors, will be used in this study to quantify inter- and intramolecular binding events in multivalent interactions on surfaces.

Host-guest studies performed with small monovalent guests have shown that the molecular recognition properties of β-cyclodextrin (β-CD) cavities at a β-CD SAM were unaltered by the surface immobilization.[7,8] An analysis of the thermodynamics of binding of the divalent complex between a bis-adamantyl calix[4]arene guest with flexible tetra(ethylene glycol) linkers and a bis-cyclodextrin host has shown that this system can be described with multivalency effects only, without cooperativity.[9] The concept of C_{eff} has been used to build a model for describing the thermodynamics of multivalent host-guest interactions at interfaces.[10] The model assumes that all individual host-guest interactions in solution, as well as on the surface, are independent and multivalent interactions can be rationalized as sequential binding events described with the help of C_{eff}. The model was successfully used to describe the thermodynamics of binding of multivalent guests to β-CD SAMs in the presence of a monovalent competitor in solution.

Compared to Chapter 5, additional spreading experiments are presented in this Chapter, to further investigate the nature of the multivalent spreading at a molecular level, by eliminating the concentration gradient difference on the surface and by

changing the intrinsic binding constant of the guest moieties. The dynamics of mono-, di- and trivalent host-guest interactions on the molecular printboard in the presence of competitive β-CD in the surrounding solution is analyzed, simulated and discussed with the help of C_{eff} and kinetic parameters of the intrinsic binding of the guest moieties to β-CD.

6.2 Results

In the previous chapter it was shown that mono-, di- and trivalent fluorescent guest molecules, printed on a β-CD SAM, spread onto the empty molecular printboard areas in the presence of water with and without native β-CD. A change in the spreading rate of all studied guests was induced by increasing the host concentration in solution (see Figure 6.1).
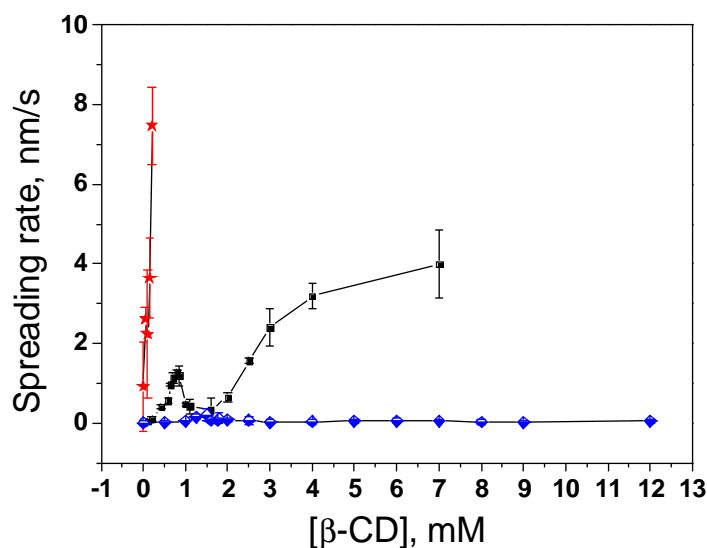
Figure 6.1 Spreading rate of the fluorescent dyes lissamine-Ad (★), lissamine-Ad$_2$ (■) and lissamine-Ad$_3$ (◆) on the molecular printboard as a function of the β-CD concentration in the surrounding solution.

It was concluded that monovalent guests spread in β-CD solutions by complete desorption followed by re-adsorption. The spreading rate profile of the divalent guest with a local maximum at 0.8 mM β-CD suggested the occurrence of multiple spreading mechanisms, where the divalent molecules spread by 'walking' in pure water, by complete desorption and re-adsorption at high β-CD concentrations and possibly by a 'hopping' mechanism at intermediate β-CD concentrations. The high

binding strength of the trivalent guest to the surface reduced the surface spreading and only a moderate spreading rate maximum was observed, however spreading mechanisms similar to the divalent system were suspected to control the surface dynamics.

In the experiments described in Chapter 5, printing establishes a steep gradient of guest molecules, which increases in length and decreases in steepness upon spreading. This is accompanied by a similarly changing gradient of empty surface β-CD sites, and thus of C_{eff}. To investigate a potentially directional driving force of the C_{eff} gradient on the spreading, here, the spreading of the divalent guests on a fully and uniformly covered printboard was investigated.

Fluorescence recovery after photo-bleaching (FRAP) experiments were performed by deposition of a uniform SAM of lissamine-Ad$_2$ on a fresh β-CD printboard followed by local irradiation of the surface, in order to induce photo-bleaching on the selected areas. However, FRAP experiments followed by spreading tests in water with and without β-CD were not successful due to the poor edge resolution of the bleached areas.
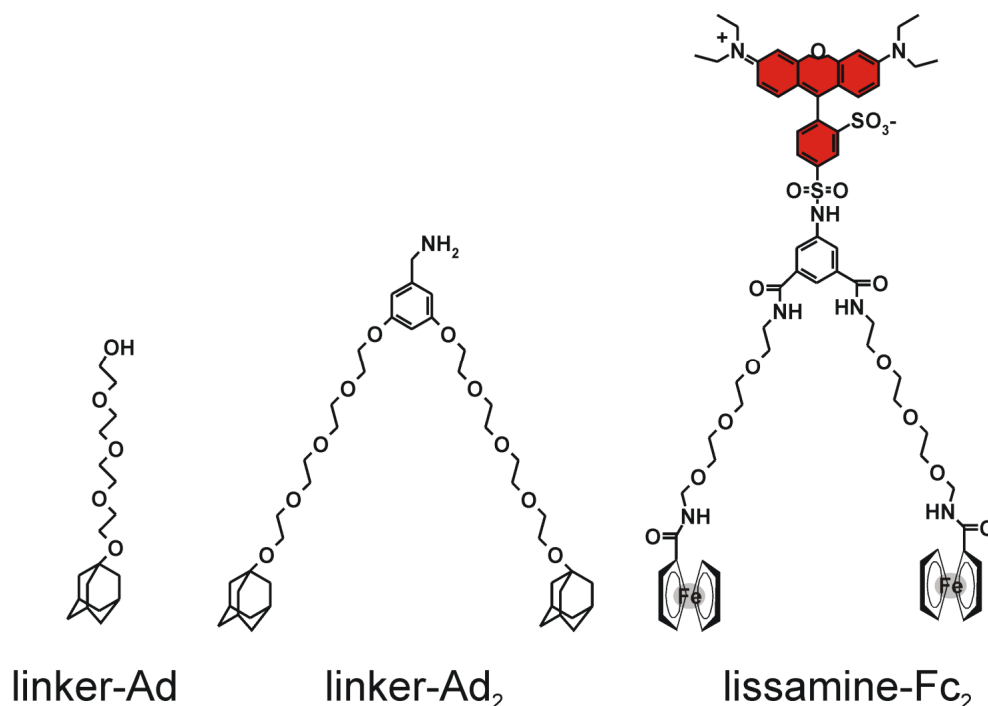
Chart 6.1 Guest molecules used in this study.

This problem was overcome by patterning the surface with fluorescent lines by microcontact printing of lissamine-Ad$_2$ and backfilling the rest of the surface in solution with the non-fluorescent linker-Ad$_2$ (see Chart 6.1). The backfilling step may

result in some exchange of fluorescent by non-fluorescent guests, but the coverage will be homogeneous and only relative intensities are used.

High ($\geq$ 90 %) and low ($\approx$ 50 %) coverages of the surface after backfilling were achieved through rinsing the samples with water and a 20:80 (v:v) mixture of ethanol:water, respectively. Rinsing with water was necessary to remove any physisorbed molecules, while rinsing with ethanol-containing water leads to efficient decrease of the surface coverage. Spreading experiments were carried out with fluorescent lines of 5 µm with a 20 µm period, in water and in 0.8 mM β-CD (Figure 6.2). The choice for the later concentration is given by the observed spreading rate maximum at this β-CD concentration (Figure 6.1).
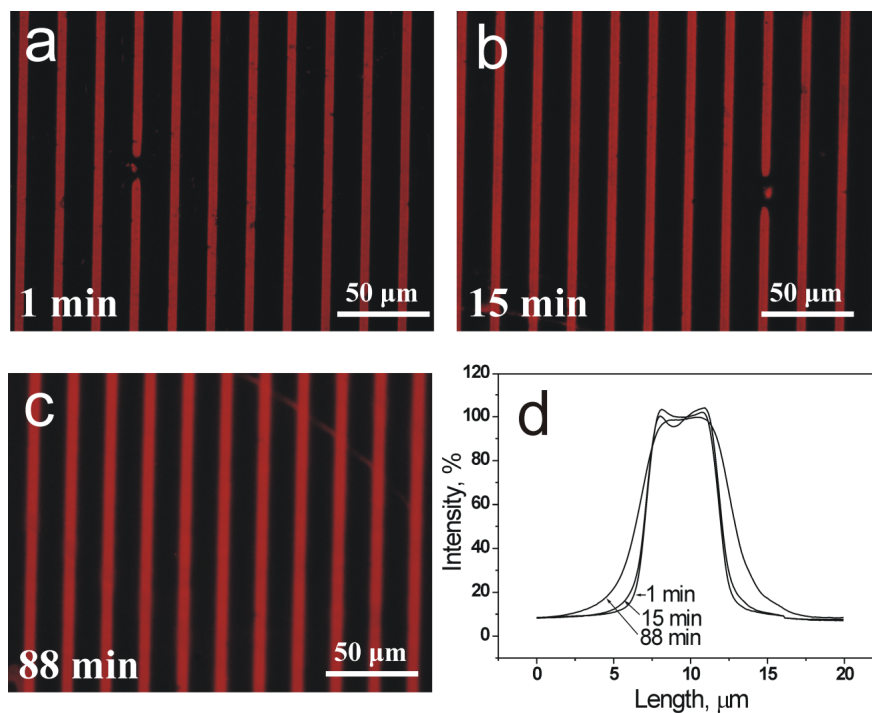
Figure 6.2 Spreading of lissamine-Ad$_2$ on the fully covered molecular printboard with high coverage: fluorescence micrographs (a, b and c) and the average normalized line profiles (d) when the guest-printed substrates were immersed in 0.8 mM β-CD solutions.

In Figure 6.3, the maximum peak intensity (I_{max}) of the patterns is plotted as a function of time. The I_{max} from the first measurement (t = 1 min) at high coverage was set to 100 %. Lower fluorescence intensities reflect lower surface concentrations of the divalent guest.
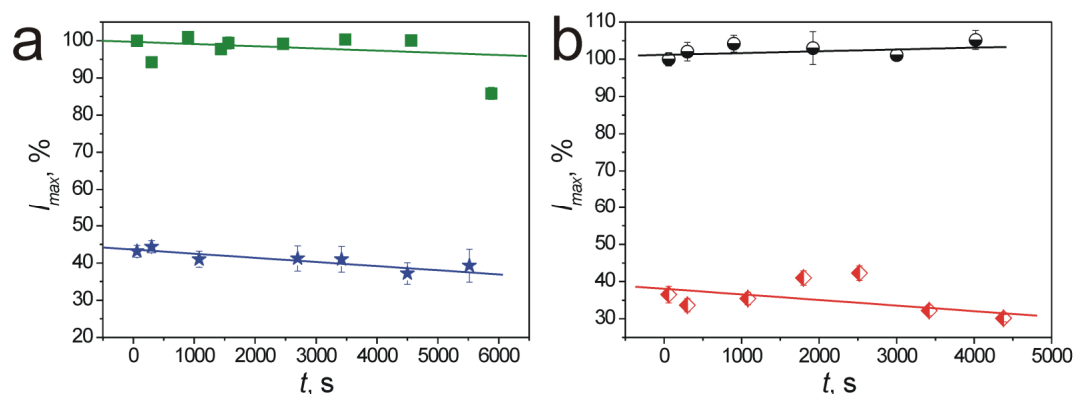
Figure 6.3 The plot and the linear fit of I_{max} as a function of time in water (a) at high (■) and low surface coverage (★); in 0.8 mM β-CD (b) at high (◖) and low surface coverage (◆).

In all cases I_{max} did not change significantly during the measurements indicating a low desorption of the fluorescent guests. The linear fit of the change of the peak width in time (Figure 6.4) gives the spreading rate of the divalent molecules (see Chapter 5).
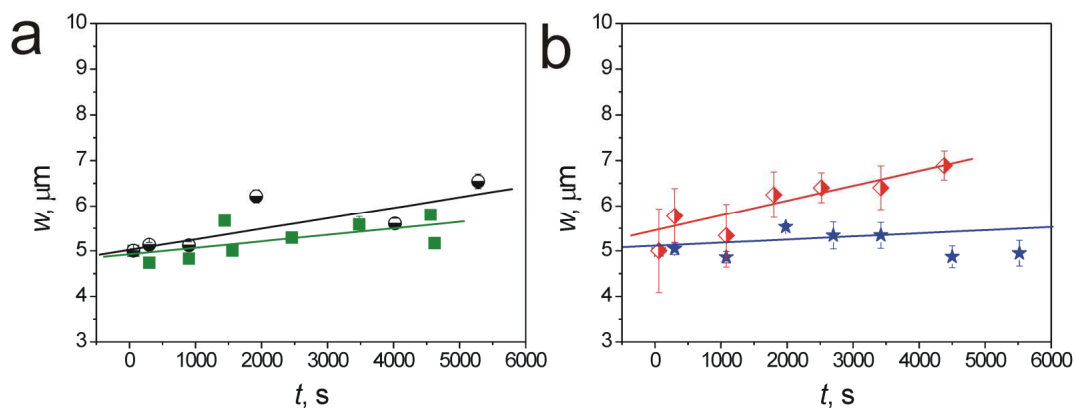

Figure 6.4 The plot and the linear fit of w as a function of time at high surface coverage (a) in water (■) and in 0.8 mM β-CD (◖), and at low surface coverage (b) in water (★) and in 0.8 mM β-CD (◆).

The obtained spreading rates are listed in Table 6.1. In pure water, the surface coverage, and the associated C_{eff}, did not affect measurably the spreading rate. In both cases the rates were close to the value measured on printed, non-backfilled samples, as presented in Chapter 5.

Table 6.1 Measured surface spreading rates of lissamine-Ad$_2$ on fully covered printboards (high and low coverage) and on patterned printboards.

	rates in water (nm/s)	rates in 0.8 mM β-CD (nm/s)
fully covered, high coverage	0.05 ± 0.04	0.19 ± 0.02
fully covered, low coverage	0.07 ± 0.04	0.3 ± 0.1
patterned printboard (Chapter 5)	0.02 ± 0.01	1.3 ± 0.1

At a 0.8 mM β-CD concentration, a slightly higher spreading rate was observed at low surface coverage, which suggests a coverage- and C_{eff}-dependent spreading mechanism under these conditions. However, on both uniformly covered printboards, the spreading rates were significantly lower than the rate observed on a patterned, non-backfilled surface. This is a clear indication that spreading of the divalent guest on the printboard is directional and is driven by the C_{eff} difference between neighboring areas.

The effect of the binding strength on the multivalent dynamics on surfaces was studied by performing spreading experiments in which the intrinsic stability constant of the guest moiety to β-CD was varied. The intrinsic binding constant (K_i) of a simple, monovalent host-guest interaction is determined by the association ($k_{a,i}$) and dissociation ($k_{d,i}$) rate constants:

$$K_i = \frac{k_{a,i}}{k_{d,i}} \tag{6.1}$$

Two different strategies were used to change K_i, one by changing the solvent while studying the spreading of Ad-functionalized guests, and another in which the guest moiety was the weaker binding ferrocenyl (Fc).

First, the spreading of patterned SAMs of lissamine-Ad$_2$ and lissamine-Ad$_3$ was studied in a methanol-water mixture. Addition of cosolvents, such as alcohols, typically decreases the equilibrium constants of guests with cyclodextrin.[11] Since the association is usually assumed to be diffusion-controlled, lowering of K_i is expected

to be accompanied by an increase of $k_{d,i}$. However, fluorescence and laser flash photolysis experiments have shown that the equilibrium constant of xantone / β-CD complexes in the presence of alcohols decreased together with the observed dissociation rate constant $(k^*_{d,i})$.[12] This led to the proposal that, in this case, alcohol molecules, in addition to filling the empty spaces inside the β-CD cavity, also provide a shielding of the cavity by preferential solvation of the rim.[12]

Binding studies with tetra(ethylene glycol)-functionalized adamantyl (linker-Ad; see Chart 6.1) in aqueous solution using isothermal titration calorimetry (ITC) showed that the binding constant of an individual adamantyl - β-CD interaction is 5.7×10^4 M^{-1} (Figure 6.5; Table 6.2). This value closely resembles the intrinsic binding constant from the literature.[9,13] Calorimetric titration of linker-Ad with β-CD in 10 % methanol gave a binding constant of $3.2 \times 10^4 \, M^{-1}$ (Table 6.2).
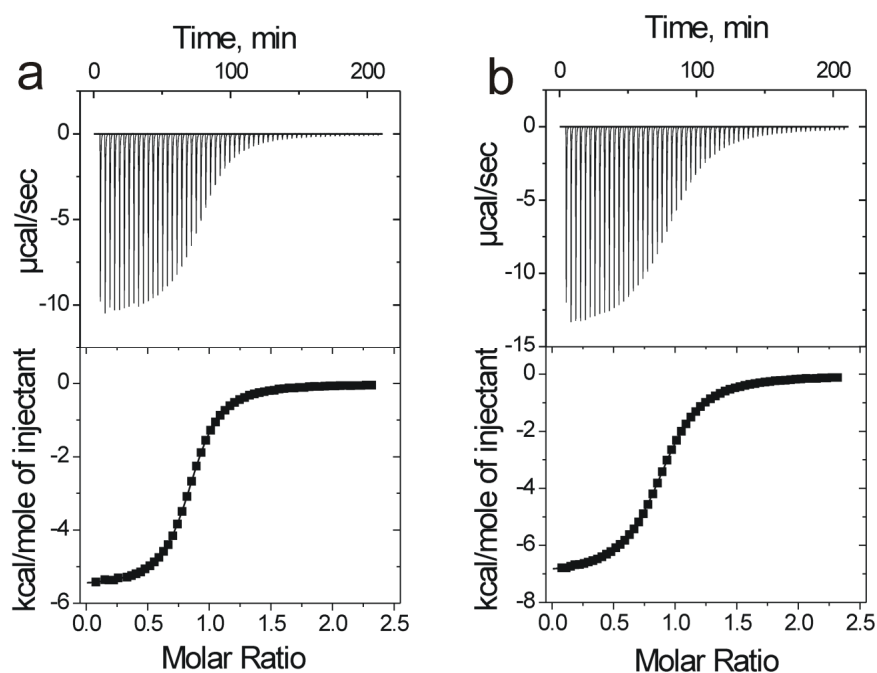
Figure 6.5 Data of heat evolution upon injection of an aqueous solution of β-CD and resulting binding curves (markers) and best fits (line) to a 1:1 model from calorimetric titrations of linker-Ad (1 mM) with β-CD (10 mM) in water (a) and in a methanol:water (10:90 v/v) mixture (b) at 25°C.

Table 6.2 Thermodynamic parameters of the complexation of linker-Ad to β-CD in water and in a methanol:water (10:90 v/v) mixture, as determined by ITC at 298 K.

methanol:water ratio	K (M^{-1})	ΔG^0 (kcal/mol)	ΔH^0 (kcal/mol)	$T\Delta S^0$ (kcal/mol)
0:100	5.7×10^4	-6.5	-5.7	0.8
10:90	3.2×10^4	-6.1	-7.1	-1.0

The surface spreading of the divalent lissamine-Ad_2 and the trivalent lissamine-Ad_3 on the β-CD-based molecular printboard was studied in 10 % methanol in water, without backfilling. The spreading rate of the divalent lissamine-Ad_2 on the β-CD-based molecular printboard in the methanol:water (10:90) mixture (0.2 nm/s) showed an increase of one order of magnitude compared to the value obtained in the presence of pure water (0.02 nm/s). Similarly, the spreading rate of the trivalent guest in the same methanol:water mixture showed a spreading rate of 0.03 nm/s, which is also one order of magnitude higher than the spreading rate measured in the presence of pure water. In conclusion, these experiments confirm qualitatively the expected behavior that a decrease of K_i leads to an increase of $k_{d,i}$ and thus of the spreading rate.

In a second strategy, divalent molecules equipped with ferrocene moieties were patterned on the printboard and the spreading in presence of water with and without β-CD was studied. Ferrocene forms inclusion complexes with β-CD with an equilibrium binding constant of 1.1×10^3 M^{-1}.[13]

Pattern evolution of lissamine-Fc_2 (Chart 6.1) printed on the printboard, followed by immersion water and in 0.1 mM and 0.2 mM β-CD solutions, was investigated in time. I_{max} was decreasing in all cases, while w was also slightly decreasing with time (Figure 6.6). Surprisingly, no surface spreading could be observed. Apparently, complete desorption dominates spreading for this system.
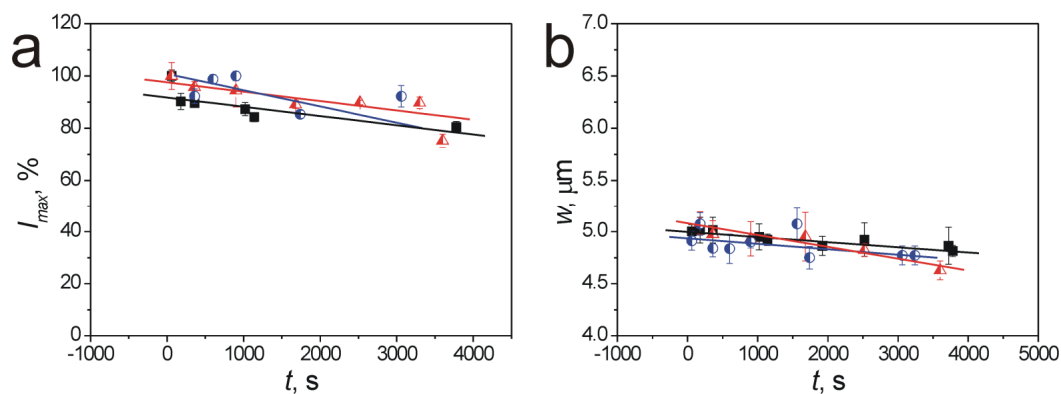
Figure 6.6 Spreading of lissamine-Fc$_2$ on the molecular printboard: (a) The plot and the linear fit of I_{max} as a function of time; (b) The plot and the linear fit of the peak width w at half maximum in function of time in different β-CD concentrations: (■) water, (▲) 0.1 mM β-CD and (◐) 0.2 mM β-CD.

6.3 Discussion

6.3.1 Thermodynamic equilibrium considerations

Binding of mono- or multivalent guests to the β-CD printboard is a reversible interaction governed by an intrinsic binding constant (see Equation 6.1). Competition for guest binding with monovalent hosts in solution infers additional equilibria.

All equilibria of lissamine-Ad with β-CD SAMs in the presence of competitive β-CD in solution are shown in Scheme 6.1. The monovalent equilibria contain two solution guest species (G^I and $G^I H_l$) and one surface complex ($G^I H_s$) and they describe the interaction of lissamine-Ad with β-CD in solution (from top to bottom) and with β-CD at the surface (from left to right).
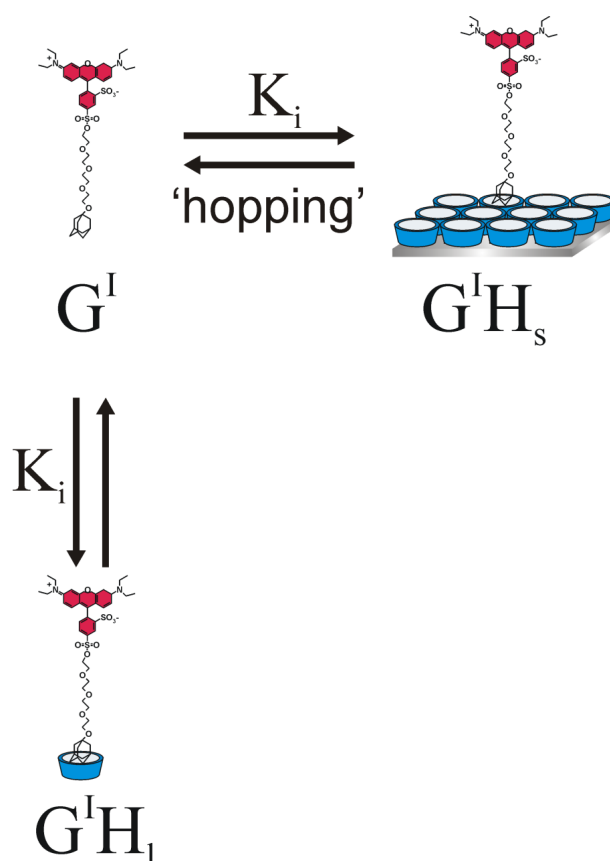
Scheme 6.1 Equilibria of the binding of lissamine-Ad (G^I) to a β-CD at a surface (H_s) and to β-CD in solution (H_l).

The binding constants can be expressed in terms of intrinsic binding constants for binding to a surface host ($K_{i,s}$) and to a solution host ($K_{i,l}$). It has been shown previously that the binding strength of a guest to a β-CD from solution is equal to the binding strength to a β-CD of the surface,[8] therefore a common intrinsic binding constant (K_i) will be used here for all the involved equilibria (Scheme 6.1) as shown in Equation 6.2:

$$K_i = K_{i,s} = K_{i,l} = \frac{[G^I H_s]}{[G^I] \cdot [H_s]} = \frac{[G^I H_l]}{[G^I] \cdot [H_l]} \qquad (6.2)$$

where *[H_s]* represents the unbound, surface-confined host concentration and *[H_l]* the concentration of unbound β-CD cavities in the solution. The equilibrium constants are expressed in terms of volume concentrations (in M), using the fixed volume of the experimental cell to calculate the concentrations of the surface species.

The extension of the monovalent binding scheme to a divalent system requires the introduction of the parameter C_{eff}. Scheme 6.2 depicts all equilibria for the sequential divalent binding of lissamine-Ad$_2$ to β-CD SAMs and to β-CD in solution. The equilibria contain surface species as a consequence of interaction of the divalent guest (G^{II}) with surface-confined hosts (from left to right) and solution species upon interaction with β-CD in solution (from top to bottom). The sequential binding events in the solution and at the surface are considered equal and independent.[9,10]
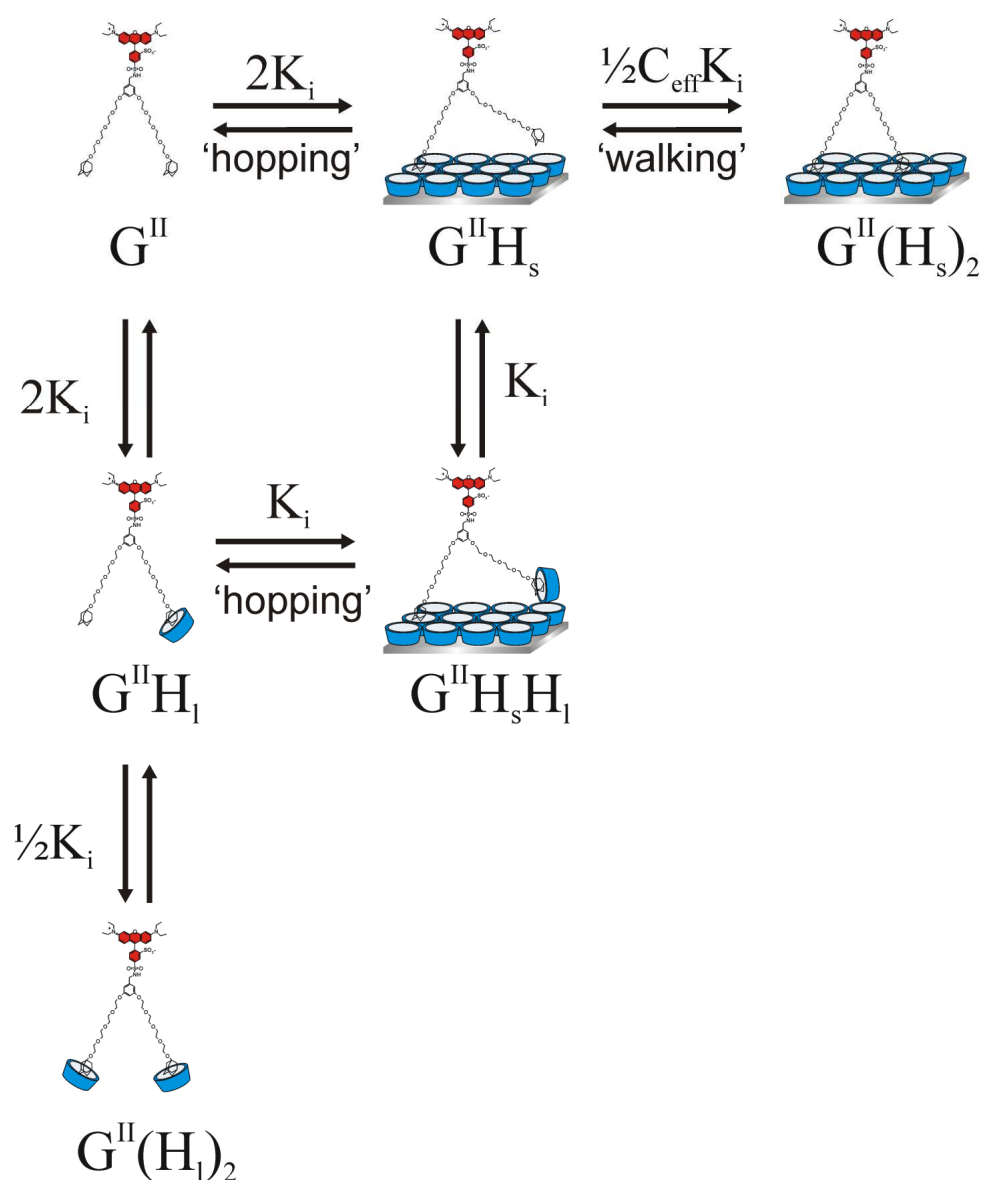
Scheme 6.2 Equilibria for the sequential binding of the divalent lissamine-Ad$_2$ (G^{II}) to the β-CD printboard and to β-CD in solution.

The first, intermolecular binding event of lissamine-Ad$_2$ to a host is given by Equation 6.3:

$$2 \cdot K_i = \frac{[G^{II}H_s]}{[G^{II}] \cdot [H_s]} = \frac{[G^{II}H_l]}{[G^{II}] \cdot [H_l]} \tag{6.3}$$

The second, intramolecular, interaction at the printboard surface is the product of K_i and C_{eff}. The concentration of accessible, unbound host sites in the probing volume of the unbound guest moiety, C_{eff}, is dependent on the coverage of free host sites. It is equal to the limiting value reached at infinitely low surface coverage ($C_{eff,max}$) multiplied by the fraction of unbound surface host sites (Equation 6.4).[9,10]

$$C_{eff} = C_{eff,max} \cdot \frac{[H_s]}{[H_s]_{tot}} \tag{6.4}$$

Previous studies with a divalent bis-adamantyl calix[4]arene guest with flexible tetra(ethylene glycol) linkers have found 0.2 M as an approximate value for $C_{eff,max}$.[9] The equilibria of the trivalent lissamine-Ad$_3$ to the printboard contain surface and solution species (Scheme 6.3) and the transition from the fully surface-bound form (top row, right end) to the form where the trivalent guest G^{III} binds only to solution hosts (most left column) is abundantly represented by various surface-bound forms of the trivalent guest.
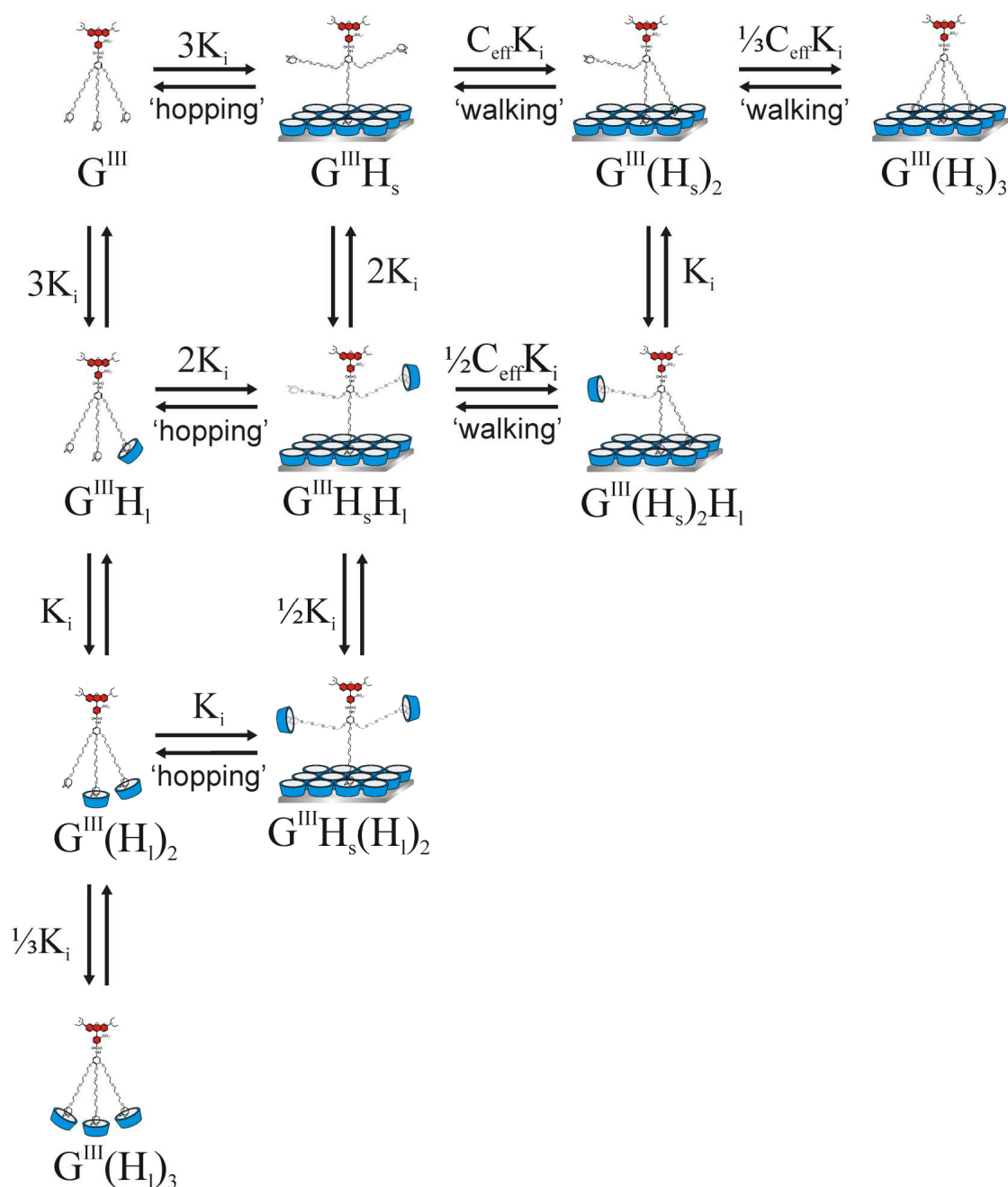
Scheme 6.3 Equilibria for the sequential binding of the trivalent lissamine-Ad_3 (G^{III}) to the β-CD printboard and to β-CD in solution.

Schemes 6.1-6.3 represent all species that can be present, as well as the elementary association and dissociation steps. 'Walking' is defined as the dissociation of a surface-bound site of a multivalently bound guest species and its re-association to another free host site on the surface. It can therefore only occur for multivalent guests, according to the steps indicated in Schemes 6.2 and 6.3. 'Hopping' is defined as the dissociation of the surface-bound site of a monovalently bound guest species and the

re-association of any available site of the molecule to another free host site on the surface. The dissociated guest molecule with at least one unsaturated site diffuses close to the printboard surface and travels a mean path length determined by its lifetime. Binding of all free sites of the dissociated guest molecule to β-CDs from solution initiates the complete desorption followed by re-adsorption mechanism, where the fully saturated guest molecule diffuses into the bulk and after the stochastic re-approaching to the printboard surface and dissociation of a β-CD moiety from the solution, the association to a free host site on the surface can occur.

The initial aim was to calculate the concentrations of all species as a function of the β-CD concentration in solution to verify whether trends in the concentrations of the species could be related to the observed trends of the spreading rates. Since the observed spreading phenomena take places over the course of minutes and hours, while the elementary dissociation of a β-CD-guest interaction is in the order of μs-ms, it is assumed that very close to the surface, all species are locally in thermodynamic equilibrium.

Assuming equilibrium close to the surface in a system similar to the experimental setup, where a β-CD printboard homogeneously covered with a guest SAM is placed in a solution with or without native β-CD, the equilibrium concentrations of all species present in the system can be calculated. Assuming that the free β-CD concentration in solution close to the surface is equal to the free β-CD concentration in the bulk (for which $[H_l] = [H_l]_{tot}$; see 6.3.1), the combination of the equilibrium constant definitions with the mass balances for the total surface-confined host concentration $[H_s]_{tot}$ and the total guest concentration (for mono-, di- and trivalent systems $[G^I]_{tot}$, $[G^{II}]_{tot}$ and $[G^{III}]_{tot}$, respectively) gives numerically solvable sets of equations. Printboard surfaces before immersion in water (with or without β-CD), with 90 % of surface-confined β-CDs bound to guest moieties (the printed guest SAMs were rinsed with water and therefore 10 % loss of the guest moieties from the surface is assumed) were used to simulate the experimental conditions, and calculate the equilibrium concentrations of all species for the mono-, di- and trivalent systems.

Spreading of the monovalent guest is realized by a sequence of events including desorption of $G^I H_s$ from the printboard to form G^I which after a certain stay in the solution readsorbs to the surface. Formation of $G^I H_l$ increases the time of stay in the solution, and thus the diffusion length, because only after the dissociation of $G^I H_l$ re-adsorption of G^I to the surface can take place. Figure 6.7 shows the calculated

concentrations of all species in the monovalent system (Scheme 6.1) as a function of the β-CD concentration in solution. In pure water, only 'hopping' of the guest (G^IH_s → G^I → G^IH_s) can contribute to spreading (which is here indistinguishable from the regular desorption and re-adsorption). Because the concentration of both species contributing to hopping (G^IH_s and G^I) are decreasing upon increase of the β-CD concentration in the solution, the increased spreading rate can be assigned to desorption and formation of G^IH_l, which is increasing in concentration (Figure 6.7).
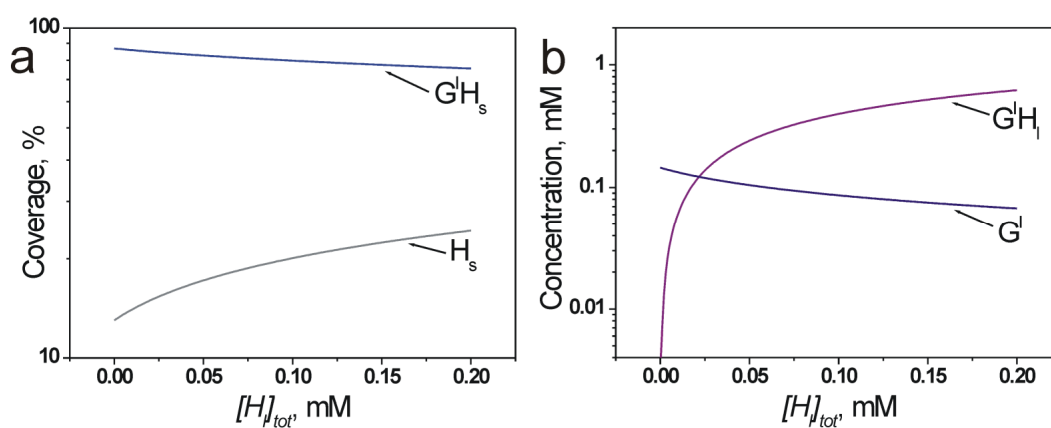
Figure 6.7 Equilibrium concentrations of lissamine-Ad (G^I) species at the surface (a) and in solution (b) as a function of the β-CD concentration in the surrounding solution.

Spreading of the divalent guest occurs according to different spreading mechanisms as a function of $[H_l]_{tot}$, as already qualitatively indicated in Chapter 5. In pure water, only walking and hopping can occur. 'Walking' (Scheme 6.2) starts with the dissociation of one guest site of $G^{II}(H_s)_2$, while 'hopping' involves a similar dissociation step of $G^{II}H_s$. Because the intrinsic attempt frequency of the dissociation of $G^{II}(H_s)_2$ is twice as likely and the concentration of $G^{II}(H_s)_2$ is more than two orders of magnitude larger, 'walking' is most likely the only spreading mechanism under these conditions. Upon increase of $[H_l]_{tot}$, the concentrations of both species involved in walking ($G^{II}(H_s)_2$ and $G^{II}H_s$) decrease monotonously (Figure 6.8a), indicating that the observed increase in spreading rate is caused by another mechanism.
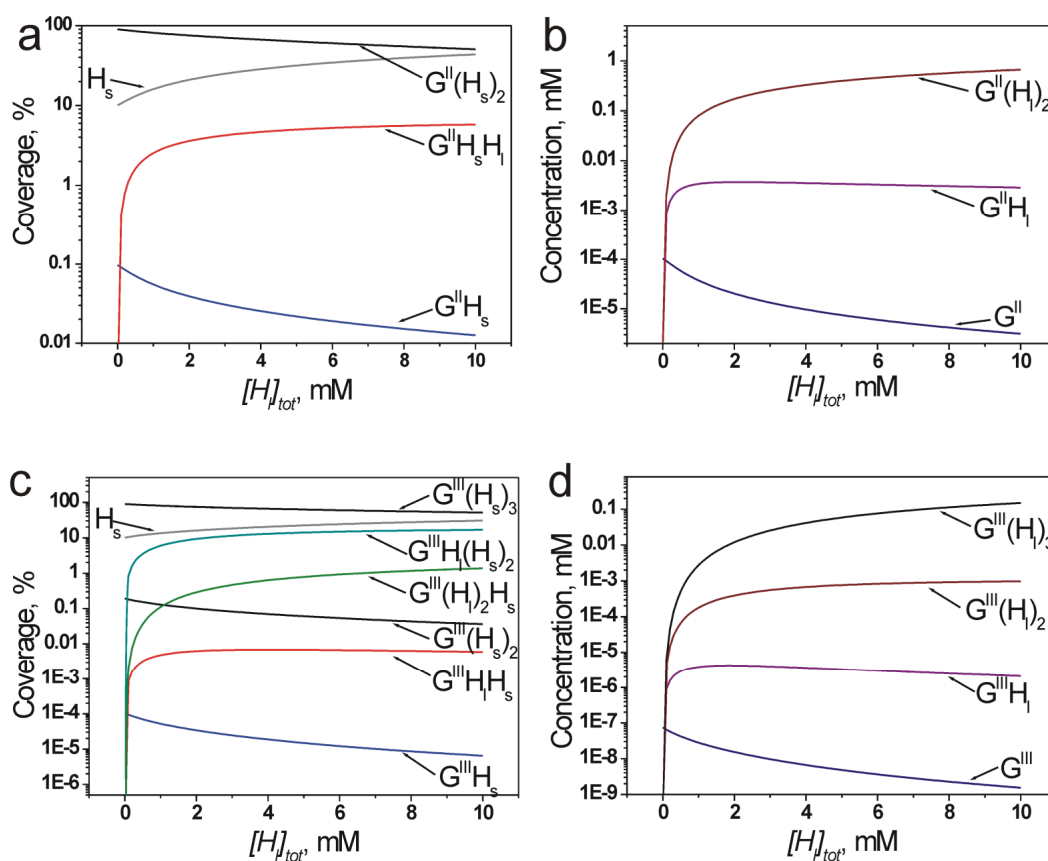
Figure 6.8 The variation of equilibria-concentration of lissamine-Ad$_2$ surface (a) and solution (b), and lissamine-Ad$_3$ surface (c) and solution (d) species on the molecular printboard as a function of the β-CD concentration in the surrounding solution.

Desorption, involving $G^{II}(H_l)_2$, is experimentally only observed at $[H_l]_{tot} > 1.5$ mM. Therefore, both the increase and the decrease of spreading rate, observed at $0 < [H_l]_{tot} < 0.8$ mM and $0.8 < [H_l]_{tot} < 1.5$ mM, respectively, must be explained by the 'hopping' mechanism. Figure 6.8a and b show clearly the rapid increase of the concentrations of the species bound to one H_l unit that could contribute to 'hopping' ($G^{II}H_sH_l$ and $G^{II}H_l$), which can explain the observed spreading rate increase up to 0.8 mM of H_l. However, their concentrations level off at higher $[H_l]_{tot}$, indicating that the overall attempt frequencies are not able to explain the rate decrease at $[H_l]_{tot} > 0.8$ mM. The decrease can potentially arise from the increase of $[H_s]$ which increases the chance of rebinding of $G^{II}H_l$ to the surface, thus effectively reducing its lifetime and, concomitantly, the average distance this species travels before rebinding. Qualitatively, however, it seems unlikely that the less than 2-fold increase of $[H_s]$ over $[H_l]_{tot} = 0 – 1.5$ mM can explain fully the > 5-fold decrease in spreading rate

observed between $[H_l]_{tot} = 0.5 - 1.5$ mM. Most likely, the explanation needs also to involve the relative frequencies of rebinding to the *same* surface site (leading to absence of spreading, an '*unsuccessful* event') and to *another* surface site ('*successful* event') (see below).

Figure 6.8c and d presents the calculated concentrations of all species involving the trivalent guest (G^{III}) (Scheme 6.3) as a function of the β-CD concentration in the solution. Many species ($G^{III}H_s$, $G^{III}H_l$ and G^{III}) have insignificantly low equilibrium concentrations and their contribution to spreading can be ignored. Thus, similarly to the divalent system, 'walking' of the molecules causes the spreading in water involving several surface-bound guest species, as indicated in Scheme 6.3. According to the high affinity of the trivalent guest to the printboard, no desorption of $G^{III}(H_s)_3$ was observed experimentally within the studied host concentration range and thus no complete desorption followed by re-adsorption contributes to the spreading. In presence of low amounts of β-CD in the solution, the concentrations of species involved in 'walking' decrease monotonously (Figure 6.8c), with the exception of $G^{III}(H_s)_2H_l$ and $G^{III}H_sH_l$. Dissociation and association of one guest site of $G^{II}(H_s)_2H_l$ can contribute to the spreading of the trivalent molecule. The rapid increase of the concentrations of $G^{III}H_s(H_l)_2$ and $G^{III}(H_l)_2$ can also contribute to the increase of the spreading rate by a 'hopping' mechanism. Their equilibrium concentrations are about one order of magnitude lower than $G^{II}H_sH_l$ and $G^{II}H_l$ in the divalent system. The contribution to spreading of other species possibly involved in a 'hopping' mechanism is minimal due to their significantly lower equilibrium concentrations. Thus, both 'walking' of $G^{III}(H_s)_2H_l$ and 'hopping' of $G^{III}H_s(H_l)_2$ may induce a spreading rate increase at $0 < [H_l]_{tot} < 1.5$ mM. The maximum in spreading rate occurs at higher $[H_l]_{tot}$ than in the case of the divalent system, indicating the need of a higher amount of β-CD in the spreading mechanism. This suggests that 'hopping' of $G^{III}H_s(H_l)_2$ is the main contributor to the spreading, because its formation requires a higher concentration of H_l compared to the equivalent $G^{II}H_sH_l$ in the divalent case. The decrease of the spreading rate at $[H_l]_{tot} > 1.5$ mM is possibly caused by the reduced lifetime of the involved unsaturated species and the increased frequency of 'unsuccessful events' (see below).

In the presence of 10 % methanol in the surrounding solution, the binding strength of an adamantyl moiety to β-CD changes with a factor of about $2 - 3$, as shown by ITC measurements with linker-Ad. The spreading rate of lissamine-Ad$_2$ on the printboard

is proportional to the concentration of $G^{II}H_s$ and $k_{d,i}$ of an individual Ad - β-CD interaction. A decrease of K_i causes an increase of $k_{d,i}$ with the same factor (Equation 6.1 assuming $k_{a,i}$ is constant) and a similar increase of $[G^{II}H_s]$ (Equation 6.3). Therefore, the spreading rate may increase with the square of this factor. The observed spreading rate increase of one order of magnitude can thus be explained with the weakening of the Ad-β-CD interaction of only a factor 3, which is within experimental error of the observed value.

6.3.2 A molecular picture of the 'hopping' mechanism

Spreading of multivalent molecules on the molecular printboard via the 'walking' or 'hopping' mechanisms is realized by a dissociation step followed by an association step. The spreading rate is determined by the frequency of those dissociation and association cycles which end up in binding to different surface-confined host cavities (Scheme 6.4). No spreading occurs when the guest site rebinds to the β-CD cavity from which it originates.
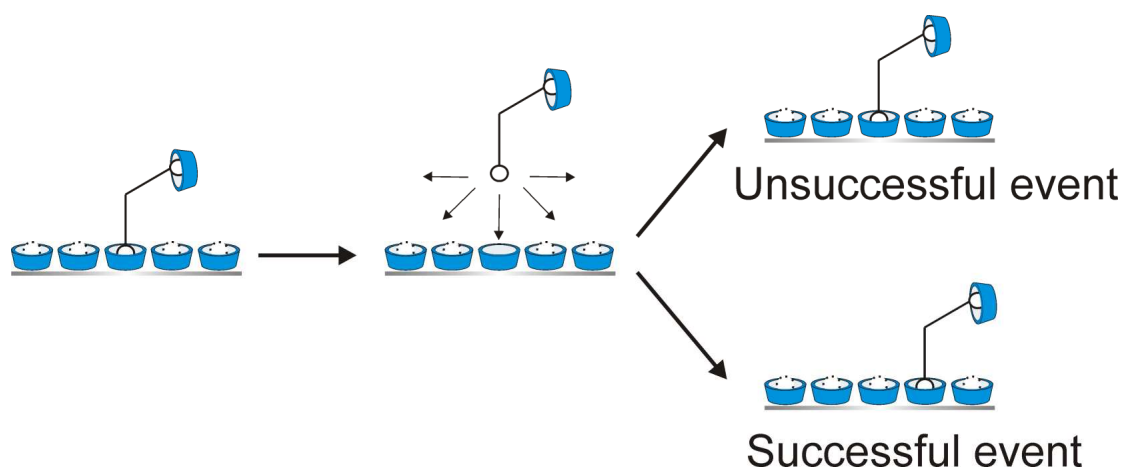
Scheme 6.4 Schematic representation of rebinding to the same surface site (unsuccessful event) and to another surface site (successful event) by 'hopping' of the divalent guest. Dashed circles in the β-CD cavities represent potentially bound guest moieties.

Spreading by 'walking' or 'hopping' of a divalent guest (Scheme 6.2), and analogously any multivalent guest, is a directional process, in which the probability of the re-adsorption to the same or another β-CD is dependent on the coverage of the printboard. The direction in which the molecules move is driven by the concentration differences of the free surface-confined host sites.

It was shown in the previous section that an increase of $[G^{II}H_l]$ and $[G^{II}H_sH_l]$ indicates an increasing spreading rate by 'hopping' of the molecules. However, the spreading rate maximum and the following rate decrease could not be explained by the equilibrium concentrations of the involved species, which did not decrease significantly. In this spreading mechanism, the lifetime of $G^{II}H_l$ has a significant effect on the fraction of the successful dissociation and association cycles for which binding to new hosts occurs. The longer the lifetime of the unsaturated $G^{II}H_l$, the higher is the chance to travel to a new surface-confined host and thus the higher is the fraction of successful cycles. The increasing $[H_l]$ and $[H_s]$ have a direct lifetime-reducing effect, because the probability to bind to a new available host becomes larger. The lifetime τ of the unsaturated $G^{II}H_l$ is:

$$\tau = \frac{\ln 2}{k} \tag{6.5}$$

Where k is:

$$k = k_{a,i} \cdot [H_s]_{same} + k_{a,i} \cdot [H_s]_{other} + k_{a,i} \cdot [H_l] \tag{6.6}$$

Here, $[H_l]$ is the concentration of unbound β-CD cavities in the solution, while $[H_s]_{same}$ and $[H_s]_{other}$ are concentrations of free surface hosts experienced by the guest *locally*, and thus resemble more closely C_{eff}.

Assuming an average association rate constant[11] of $k = 10^8 - 10^9$ M^{-1}s^{-1}, the calculated lifetime is expected to be in the range of ns, which allows a few nm mean path length. It has been confirmed by AFM that the β-CD cavity lattice periodicity on the printboard is around 2 nm.[14] The travelled mean displacement during the lifetime of $G^{II}H_l$ decreases when τ decreases, therefore the fraction of successful cycles also decreases. Upon further increase of $[H_l]_{tot}$, although the concentrations of $G^{II}H_sH_l$ and $G^{II}H_l$ remain high, as well as the overall 'hopping' frequency, an increased fraction of the involved guest moieties rebind to the host of origin, suppressing the observed spreading rate. When the β-CD concentration exceeds 2 mM, the lifetime of $G^{II}H_l$ becomes less important because most of the species forms by the dissociation of $G^{II}(H_l)_2$ (Scheme 6.2), and full desorption starts to take over the spreading.

6.3.3 Diffusion of the guests from the surface into the bulk

When a β-CD printboard covered with a SAM of guest molecules is immersed in an aqueous solution, desorption from the surface can take place. The rate of this desorption is mainly determined by the binding affinity of the guest molecules and the surface coverage, and thus the C_{eff} on the surface, which determines the fraction of the free solution species. As a function of valency, coverage and β-CD concentration in solution, a certain concentration of guest species is established near the interface assuming equilibration is rapid. These concentrations can be calculated as described above (see 6.3.1). The guest species in solution, formed near the interface upon desorption, will diffuse into the bulk according to Fick's laws of diffusion. Similarly, when β-CD in solution is present, the desorption near the interface leads to complexation of guest with H_l and therefore, potentially, to depletion of H_l near the interface.

To evaluate: (i) whether equilibration near the interface is fast relative to diffusion into the bulk, (ii) what the expected timescales are for desorption as a function of valency, and (iii) whether depletion of H_l is expected near the interface, model calculations based on Fick's laws were performed. The maximum desorption rates for all the guests can be calculated assuming that the guest-covered printboard functions as an infinite source of the free guest (concentrations summed for all $G(H_l)_n$, where $n = 0 - n_{max}$).

As an example, Figure 6.9 depicts the evolution of the concentration profile of the solution species G^{II} desorbed from a lissamine-Ad$_2$ SAM-covered printboard in pure water. Upon increase of $[H_l]_{tot}$, the time dependence of these curves does not change, only the absolute values. The calculations show that diffusion for > 1 μm takes > 1 ms, while equilibration occurs on the order of the lifetime of an individual β-CD-Ad interaction, which is < 0.1 ms. This confirms that equilibration is rapid compared to diffusion.
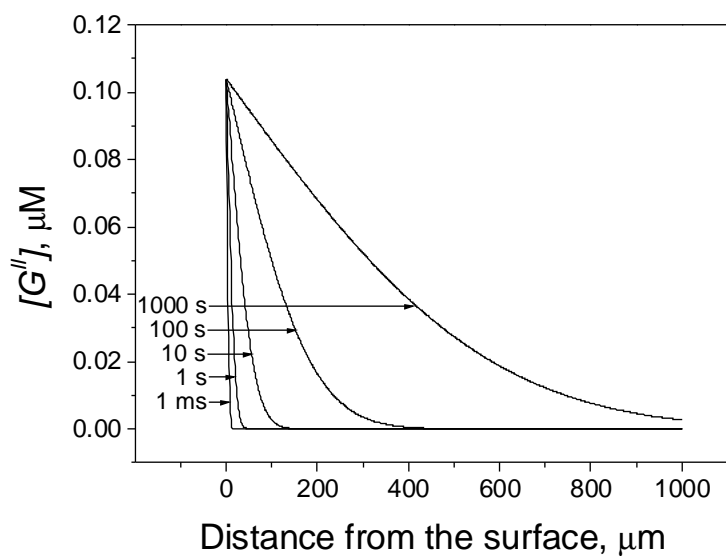
Figure 6.9 Diffusion profiles of G^{II} after its desorption from a divalent guest SAM-covered printboard in water.

The integration of the concentration profiles of Figure 6.9 gives the amounts of desorbed guests per surface area, *M*, after time *t*. Figure 6.10 shows the calculated maximum amounts (in mol/m^2) of desorbed guests (*M*) after a time period of 1 h.
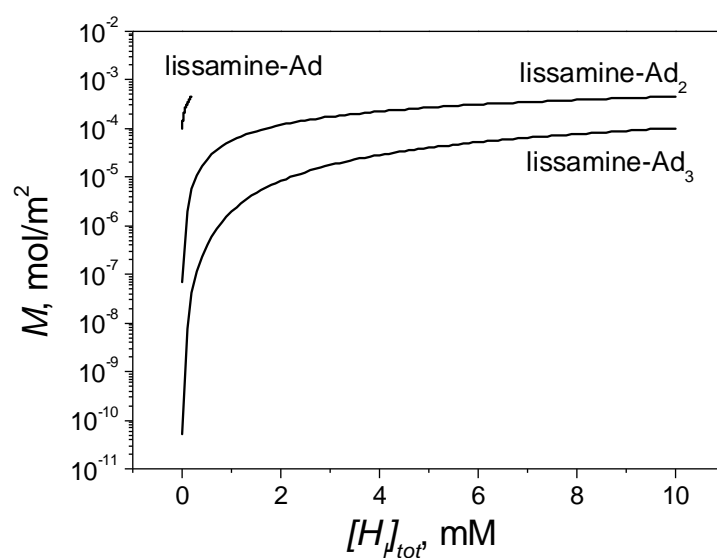

Figure 6.10 Calculated amounts of desorbed mono-, di- and trivalent guests after 1 h as a function of the β-CD concentration in the surrounding solution. The source at the surface is assumed to keep the concentration of solution species near the surface constant.

The guest concentration on the surface at 90 % coverage is in the range of 10^{-7} mol/m^2. In pure water, the trends are as expected: the monovalent guest is desorbing very quickly (order of seconds), while the divalent (on the order of 10^2 h) and trivalent ($\sim 10^6$ h) are stably anchored (see Figure 6.11). However, upon only small concentrations of H$_l$, the concentration of free guest species in solution rapidly increases (Figure 6.7 and 6.8). This (Figure 6.10) suggests that the divalent and even the trivalent guest, at relatively low *[H$_l$]* would completely desorb from the surface within the given timeframe. However, in real experimental conditions the concentrations of solution species near the interface are rapidly decreasing when the guest coverage on the surface is decreasing due to desorption. This effect is exemplified in Figure 6.12, where the concentration of the divalent solution species *[G^{II}]*, plotted as a function of coverage, decreases with three orders of magnitude upon the decrease of the coverage from 90 to 10 %. This significant decrease of available solution species close to the surface will lower the desorption rate and the concomitant diffusion into the bulk, and thus quickly enhance the projected timescales.
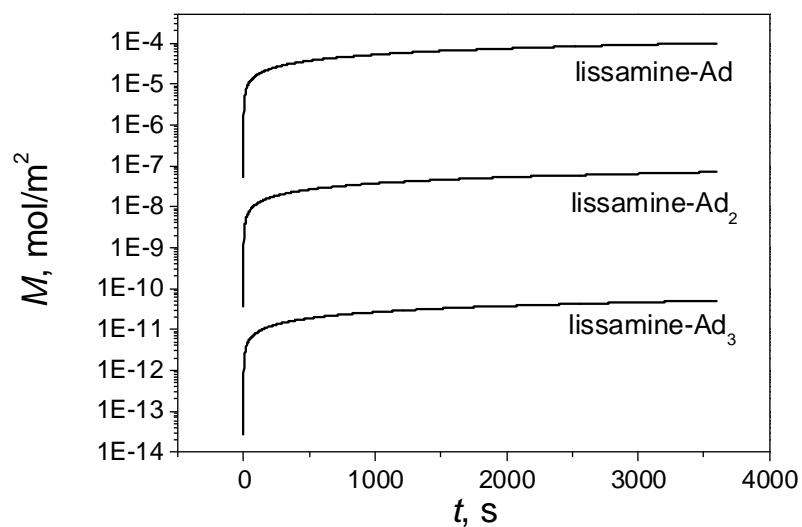

Figure 6.11 Variation of *M* as a function of time *t* and valency. The calculations were performed for a surface 90 % covered by guest molecules in pure water and the source at the surface was assumed to keep the concentration of solution species near the surface constant.
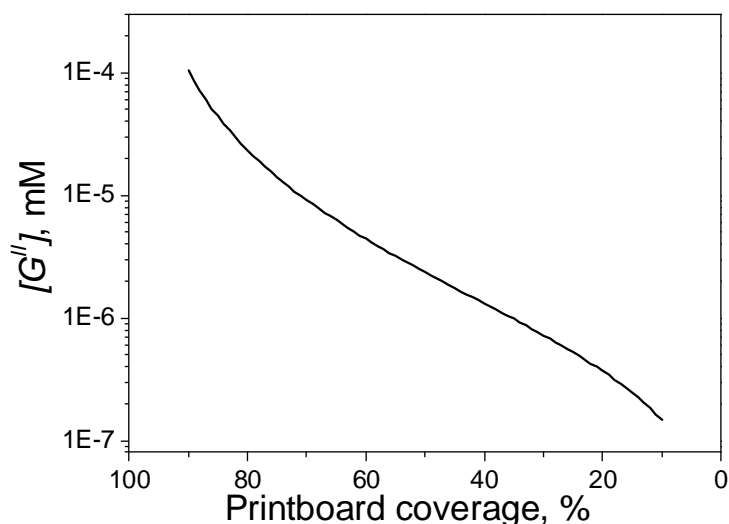
Figure 6.12 Calculated concentration of solution guest species $[G^{II}]$ in pure water as a function of the surface coverage.

For evaluating the effect of depletion of H_l, similar calculations were used. From the fact that the $[H_l]_{tot}$ is always the same or (much) higher than the free guest concentration formed near the surface, rapid repletion of β-CD from the solution is always expected, thus confirming the assumption made above (6.3.1) that $[H_l]$ near the surface is equal to $[H_l]_{tot}$ of the bulk.

6.3.4 Computational modeling of multivalent surface spreading

To complement the kinetic experiments, fully atomistic molecular dynamics (MD) simulations, including an explicit representation of the molecular printboard surface, were used to explore the conformational space available to strongly bound multivalent dendrimers functionalized with ferrocene moieties.[15,16] These simulations allowed to describe the effective concentration of unbound guest moieties at the printboard and to estimate the likelihood of an additional binding interaction. Several nanosecond MD simulations were performed with ferrocenyl-functionalized 0th generation poly(amidoamine) (G0-PAMAM-(Fc)$_4$) and 1st generation poly(propylene imine) (G1-PPI-(Fc)$_4$) dendrimers (Scheme 6.5) bound to the β-CD-based molecular printboard. Although both dendrimers have four end-groups, MD calculations were effectuated using a situation where these ferrocenyl-functionalized dendrimers bind to the printboard with only one or two guest moieties, in accordance with experimental observations.[15]
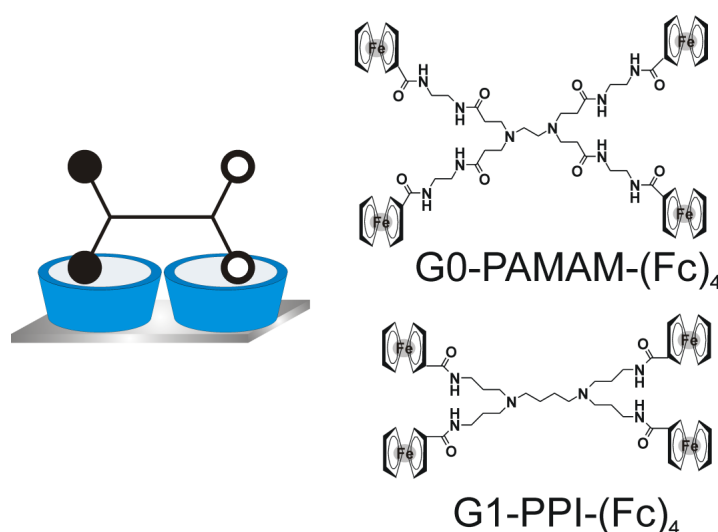
Scheme 6.5 Schematic representation of a dendrimer with four equivalent end-groups using two guest moieties from opposite-branch end-groups (black and hollow) to bind to surface-confined hosts (left); the structures of G0-PAMAM-(Fc)$_4$ (upper right) and G1-PPI-(Fc)$_4$ (lower right).

The results showed that the monovalently bound G0-PAMAM-(Fc)$_4$ has a higher population of unbound guests at positions facilitating the formation of a divalently bound complex by an additional binding interaction. Unbound guest sites of both G0-PAMAM-(Fc)$_4$ and G1-PPI-(Fc)$_4$ on the branch opposite the bound anchor were closest to empty printboard binding sites. Monovalent G0-PAMAM-(Fc)$_4$ adopted a surface-close orientation after approximately 3 ns of dynamics and core:printboard interactions dominated for ~70% of the remaining 7 ns, with distances of 1.5 – 2.0 Å between a dendrimer core proton and secondary hydroxyl oxygens at the entrance to the β-CD cavity, "localizing" the dendrimer at the printboard. The more compact G1-PPI-(Fc)$_4$ maintained a core:β-CD interaction for ~80% of its 10 ns trajectory and so unbound G1-PPI-(Fc)$_4$ anchors remained exclusively at one side of the printboard.

The monovalent G0-PAMAM-(Fc)$_4$ placed in a partial unbinding position showed the movement of the released anchor to the periphery of the dendrimer binding hemisphere (in about 0.5 ns) and then re-approached to the printboard (a further 2.0 ns). This supports the 'walking' mechanism for multivalent dendrimer surface-spreading at low solution β-CD concentrations, involving switching between monovalent and multivalent states and minimizing complete unbinding to bulk solution.

As a support of the 'hopping' mechanism, coarse-grained molecular dynamics simulations with monovalently bound G1-PPI-(Fc)$_4$ on the molecular printboard showed that the dendrimer can dissociate from the surface and diffuse short distances above the printboard before rebinding.[17]

6.4 Conclusions

The intrinsic binding kinetics of a single guest moiety to a β-CD cavity, the equilibrium concentrations and the lifetime of the active species influence the surface spreading rate of a multivalent guest molecule on the β-CD-based molecular printboard. The directional spreading is an C_{eff}-driven process. The thermodynamic overview of the monovalent equilibria was successfully extended to di- and trivalent systems with the use of the theoretical parameter C_{eff}, allowing the numerical calculation of the equilibrium concentrations. These equilibrium concentrations can explain the rate *increase* but not the *decrease* for multivalent spreading rates. The lifetime decrease of the unsaturated guest in the solution causes a decreasing mean displacement and a lower fraction of successful dissociation-association cycles explaining the spreading rate decrease by a 'hopping' mechanism at intermediate β-CD concentrations.

The molecular understanding of the kinetics of multivalent interactions on surfaces offers an increased insight into recognition processes on biological cell membranes and new strategies for the design of pharmaceutical agents based on multivalency.

6.5 Experimental

Synthesis. All starting materials are commercially available and were used as received. Linker-Ad, linker-Ad$_2$ were synthesized according literature procedures.[18] Lissamine-Fc$_2$ was synthesized by Henk Dam. The synthesis of [[[2-[2-(2-aminoethoxy)ethoxy]ethyl]amino]carbonyl]-ferrocene has been described before,[15] we used, however, a modified procedure which consists of only two steps starting from the commercially available (Fluka) 11-Azido-3,6,9-trioxaundecan-1-amine and ferrocenylcarbonyl chloride, giving [[[2-[2-(2-azidoethoxy)ethoxy]ethyl]-amino]carbonyl]-ferrocene in 75% yield. 5-[(tert-Butyloxycarbonyl)amino]isophthalic acid was then synthesized starting from the commercially available (Aldrich) 5-aminoisophthalic acid according to a literature procedure in 74% yield.[20] The obtained

diacid was subsequently converted to its diacylchloride. In the ^{1}H NMR spectrum from the diacylchloride the two peaks coming from the phenyl protons were shifted to lower field with respect to the phenyl protons from the diacid. The diacylchloride was then coupled with Fc-PEG$_4$NH$_2$ giving the divalent ferrocenyl linker. The coupling of Fc-PEG$_4$NH$_2$ with lissamine rhodamine B sulfonyl chloride was performed according to the procedure described in Chapter 5.

[[[2-[2-(2-Azidoethoxy)ethoxy]ethyl]amino]carbonyl]-ferrocene. A suspension of 11-azido-3,6,9-trioxaundecan-1-amine (1.56 g, 7.14 mmol), ferrocenylcarbonyl chloride (1.78 g, 7.14 mmol) and K$_2$CO$_3$ (4.9 g, 35.7 mmol) was stirred at rt in 40 ml CH$_2$Cl$_2$ for 15 h. The K$_2$CO$_3$ was filtered over celite. Evaporation of the volatiles afforded a red brown oil which was subjected to column chromatography (eluent CH$_2$Cl$_2$/MeOH, 14/1) yielding the product (2.30 g, 75%) as a dark red oil. ^{1}H NMR (ppm): δ = 6.23 (1 H, bs, N*H*), 4.68 (2 H, s, Fc), 4.33 (2 H, s, Fc), 4.20 (5 H, s, Fc), 3.70-3.58 (16 H, m, NHC*H*$_2$C*H*$_2$OC*H*$_2$C*H*$_2$O-), 3.38 (2 H, t, *J* 5.1, CH$_2$C*H*$_2$N$_3$). ^{13}C NMR (ppm): δ = 170.5, 167.9, 72.92, 72.68, 71.02-69.95, 68.38, 50.85, 39.45. MALDI-TOF-MS *m/z* = 430.3 [M]$^{+}$, calcd. 430.3.

[[[2-[2-(2-Aminoethoxy)ethoxy]ethyl]amino]carbonyl]-ferrocene. 11-Azido-3,6,9-trioxaundecan-1-ferrocenylamide (1.81 g, 4.20 mmol) was hydrogenated under 1 bar of H$_2$(g) atmosphere by stirring for 5 h at rt in 50 ml methanol with a catalytical amount of 10% Pd/C. The catalyst was removed by filtration over celite. Evaporation of the volatiles yielded the pure product as a red oil (1.64 g, 97%). The results of the analytical analysis (^{1}H NMR and mass spectrometry) corresponded with the data described in literature.[19]

***N*-[3,5-bis[[[2-[2-(2-Aminocarbonylferroceneethoxy)ethoxy]ethyl]-1-ylamine]-carbonyl]phenyl]-,1,1-dimethylethylester.** 5-[[(1,1-Dimethylethoxy)carbonyl]-amino]-1,3-benzenedicarboxylic acid (1.22 g, 4.35 mmol) was suspended in a mixture of toluene (70 ml) and DMF (0.5 ml), to this was added pyridine (4.2 ml) and oxalylchloride (1.49 ml, 17.4 mmol). After stirring the mixture for 7 h at rt the formed precipitate was removed by filtration, the residue was washed with toluene. The volatiles of the filtrate were evaporated under reduced pressure at rt to give 1.30 g of

N-[3,5-bis(chlorocarbonyl)phenyl-,1,1-dimethylethylester which was directly used without further purification due to its hygroscopic properties. The diacid chloride (0.086 mg, 0.27 mmol) was dissolved in 0.5 ml pyridine, to this was added a solution of [[[2-[2-(2-Aminoethoxy)ethoxy]ethyl]amino]carbonyl]-ferrocene (0.219 g, 0.541 mmol) in 0.5 ml pyridine and 1 ml DMF. The resulting solution was stirred for 32 h at rt. After the volatiles were removed under reduced pressure at rt, the residue was taken up in 20 ml CH_2Cl_2 and washed (3 × 10 ml H_2O). The organic layer was dried with $MgSO_4$. Evaporation of the solvent gave 0.126 g of a red oil which was subjected to column chromatography (eluent CH_2Cl_2/MeOH, 9/1) yielding the product (0.025 g, 9%) as a red oil. ^{1}H NMR (ppm): δ = 8.04 (2 H, s, PhH), 7.93 (1 H, s, PhH), 7.21 (2 H, s, NH), 6.49 (2 H, s, NH), 4.69 (4 H, t, *J* 1.8, Fc), 4.29 (4 H, s, Fc), 4.17 (10 H, s, Fc), 3.74-3.58 (28 H, m, NHC*H₂*C*H₂*OC*H₂*C*H₂*O), 3.52 (4 H, t, *J* 5.4, (C*H₂*NHC(O)Ph), 1.51 (9 H, s, NHC(O)C(C*H₃*)₃. ^{13}C NMR (ppm): δ = 170.6, 166.7, 152.9, 139.4, 135.6, 120.2, 120.0, 70.52-70.10, 69.77, 68.24, 40.02, 39.30, 28.36. MALDI-TOF MS *m/z* = 1055.6 [M]$^+$, calcd. 1055.7.

[3,5-bis[[[2-[2-(2-aminocarbonylferroceneethoxy)ethoxy]ethyl]-1-ylamine]carbonyl]phenylamine (Fc-PEG₄NH₂). N-[3,5-bis[[[2-[2-(2-Amino-carbonylferrocene-ethoxy)ethoxy]ethyl]-1-ylamine]-carbonyl]phenyl]-,1,1-dimethylethylester (0.050 g, 0.047 mmol) was dissolved in CH_2Cl_2 (1 ml). Slowly a mixture of TFA (0.11 ml) and CH_2Cl_2 (0.5 ml) was added at rt. The resulting mixture was stirred at rt for 220 min. The mixture was diluted with CH_2Cl_2 (10 ml) and washed (2 × 5 ml 0.1 M NaOH). The organic layer was dried with $MgSO_4$. Evaporation of the volatiles at reduced pressure gave 0.051 g of crude product which was subjected to column chromatography (eluent CH_2Cl_2/MeOH, 10/1) yielding the product (0.025 g, 55%) as a red oil. ^{1}H NMR (ppm): δ = 7.54 (1 H, s, PhH), 7.23 (2 H, s, PhH), 6.94 (2 H, s, NH), 6.40 (2 H, s, NH), 4.70 (4 H, t, *J* 1.8, Fc), 4.31 (4 H, t, *J* 2.1, Fc), 4.19 (10 H, s, Fc), 3.66-3.59 (28 H, m, NHC*H₂*C*H₂*OC*H₂*C*H₂*O), 3.51 (4 H, t, *J* 5.4, (C*H₂*NHC(O)Ph). ^{13}C NMR (ppm): δ = 170.5, 167.2, 147.3, 135.9, 116.2, 114.9, 70.36-69.67, 68.84, 68.24, 68.13, 39.88, 39.26. MALDI-TOF MS *m/z* = 954.3 [M]$^+$, calcd. 953.6.

[3,5-bis[[[2-[2-(2-aminocarbonylferroceneethoxy)ethoxy]ethyl]-1-ylamine]carbonyl]phenyllissamide (Lissamine-Fc₂). Fc-PEG₄NH₂ (0.072 g, 0.076

mmol), lissamine rhodamine B sulfonyl chloride (0.088 g, 0.151 mmol) and diisopropylethylamine (DIPEA) (0.16 ml, 1.51 mmol) was dissolved in CH_2Cl_2 (3 mL) and stirred at rt for 76 h. Evaporation of the volatiles at reduced pressure gave 0.305 g crude product which was subjected to column chromatography (eluent CH_2Cl_2/MeOH, 10/1) yielding 0.100 g of a purple oil consisting of a mixture of 70% lissamine-Fc$_2$ and 30% Fc-PEG$_4$NH$_2$ (58% yield of lissamine-Fc$_2$) as judged from the integration of the PhH peak at 7.89 ppm of the product and that of the PhH of the starting amine at 7.54 ppm. MALDI-TOF MS m/z = 1494.6 [M]$^+$ and 954.3 [M]$^+$ (amine), calcd.+ 1494.6 and 953.6.

Calorimetry. Calorimetric measurements were carried out using a Microcal VP-ITC instrument with a cell volume of 1.4115 mL. Solutions for titration were prepared in Milipore water and in 10 % methanol containing aqueous mixtures. Titrations were performed by adding 5 μL aliquots of a 10 mM β-CD solution to a 1 mM solution of tetraethylene glycol-functionalized adamantyl.

Spreading experiments. Substrate preparation, microcontact printing and spreading experiments have been described in the previous chapter (Chapter 5), and the same procedure was used here. Backfilling with linker-Ad$_2$ was achieved by immersion of the samples in a 0.1 mM linker-Ad$_2$ aqueous solution for 10 s. Low coverage of the mixed divalent SAM was achieved by rinsing with 20 % ethanol in water for 30 s.

Theoretical calculations. Numerical calculations of the equilibria[10] concentrations and the diffusion profiles were performed using Matlab software. Values of 4.6×10^4 M^{-1} for the intrinsic binding constant, 0.2 M for the maximum effective concentration, 2 nm for the β-CD cavity lattice periodicity on the printboard and 10^{-10} m^2/s for the diffusion constant of the solution species were used to perform the calculations.
MD simulations were performed by Damien Thompson at Tyndall National Institute, Cork, Ireland. The four-legged dendrimer molecules G0-PAMAM-(Fc)$_4$ and G1-PPI-(Fc)$_4$, were each built with protonated core amines to simulate the low-pH conditions. β-CD molecules were then added to make dendrimer:printboard complexes. A 70 Å cubic box of water was overlaid, and waters overlapping the complex removed. Periodic boundary conditions were assumed; i.e. the entire 70 Å box was replicated

periodically in all directions, completely solvating the complex. Standard CHARMM22 force field parameters were used for β-CD and the dendrimers. A slightly modified TIP3P model was used for the water. Bonds involving hydrogen were constrained to their experimental lengths with the SHAKE algorithm, allowing the use of a 2 fs timestep for dynamics. A CHARMM program version c31b2 was used for all calculations.

Ten nanoseconds (10 ns) of molecular dynamics were performed (for each system) at constant, room temperature and pressure with a Nosé-Hoover algorithm, following 100 picoseconds of thermalisation.

6.6 References

1   J. Huskens, *Curr. Opin. Chem. Biol.* **2006**, *10*, 537.

2   M. J. W. Ludden, D. N. Reinhoudt, J. Huskens, *Chem. Soc. Rev.* **2006**, *35*, 1122.

3   M. Mammen, S. K. Choi, G. M. Whitesides, *Angew. Chem. Int. Ed.* **1998**, *37*, 2755.

4   B. T. Houseman, M. Mrksich, in *Host-Guest Chemistry*, 218, **2002**, 1.

5   A. Mulder, J. Huskens, D. N. Reinhoudt, *Org. Biomol. Chem.* **2004**, *2*, 3409.

6   L. Mandolini, *Adv. Phys. Org. Chem.* **1986**, *22*, 1.

7   T. Auletta, M. R. de Jong, A. Mulder, F. van Veggel, J. Huskens, D. N. Reinhoudt, S. Zou, S. Zapotoczny, H. Schonherr, G. J. Vancso, L. Kuipers, *J. Am. Chem. Soc.* **2004**, *126*, 1577.

8   M. R. de Jong, J. Huskens, D. N. Reinhoudt, *Chem. Eur. J.* **2001**, *7*, 4164.

9   A. Mulder, T. Auletta, A. Sartori, S. Del Ciotto, A. Casnati, R. Ungaro, J. Huskens, D. N. Reinhoudt, *J. Am. Chem. Soc.* **2004**, *126*, 6627.

10   J. Huskens, A. Mulder, T. Auletta, C. A. Nijhuis, M. J. W. Ludden, D. N. Reinhoudt, *J. Am. Chem. Soc.* **2004**, *126*, 6784.

11   C. Bohne, *Langmuir* **2006**, *22*, 9100.

12   Y. Liao, C. Bohne, *J. Phys. Chem.* **1996**, *100*, 734.

13   M. V. Rekharsky, Y. Inoue, *Chem. Rev.* **1998**, *98*, 1875.

14   M. W. J. Beulen, J. Bügler, M. R. de Jong, B. Lammerink, J. Huskens, H. Schönherr, G. J. Vancso, B. A. Boukamp, H. Wieder, A. Offenhauser, W. Knoll, F. C. J. M. van Veggel, D. N. Reinhoudt, *Chem. Eur. J.* **2000**, *6*, 1176.

15   C. A. Nijhuis, F. Yu, W. Knoll, J. Huskens, D. N. Reinhoudt, *Langmuir* **2005**, *21*, 7866.

16   D. Thompson, *J. Phys. Chem. B* **2008**, *112*, 4994.

17   M. Cieplak, D. Thompson, *J. Chem. Phys.* **2008**, *128*, 234906.

18   A. Mulder, S. Onclin, M. Péter, J. P. Hoogenboom, H. Beijleveld, J. ter Maat, M. F. García-Parajó, B. J. Ravoo, J. Huskens, N. F. van Hulst, D. N. Reinhoudt, *Small* **2005**, *1*, 242.

19   A. Aguilar-Aguilar, A. D. Allen, E. P. Cabrera, A. Fedorov, N. Y. Fu, H. Henry-Riyad, J. Leuninger, U. Schmid, T. T. Tidwell, R. Verma, *J. Org. Chem.* **2005**, *70*, 9556.

20   J. Bitta, S. Kubik, *Org. Lett.* **2001**, *3*, 2637.

Self-assembled monolayers of α-cyclodextrin derivatives on gold and their host-guest behavior

Three sulfur-modified α-CD derivatives formed ordered monolayers on gold surfaces as confirmed by water contact angle goniometry, electrochemistry, X-ray photoelectron spectroscopy and atomic force microscopy measurements. SAMs of the adsorbates showed high polarity, uniform monolayer arrangement and low charge-transfer resistance. Electrochemical capacitance measurements were used to determine the binding affinity of aliphatic carboxylic acid salts with four, six and eight carbon atoms. The non-methylated cyclodextrin host-guest pairs showed 1-2 orders of magnitude higher binding constants on surfaces than in solution.

7.1 Introduction

The molecular recognition ability of self-assembled monolayers (SAMs) of host molecules on surfaces offers a selective attachment and accurate, but reversible, positioning of molecules.[1] These characteristics are the main prerequisites for the development of sensing applications and molecular electronics.[2-4] A high degree of order and packing in the host SAM is needed in order to render the surface-confined cavities identical for complexation and to minimize nonspecific adsorption.

Cyclodextrins (CDs) are naturally occurring water-soluble cyclic oligosaccharides consisting of glucose units connected via α-1,4-glycosidic linkages.[5,6] All the naturally occurring CDs (α-CD consists of 6, β-CD of 7 and γ-CD of 8 glucose units) have a truncated cone shape with a hollow, tapered cavity.

Sulfur-modified CD derivatives have been used previously for the preparation of SAMs on gold, and most of the work has been performed with β-CD and some with α-CD derivatives.[7-11] Perthiolated CD derivatives, in which all the primary hydroxyl groups have been replaced by thiol groups, form SAMs with a relatively poor coverage, due to the multiple and strong thiol-gold interaction which prevents self-correction during SAM formation. Our group has introduced and extensively studied SAMs of CD heptathioether derivatives on gold.[12,13] These molecules form well ordered and densely packed SAMs exposing the secondary sides of the CD rings to the solution. The cross-section of the supporting alkyl chains was estimated to be larger than the cross-section of the CD ring, resulting in the complete filling of the space underneath the CD headgroup, and thus intercalation in the monolayer of other molecules was prevented. However, the dense alkyl layer can act as an insulator and impede applications where electron transfer to and from the gold surface is involved.

In this chapter, the SAM formation ability of sulfur-modified α-CD derivatives without alkyl chains is investigated. The SAMs of three α-CDs with different anchoring configurations have been characterized by means of water contact angle goniometry, electrochemistry, X-ray photoelectron spectroscopy (XPS) and atomic force microscopy (AFM). The host-guest complexation of the host adsorbates has been studied by electrochemical capacitance measurements.

7.2 Results and discussion

7.2.1 Preparation and characterization of the CD SAMs

$6^A,6^B$-Di-sulfanil-α-CD (**1**), α-CD-intramolecular disulfide (**2**) and permethylated α-CD dithioether (**3**) were used as host adsorbates in this study (see Chart 7.1).
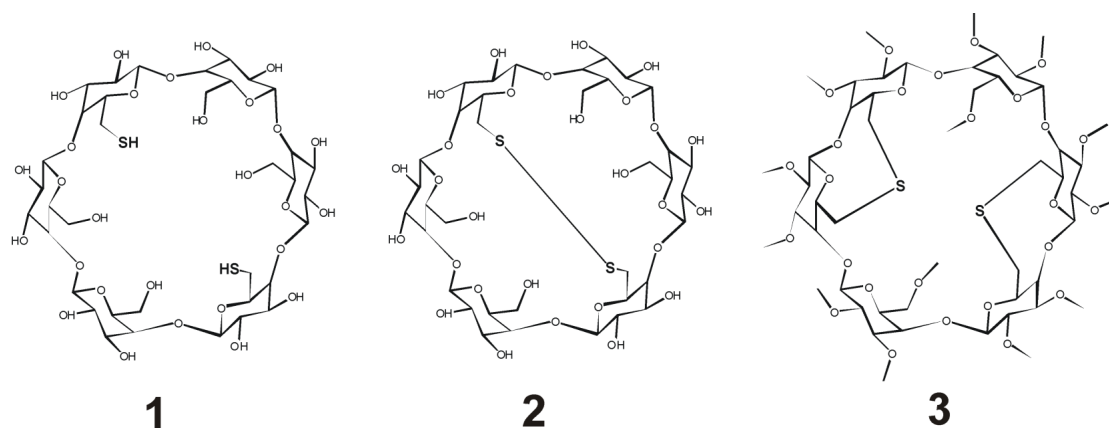

Chart 7.1 Host adsorbates used in this study.

Monolayers of **1**, **2** and **3** were prepared by immersion of clean gold substrates in 0.1 mM adsorbate solutions, in ethanol, overnight at room temperature. Table 7.1 summarizes the main characterization results.

Table 7.1 Properties of the prepared SAMs.

SAM	θ_a/θ_r (H$_2$O, deg)[a]	C_{ml} (F/m^2)[b]	R_{CT} (Ω)[c]	XPS-S$_{2p}$ (% S bound)[d]	AFM thickness (nm)[e]
1	26 / <10	0.21	400	77	0.7
2	23 / <10	0.15	110	81	0.7
3	69 / 42	0.07	20	44	0.5

[a] Advancing (θ_a) and receding (θ_r) contact angles of the monolayer with water. [b] Capacitance of the monolayer determined by cyclic voltammetry at a scan rate of 0.1 V/s at -0.25 V. [c] Charge-transfer resistance of the monolayer determined by impedance spectroscopy. [d] Percentage of sulfur bound to gold. [e] Monolayer thickness determined by AFM "molecular ruler" experiments.

Contact angle goniometry provides information about the polarity of the SAM. The low θ_a of the SAMs of dithiol **1** and disulfide **2** indicates a polar surface, which is in accordance with the hydroxyl groups of the rim of the CD exposed to the solution.

Bis-thioether **3** contains methoxy groups exposed to the solution, and thus shows higher θ_a and θ_r values.

Cyclic voltammetry in an inert electrolyte was used to determine the capacitance of the monolayers.[14-16] If no electrochemical reactions occur in the applied potential range, it may be assumed that nonfaradaic processes govern the changes at the electrode-solution interface. The electrode adsorbs ions, resulting in an electrical double layer, which provides a capacitance to the surface. This capacitance of the electrical double layer (C_{dl}) can be calculated from the measured current intensity:

$$C_{dl} = \frac{i}{A \cdot v} \qquad\qquad (7.1)$$

where i is the current intensity, A is the area of the electrode and v is the scan rate of the voltammetry measurement. In the presence of a monolayer on the electrode surface, the additional capacitance of the monolayer (C_{ml}) is significantly lower than C_{dl}. This system can be represented as a circuit containing two capacitors in series; therefore the total capacitance of the surface is equal to C_{ml} (since $1/C_{tot} = 1/C_{dl} + 1/C_{ml}$).

In Figure 7.1, the cyclic voltammograms of the studied SAMs taken in 0.1 M K_2SO_4 electrolyte solutions are presented. The halve of the current intensity difference between the forward and the reverse scans in the voltammograms was used to calculate the capacitance of the monolayers (Equation 7.1).

The capacitance of a monolayer is related to the effective thickness, the dielectric constant and the order of the SAM.[16] The higher C_{ml} of the dithiol **1** samples suggests less order or more water molecules present on the dithiol SAM-covered gold surface. Both **1** and **2** showed capacitances similar to the value reported by Kaifer (0.11 F/m^2) for a monolayer of per-7-deoxy-(7-thio)-β-cyclodextrin.[7] The decreased C_{ml} of **3** is probably caused by the presence of additional methoxy groups which lowers the dielectric constant of **3**.
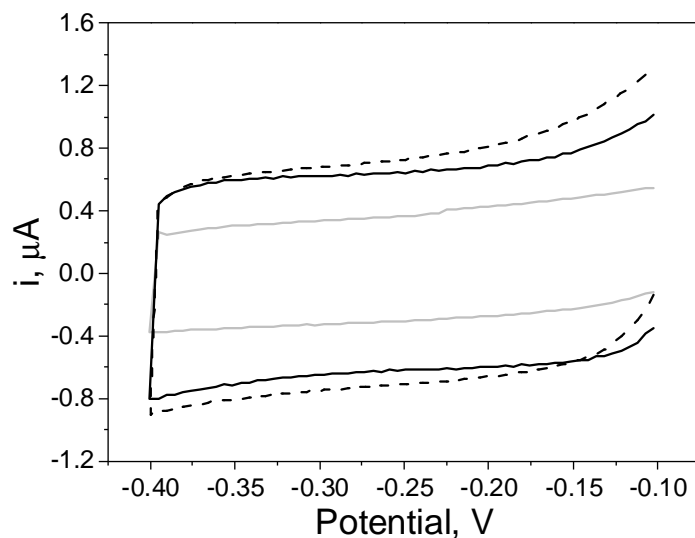
Figure 7.1 Cyclic voltammograms of the dithiol **1** (dashed), the disulfide **2** (black) and bis-thioether **3** (grey) SAM-covered gold electrodes. Supporting electrolyte was 0.1 M K_2SO_4, scan rate 100 mV/s

The ionic insulating properties of SAMs can be measured by electrochemical impedance spectroscopy.[17] This is an alternating current technique and uses very small alternating excitation amplitudes, the frequency of which is varied in the presence of an electrochemically active species. The resulting current has an amplitude and phase which differ from the applied potential. Impedance data are represented as a plot of the real part of the impedance (Z_{real}) versus the imaginary part (Z_{imag})[18] (see Figure 7.2).

All tested samples showed low insulating properties in comparison with long-chain alkanethiol SAMs, which show resistances on the order of several kΩ, suggesting that $Fe(CN)_6^{3-}$ / $Fe(CN)_6^{4-}$ could easily access the gold surface. The resistance of a SAM of **3** toward the external ferro/ferri cyanide redox couple was the smallest, indicating a high number of pinholes present in the monolayer.
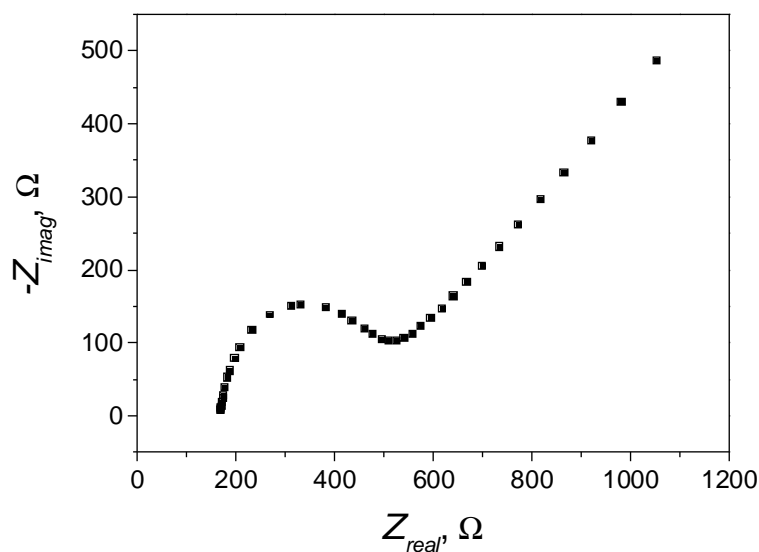
Figure 7.2 Nyquist plot of a SAM of dithiol **1** determined by electrochemical impedance spectroscopy in 1 mM $Fe(CN)_6^{3-}$ / $Fe(CN)_6^{4-}$ and 0.1 M K_2SO_4.

XPS was used to determine the average ratio of bound to unbound sulfur in the studied SAMs.[19] Adsorption of sulfur to gold results in a shift to lower energies of the XPS signal. $S_{2p\ 3/2}$ and $S_{2p\ 1/2}$ peaks from the sulfur signal were monitored, and the fitting with two double S_{2p} peaks was used to determine the fraction of bound sulfur (see Figure 7.3).
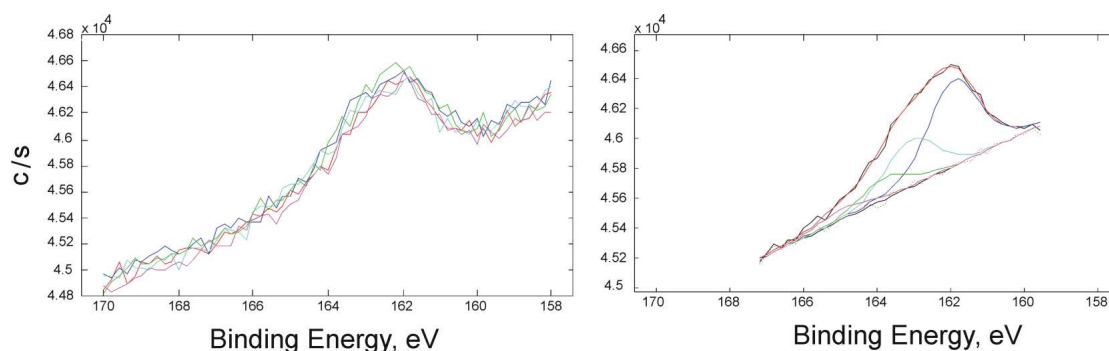
Figure 7.3 S_{2p} region of the XPS spectrum of a SAM of **2** on 20 nm evaporated gold (left: five spectra; right: fitting of the average spectrum).

Sulfur gives a very weak signal in XPS, especially when SAMs of adsorbates with a low sulfur fraction are used. The fit to the XPS spectra of Figure 7.3 provides more an approximate indication of the bound fraction rather than a reliable value. The results show that most of the adsorbate molecules use both their sulfur atoms to bind to the

gold surface, which indicates a relatively ordered monolayer where the CD molecules expose their secondary sides to the solution. Bis-thioether **3** uses on average less sulfur to bind to the gold, and thus indicates a less ordered SAM.

"Molecular ruler"[20] experiments were performed by AFM to determine the thickness of the CD SAMs prepared by immersion in solution. Octadecanethiol (ODT) stripes were microcontact printed on bare gold substrates which were afterwards immersed in 0.1 mM adsorbate solutions in ethanol to grow CD SAMs on the free parts of the gold surface. By measuring the height difference in- and outside the ODT SAM areas before and after CD monolayer formation, the thickness of the formed CD SAMs was estimated (Table 7.1, Figure 7.4).
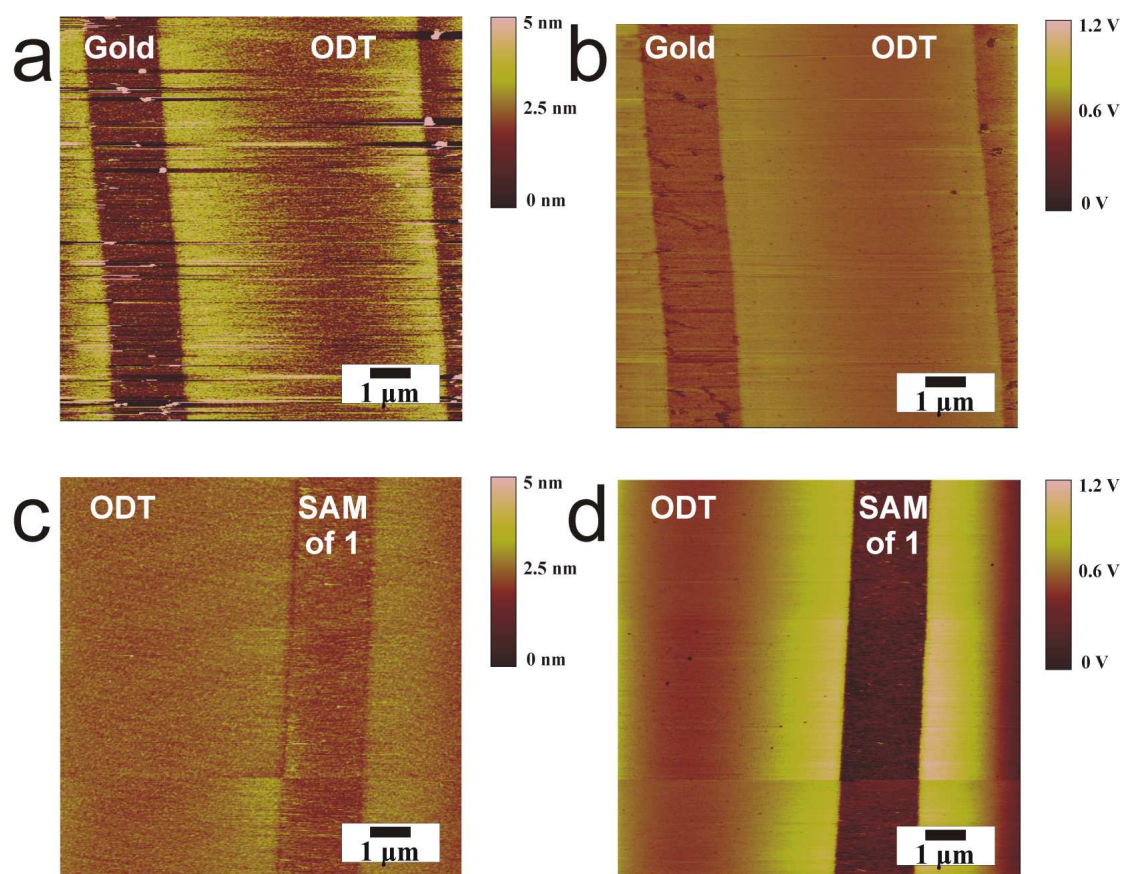
Figure 7.4 Contact mode AFM height (a, c) and friction (b, d) images of a gold surface patterned by µCP of ODT before (a, b) and after (c, d) immersion into a solution of **1**.

A clear change in the height difference between Figure 7.4a and c is attributed to SAM formation of **1** on gold in the empty areas. The measured height differences suggested a monolayer thickness of 0.7 nm for both the dithiol **1** and the disulfide **2**,

which is in a good agreement with the dimensions of a CD molecule. Compound **3** showed a SAM thickness of 0.5 nm.

The characterization of the CD monolayers suggests that all studied compounds form stable monolayers on gold. SAMs of dithiol **1** and disulfide **2** showed better order than SAMs of bis-thioether **3**. The packing and the quality of all monolayers proved to be good enough to perform host-guest complexation studies on these SAMs.

7.2.2 Complexation of guests at SAMs studied by capacitance measurements

It was shown in the previous section that cyclic voltammetry in simple electrolytes gives information about the capacitance of the monolayer on the electrode surface. If the monolayer is impermeable to the ionic species in the electrolyte, it behaves like an ideal capacitor with the capacitance given by the relation:[14,16]

$$C_{ml} = \frac{\varepsilon \cdot \varepsilon_0}{d_{eff}} \qquad (7.2)$$

where ε is the dielectric constant of the SAM, ε_0 is the permittivity of vacuum (8.9×10^{-12} F/m) and d_{eff} is the effective thickness of the SAM. Therefore, the capacitance of a SAM increases with a decreasing separation between the electrode surface and the plane of the closest approach of ionic species from the electrolyte (d_{eff}) and also increases with the polarizability of the separating medium (ε). Intercalating water molecules in the SAM have a significant influence on ε of the monolayer. During the linear potential sweep of the voltammetry measurement the charging current is independent of potential and electrolyte, and proportional to the scan rate.[15]

However, SAMs of sulfur-modified α-CD derivatives in the studied system can not be considered perfectly impermeable to the ionic species (in contrast to well-packed and ordered alkylthiol SAMs),[15] due to the hollow structure of the molecules, the absence of an alkyl layer, and the possible defects in packing. The increased permeability of the monolayer causes a larger time dependence of the measured current intensities and thus larger capacitances for slower scan rates.[14,16]

Complexation of guests to the surface-confined cavities implies the increase of the effective thickness of the monolayer and possibly causes the removal of water molecules present in the CD cavity. Generally, permeation of ionic species through guest-complexed cavities becomes less likely. At host-guest equilibrium, the surface coverage of the guest is constant at unaltered guest concentration. By increasing the

guest concentration in the solution the coverage is expected to follow a Langmuir isotherm,[12] which is reflected by changes of C_{ml}.

Potassium salts of butyric (CH_3-$(CH_2)_2$-COO^-) (ButA), hexanoic (CH_3-$(CH_2)_4$-COO^-) (HexA) and octanoic acid (CH_3-$(CH_2)_6$-COO^-) (OctA) were used as guests to study the complexation to monolayers of **1**, **2** and **3** on gold. Isothermal titration calorimetry (ITC) was used to determine the binding constant of the guests to native and permethylated α-CD in solution. ITC measurements with **1**, **2** and **3** were impossible due to the low quantity of available adsorbate molecules. It is assumed that substitution of two hydroxyl groups at the primary side of α-CD with sulfur hardly influences the complexation properties of **1** and **2**. The ITC titration curves of ButA, HexA and OctA are presented in Figure 7.5.
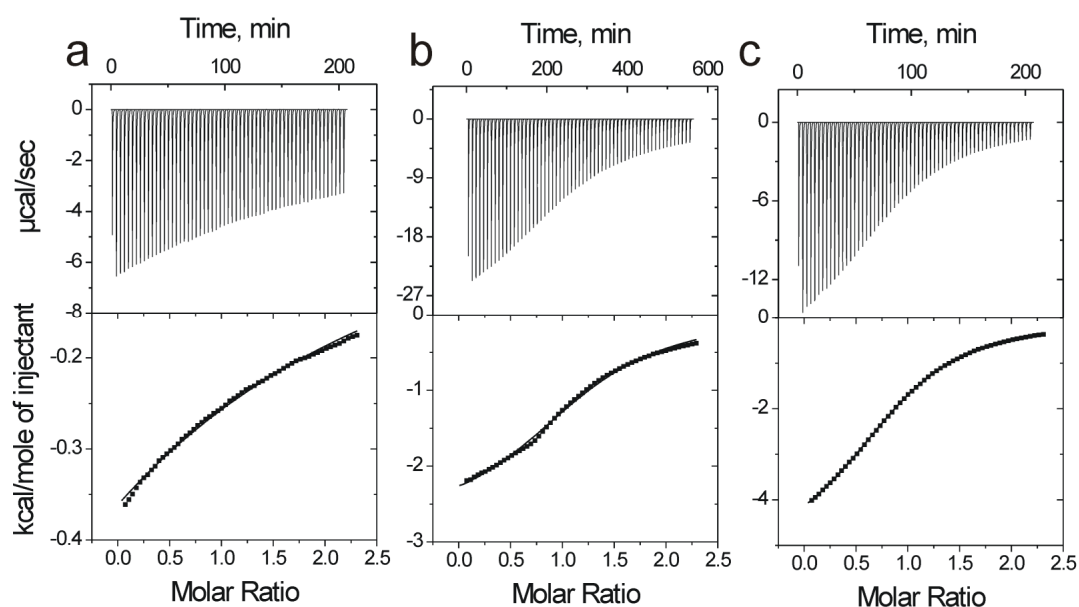
Figure 7.5 Data of heat evolution upon injection of an aqueous solution of α-CD and the resulting binding curves (markers) and best fits (line) to a 1:1 model from calorimetric titrations of (a) ButA, (b) HexA and (c) OctA (all 1 mM) with α-CD (10 mM) in 0.1 M K_2SO_4 aqueous solution at 25°C.

Table 7.2 depicts the thermodynamic parameters obtained from the calorimetric titrations of HexA and OctA with α-CD.

Table 7.2 Thermodynamic parameters of the complexation of α-CD to HexA and OctA, as determined by ITC at 298 K.

SAM	K	ΔG	ΔH	$T\Delta S$
	(M^{-1})	(kcal/mol)	(kcal/mol)	(kcal/mol)
HexA	3.5×10^2	-3.4	-4.9	-1.5
OctA	1.9×10^3	-4.5	-5.2	-0.7

No significant binding affinity of ButA to α-CD was detected (K < 50). OctA showed a significantly higher binding strength to α-CD than HexA. ITC with permethylated α-CD showed no binding affinity to any of the guests. Permethylation of CD breaks the hydrogen bond arrays, reduces rigidity, and therefore could lead to collapse of the cavity and loss of recognition ability.[5]

Electrochemical capacitance measurements on SAMs of **1**, **2** and **3** were performed at various guest concentrations. In all cases the current intensity (*i*) in the voltammograms showed a linear dependence on the scan rate (*v*), independently of the guest concentration in the electrolyte (Figure 7.6). The permeability to ionic species of the CD SAMs causes significant current intensity increase, and thus decrease of C_{ml}, with increasing scan rates.

The capacitance of the monolayer was calculated from Equation 7.1 and plotted as a function of the guest concentration in the electrolyte (Figure 7.7). As a reference a SAM of 11-mercapto-1-undecanol was used to test nonspecific adsorption of the guests. The results are presented in Figure 7.7.

In the presence of a guest, the SAM surface is a collection of free and bound cavities in parallel. The overall capacitance is therefore assumed to be linearly proportional to the coverage (because for capacitances in parallel holds: $C_{tot} = \sum_i C_i$).
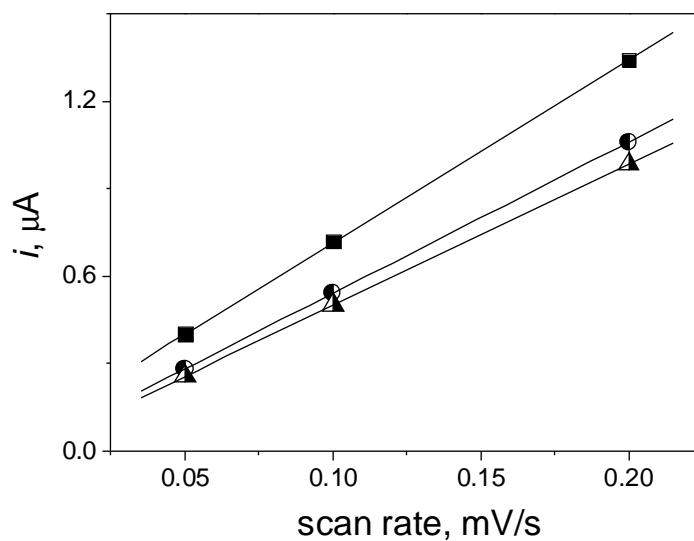
Figure 7.6 The plot and the linear fit of current intensity measured for SAMs of dithiol **1** as a function of scan rate v in 0.1 M K$_2$SO$_4$ and 0 mM (■), 0.5 mM (◐) and 5 mM (▲) HexA solutions.
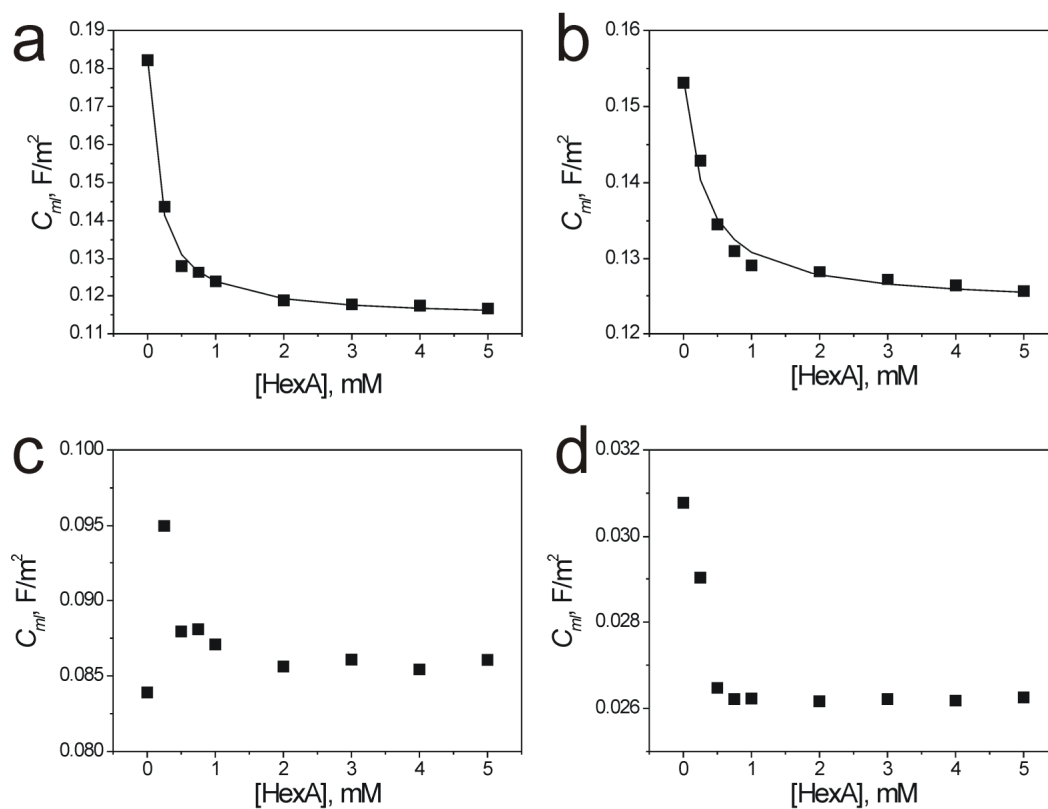

Figure 7.7 Dependence of C_{ml} (at a scan rate of 50 mV/s) of SAMs of dithiol **1** (a), disulfide **2** (b), bis-thioether **3** (c) and 11-mercapto-1-undecanethiol as a reference (d) on the concentration of HexA. The fit (solid lines) was performed based on Equation 7.5.

Therefore, assuming that C_{ml} changes linearly with the surface coverage of the guest bound at the host SAM, the binding constant of the host-guest interaction on the surface can be determined. The surface coverage of the guest (θ) on the CD monolayer is expressed by Equation 7.3:

$$\theta = \frac{K \cdot [G]}{1 + [G]} \tag{7.3}$$

where K is the binding constant and $[G]$ is the guest concentration in the solution. The capacitance of the monolayer C_{ml} is the coverage-weighed sum of the capacitance of the free, unbound surface-confined CD cavities ($C_{ml,f}$) and the capacitance of guest-bound CD molecules ($C_{ml,b}$).

$$C_{ml} = (1 - \theta) \cdot C_{ml,f} + \theta \cdot C_{ml,b} \tag{7.4}$$

Combining Equations 7.3 and 7.4, and expressing C_{ml} as a function of K gives:

$$C_{ml} = \frac{C_{ml,b} \cdot K \cdot [G] + C_{ml,f}}{1 + K \cdot [G]} \tag{7.5}$$

Variation of C_{ml} at increasing guest concentrations followed an adsorption isotherm (see Figure 7.7a and b) in case of SAMs of compound **1** and **2** as a sign of host-guest interactions on the surfaces. In case of SAMs of bis-thioether **3**, the low absolute changes of C_{ml} suggest nonspecific adsorption, and no affinity for the guests were observed (Figure 7.7c). Although some adsorption of HexA occurred on the reference monolayer at lower guest concentrations, no adsorption isotherm following Equation 7.5 was observed on the 11-mercapto-1-undecanethiol SAM (Figure 7.7d).

Fitting the experimentally obtained capacitance values with the help of Equation 7.5, the binding constants of the studied guests to the surface-confined CDs were determined (Table 7.3). Due to the permeability to ionic species of the studied CD SAMs, the measured current intensities were increasing (Figure 7.7), and the subsequently calculated capacitances were decreasing with increasing scan rates, but

the obtained binding constants did not show a significant dependence on the scan rate within the 50-200 mV/s range.

Table 7.3 Binding constants (K) of the interactions between the studied guests and surface-confined **1** and **2** on gold determined by electrochemical capacitance measurements

Guest	K ($\times 10^3$ M^{-1})	
	1	**2**
ButA	4.4	1.6
HexA	5.2	2.8
OctA	3.5	3.8

All values were obtained by averaging the binding constants determined at 50, 100 and 200 mV/s.

Binding of the guests to SAMs of dithiol **1** and disulfide **2** is characterized with high and measurable binding constants in contrast to the SAMs of bis-thioether **3** where no binding affinity could be observed. It is surprising, that higher affinity of the guests to SAMs of **1** than SAMs of **2** were observed. In comparison with the binding constants in solution obtained by ITC measurements, it can be concluded that the values obtained on surfaces are significantly higher. Similarly to the tendency of ITC measurements, the increasing chain length of the guests is associated with a higher binding affinity to surface-confined hosts too. The exception from this tendency is the binding of OctA, which may be a result of the spatial confinement of the binding sites on the surface and the blockage of one side of the cavity. Similar effects were shown before in case of host-guest interactions between steroids with long aliphatic side chains and CD heptathioether derivatives, where differences in complexation to solution and surface-confined CD cavities were observed owing to the fact that the large guests were complexed through the cavity instead of in the cavity.[21] Although host-guest studies, performed with some small monovalent guests, showed that the molecular recognition properties of heptathioether derivatives of β-CD were unaltered by surface immobilization,[21,22] other studies obtained binding constants 1-2 orders of magnitude higher than the values measured for the corresponding host-guest pairs in solution.[11]

Samples with SAMs of compound **1** were immersed in 2-mercaptoethanol (ME) solution to cover any bare gold regions possibly present on the CD adsorbate-covered surface with thiols in order to study the effect of the adsorption of the guest molecules on those areas. Capacitance measurements in increasing guest concentrations of such a mixed **1**/ME samples showed no significant change in the obtained binding constants (Figure 7.8; for **1**/ME: $K = 4.5 \times 10^3 \text{ M}^{-1}$), indicating that only host-guest interactions between the guests and CD cavities on the surface are responsible for the increasing guest coverage.
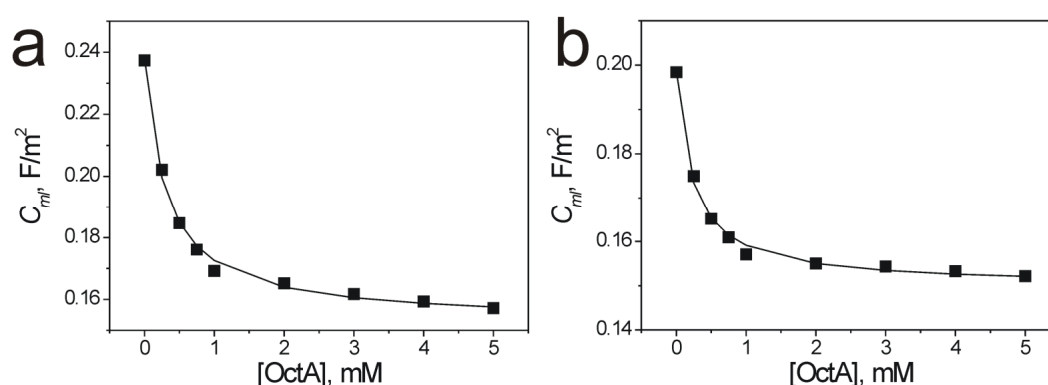
Figure 7.8 Dependence of C_{ml} (at a scan rate of 100 mV/s) of **1** (a) and mixed **1**/ME SAMs (b) on the concentration of OctA obtained by electrochemical capacitance measurements. The solid lines are fitted adsorption isotherms.

7.3 Conclusions

Sulfur-modified α-CD derivatives were used to prepare stable and ordered CD monolayers on gold, and the prepared SAMs were characterized with various techniques. The change of the capacitance of the CD SAMs was used to observe the host-guest binding of various guests. Langmuir-type adsorption isotherms allowed the estimation of the binding affinities on surfaces which showed higher values than in solution. The permethylated CD derivative showed no inclusion ability with the studied guests.

Electrochemical capacitance measurements on host monolayers without long, insulating dialkylsulfide layers offer a novel methodology to investigate host-guest binding events on surfaces and allow the determination of the binding constants.

7.4 Experimental

Materials. Compounds **1** and **2** were a generous gift of Dr Tomas Kraus (Institute of Organic Chemistry and Biochemistry, Academy of Science of the Czech Republic, Prague), compound **3** was a gift of Dr Dominique Armsprach (Louis Pasteur University, Strasbourg). All other chemicals are commercially available and were used as received.

Monolayer preparation. Oxygen plasma-cleaned gold substrates were immersed with minimal delay into a 0.1 mM solution of **1**, **2** or **3** in ethanol for 12 h at room temperature. Subsequently, the substrates were removed from the solution and rinsed with ethanol to remove any physisorbed material. Backfilling of samples of **1** with 2-mercaptoethanol (ME) was achieved through immersion in a 1 mM solution of ME in ethanol for 1 min, followed by rinsing with ethanol.

Monolayer characterization and instruments. Contact angles were measured on a Krüsss G10 contact angle setup equipped with a CCD camera. Advancing and receding contact angles were determined automatically during growth and reduction of a clean water droplet by the droplet shape analysis routine.

XPS measurements were performed on a Quantera Scanning X-ray Multiprobe instrument from Physical Electronics, equipped with a monochromatic Al Kα X-ray source producing approximatly 25 W of X-ray power. Spectra were referenced to the main C 1s peak set at 284.0 eV. A surface area of 1000 μm $\times$ 300 μm was scanned with an X-ray beam about 10 μm wide.

Electrochemical measurements were performed in a three-electrode setup using the SAM-covered gold plate as the working electrode (area = 0.44 cm^2), a platinum disc as the counter electrode and a Hg/HgSO$_4$ (MSE) as the reference electrode ($E^o_{Hg/HgSO4}$ = 0.62 V *vs.* normal hydrogen electrode (NHE)). An AUTOLAB PGSTAT10 equipped with a frequency response analysis (FRA) module for electrochemical impedance spectroscopy was used for the measurements. 0.1 M K$_2$SO$_4$, in water was used for cyclic voltammetry.

AFM analyses were carried out with a NanoScope III (Veeco/Digital Instruments, Santa Barbara, CA, USA) Multimode Atomic Force Microscope equipped with a J-scanner, in contact mode by using Si$_3$N$_4$ cantilevers (Nanoprobes, Veeco/Digital

Instruments) with a nominal spring constant of about 0.32 N m^{-1}. To ensure maximum sensitivity for lateral forces in the friction force images, the sample was scanned at 90° with respect to the long axis of the cantilever. AFM imaging was performed at ambient conditions.

Calorimetric measurements were carried out using a Microcal VP-ITC instrument with a cell volume of 1.4115 mL. Solutions for titration were prepared in 0.1 M K_2SO_4 in Milipore water. Titrations were performed by adding 5 μL aliquots of a 10 mM α-CD solution to a 1 mM solution of ButA, HexA and OctA.

Binding constant determination. The halve of the current intensity difference between the forward and the reverse scans at -0.25 V in the voltammograms was used to calculate the capacitance of the monolayers. Fitting and binding constant determination was performed with a user-defined non-linear curve fit algorithm based on Equation 7.5 (Origin program version 6.1). Separate binding constant values were determined for each applied scan rate (50, 100 and 200 mV/s) and an average constant was calculated from the obtained values.

7.5 Acknowledgement

7.6 References

1   M. J. W. Ludden, D. N. Reinhoudt, J. Huskens, *Chem. Soc. Rev.* **2006**, *35*, 1122.

2   C. Joachim, J. K. Gimzewski, A. Aviram, *Nature* **2000**, *408*, 541.

3   A. D. Mehta, M. Rief, J. A. Spudich, D. A. Smith, R. M. Simmons, *Science* **1999**, *283*, 1689.

4   S. Weiss, *Science* **1999**, *283*, 1676.

5   M. V. Rekharsky, Y. Inoue, *Chem. Rev.* **1998**, *98*, 1875.

6   J. Szejtli, *Chem. Rev.* **1998**, *98*, 1743.

7   M. T. Rojas, R. Königer, J. F. Stoddart, A. E. Kaifer, *J. Am. Chem. Soc.* **1995**, *117*, 336.

8   G. Nelles, M. Weisser, R. Back, P. Wohlfart, G. Wenz, S. MittlerNeher, *J. Am. Chem. Soc.* **1996**, *118*, 5039.

9   J. Qian, R. Hentschke, W. Knoll, *Langmuir* **1997**, *13*, 7092.

10   H. Kitano, Y. Taira, *Langmuir* **2002**, *18*, 5835.

11   A. E. Kaifer, *Acc. Chem. Res.* **1999**, *32*, 62.

12   M. W. J. Beulen, J. Bügler, M. R. de Jong, B. Lammerink, J. Huskens, H. Schönherr, G. J. Vancso, B. A. Boukamp, H. Wieder, A. Offenhauser, W. Knoll, F. C. J. M. van Veggel, D. N. Reinhoudt, *Chem. Eur. J.* **2000**, *6*, 1176.

13   M. W. J. Beulen, J. Bügler, B. Lammerink, F. A. J. Geurts, E. Biemond, K. G. C. van Leerdam, F. van Veggel, J. F. J. Engbersen, D. N. Reinhoudt, *Langmuir* **1998**, *14*, 6424.

14   C. E. D. Chidsey, D. N. Loiacono, *Langmuir* **1990**, *6*, 682.

15   C. Naud, P. Calas, A. Commeyras, *Langmuir* **2001**, *17*, 4851.

16   M. D. Porter, T. B. Bright, D. L. Allara, C. E. D. Chidsey, *J. Am. Chem. Soc.* **1987**, *109*, 3559.

17   E. Boubour, R. B. Lennox, *Langmuir* **2000**, *16*, 4222.

18   A. J. Bard, L. R. Faulker, *Electrochemical Methods: Fundamentals and Applications*, John Wiley & Sons, New York **2001**.

19   D. G. Castner, K. Hinds, D. W. Grainger, *Langmuir* **1996**, *12*, 5083.

20   S. A. Levi, P. Guatteri, F. van Veggel, G. J. Vancso, E. Dalcanale, D. N. Reinhoudt, *Angew. Chem. Int. Ed.* **2001**, *40*, 1892.

21   M. R. de Jong, J. Huskens, D. N. Reinhoudt, *Chem. Eur. J.* **2001**, *7*, 4164.

22   T. Auletta, M. R. de Jong, A. Mulder, F. van Veggel, J. Huskens, D. N. Reinhoudt, S. Zou, S. Zapotoczny, H. Schonherr, G. J. Vancso, L. Kuipers, *J. Am. Chem. Soc.* **2004**, *126*, 1577.

Summary

The focus of this thesis is on multivalent molecular self-assembly on solid surfaces studied both for fundamental reasons and technological applications. Dendrimers with thioether end-groups and sulfur-modified α-cyclodextrins have been immobilized on gold, and their monolayer formation ability has been shown. The low surface spreading of the dendritic inks was successfully used to transfer sub-micrometer features on gold. Host-functionalized stamps were used to achieve selectivity over inking and control over transfer of specific, multivalent molecules by supramolecular microcontact printing (SμCP). The kinetics of multivalent interactions on surfaces was studied by guest-functionalized fluorescent molecules, which were attached to covalently bound β-cyclodextrin (β-CD) self-assembled monolayers (SAMs) on silicon in the presence of free and competitive hosts in the solution. The dynamics of the multivalent surface spreading is disclosed by monitoring the change of the patterned guest SAMs in time.

A review about microcontact printing (μCP) has been given in Chapter 2. The spectacular evolution since the invention of the technology is presented illustrating the development of new printing schemes with improved stamp and ink materials. An additional increase of the applicability of the μCP process was achieved through surface treatment methods of the stamp and through chemical and supramolecular interactions between the ink and the substrate.

Chapter 3 describes the preparation and development of poly(propylene imine) (PPI) dendrimers with thioether end-groups as inks for positive μCP. Long (C_{10}-S-C_{10}-), medium (C_3-S-C_4-) and short (C_1-S-C_1-) thioether end-groups were attached to second and third generation PPI dendrimers. The dendritic inks flattened upon adsorption and form thin monolayers on gold. The multivalent sulfide attachment and the relatively high molecular weight of these dendrimers ensured minimal lateral ink spreading and thus optimal feature reproducibility. The spreading rates of the dendritic inks were

found to be much lower than that of pentaerythritol-tetrakis(3-mercapto-propionate). Lines of 100 nm wide were faithfully replicated with the third generation dendrimer bearing medium (C3-S-C4-) end-groups.

Poly(dimethylsiloxane) (PDMS) stamps have been functionalized with β-cyclodextrin (β-CD) receptors, as described in Chapter 4, to achieve control over inking and transfer of specific molecules by supramolecular microcontact printing (SμCP). Mono- and divalent adamantyl-functionalized ink molecules were picked up and transferred via molecular recognition by the surface-confined β-CD host cavities. A selectivity of at least 4000 was shown upon extracting a monovalent dye from a solution containing other, nonbinding molecules. Uniform, equilibrium-controlled host-guest ink transfer was achieved upon conformal contact between two β-CD-covered surfaces. A higher valency of the ink favors the adsorption from ink mixtures to the β-CD-functionalized PDMS stamp. It was proven that a host-functionalized silicon dioxide surface covered with a host-guest-bound ink monolayer can be used as an efficient supramolecular inkpad to ink a β-CD-functionalized stamp, which offers an increased control over the amount of applied ink molecules.

In Chapters 5 and 6, the multivalent binding at interfaces is discussed from a kinetic and thermodynamic point of view. Mono-, di- and trivalent fluorescent guest molecules were microcontact printed on the β-CD-based molecular printboard, and the kinetic stability of the patterned SAMs was studied by means of fluorescence microscopy. In the presence of native host sites in the surrounding aqueous solution, competition-induced surface spreading of the fluorescent molecules was observed. Surface spreading appeared to be a directional, effective molarity-driven, process. The effect of the thermodynamic equilibrium concentrations of the various species was used to evaluate potential spreading mechanisms. Line patterns of the monovalent guest showed a spreading rate of 0.9 nm/s in the presence of water, which increased when the native β-CD concentration was increased in the solution. The monovalent guest spread in both pure water and β-CD solutions by complete desorption followed by re-adsorption. Experiments with the divalent guest indicated a lower spreading rate in water (0.02 nm/s) in accordance with its higher affinity to the surface, and a spreading rate maximum at 0.8 mM β-CD in the solution was observed. Different spreading mechanisms dominate the spreading of the divalent guest at different competitive host concentrations in the solution. Spreading by 'walking' in pure water, by a 'hopping' mechanism in the 0-1.5 mM β-CD concentration range and by

complete desorption and re-adsorption at higher β-CD concentrations was inferred. The lifetime decrease of an unsaturated guest species in the solution causes a decreasing mean displacement and a lower fraction of successful dissociation-association binding cycles to other empty surface-confined host cavities, which explains the observed spreading rate maximum in the 'hopping' mechanism at intermediate β-CD concentrations. Trivalent molecules followed spreading mechanisms similar to the divalent system generally with significantly lower spreading rates owing to the higher affinity to the surface.

Monolayer formation ability on gold surfaces of various sulfur-modified α-CD derivatives was shown in Chapter 7. Results of water contact angle goniometry, electrochemistry, X-ray photoelectron spectroscopy and atomic force microscopy measurements showed that the adsorbates form uniform and stable SAMs on gold. Electrochemical capacitance measurements were used to determine the binding affinities of these SAMs with aliphatic carboxylic acid salts with four, six and eight carbon atoms. The non-methylated α-CDs showed higher binding constants on surfaces than in solution. The permethylated α-CD showed no detectable binding affinity presumably due to the breaking of the hydrogen bond arrays between neighboring glucose units and the consequent collapse of the cavity.

The results presented in this thesis reveal the complexity and some important governing principles of multivalent molecular interactions on surfaces. The adequate affinity of the ink to the substrate and the simultaneous binding of multiple functionalities are both useful parameters to reliably transfer nano-sized features. A solution for the ink-spreading issue in μCP is given by the use of heavyweight, low spreading or host-guest interacting inks, upgrading soft lithography to a more powerful nanofabrication technique. The fundamental understanding of the kinetics of multivalent molecular self-assembly on surfaces plays a key role in the design of more advanced nanofabrication schemes.

Samenvatting

De focus van het werk dat is beschreven in dit proefschrift is het aanwenden van multivalente moleculaire zelf-assemblage op vaste oppervlakken wat van belang kan zijn voor zowel fundamentele wetenschappelijke vraagstukken als ook voor technologische toepassingen.

Dendrimeren, voorzien van thioether-eindgroepen, en α-cyclodextrines die met zwavel zijn gemodificeerd, zijn gebruikt om monolagen op goud te vormen waarvan de stabiliteit werd onderzocht. De spreiding van de dendritische inkt was langzaam en deze eigenschap liet het toe om sub-micrometer structuren op goud over te dragen op een succesvolle manier. Stempels, gefunctionaliseerd met gastheer-moleculen, zijn gebruikt om de selectiviteit van het inktproces te verbeteren en ook om controle te verkrijgen in het overdrachtsproces van specifieke multivalente moleculen door supramoleculair microcontact-printen (SµCP). De kinetiek van multivalente interacties op oppervlakken is bestudeerd met behulp van fluorescente moleculen die voorzien zijn van gast-functionaliteiten. Deze moleculen complexeren met covalent gebonden β-cyclodextrines in zelfgeassembleerde monolagen op silicium. In aanwezigheid van vrije en competitieve gastheermoleculen in de oplossing boven het silicium-oppervlak werden de fluorescente moleculen mobiel waardoor de dynamica van de multivalente spreiding aan de oppervlakken eenvoudig bestudeerd kan worden door het volgen van de veranderingen van de gepatroneerde gast-monolagen in de tijd.

In hoofdstuk 2 een literatuuroverzicht van microcontact-printen (µCP) weergegeven. De spectaculaire ontwikkelingen sinds de ontdekking van deze technologie, wordt beschreven samen met de ontwikkeling van nieuwe methoden, verbeterde stempels en inktmaterialen. Een verbeterde toepasbaarheid van het µCP-proces is bewerkstelligd door oppervlaktebehandelingsmethodes voor stempels te ontwikkelen en door

chemische en supramoleculaire interacties tussen inkt en oppervlakken te introduceren.

Hoofdstuk 3 beschrijft the bereiding en ontwikkeling van poly(propyleen-imine) (PPI) dendrimeren met thioether-eindgroepen als inkt voor gebruik in positief µCP. Lange (C10-S-C10), middellange (C3-S-C4) en korte (C1-S-C1) thioether-eindgroepen zijn aangebracht aan tweede- en derde-generatie PPI-dendrimeren. De dendritische inkten spreiden uit na adsorptie en vormden dunne monolagen op goud. De multivalente zwavelaanhechting en het relatief hoge moleculair gewicht van deze dendrimeren verzekerden een minimale laterale spreiding van de inkt en dus een optimale reproduceerbaarheid van de structuren. De spreidingssnelheden van de dendritische inkten waren veel lager dan die van pentaerythritol-tetrakis(3-mercapto-propionaat). Lijnen van 100 nanometer breedte zijn nauwkeurig gerepliceerd met de derde-generatie dendrimeren, met middellange eindgroepen.

Zoals beschreven staat in Hoofdstuk 4 zijn polydimethylsiloxaan (PDMS) stempels gefunctionaliseerd met β-CD-receptoren, om de controle over het inkt- en overdrachtsproces van specifieke moleculen te vergroten (SµCP). Mono- en divalente adamantyl-gefunctionaliseerde inktmoleculen zijn opgenomen en overgedragen aan oppervlakte-gebonden β-CD-gastheerholtes via moleculaire herkenning. Een selectiviteit van op zijn minst 4000 is aangetoond na extractie van een monovalente kleurstof vanuit een oplossing die andere, niet-bindende moleculen bevatte. Uniforme, evenwichtsgecontroleerde, gastheer-gast-gemedieerde inktoverdracht was mogelijk door contact te maken tussen twee β-CD-bedekte oppervlakken. Een hogere valentie van de inkt gaf aanleiding tot overwegend meer adsorptie vanuit inktmengsels aan de β-CD-gemodificieerde PDMS-stempels. Er is aangetoond dat een gastheerdragend siliciumoxide-oppervlak, dat bedekt was met een gastheer-gast-gebonden inkt-monolaag, kon worden gebruikt als een efficiënt supramoleculair stempelkussen voor β-CD-gefunctionaliseerde stempels. Dit proces bood verhoogde controle over de hoeveelheid gebruikte inktmoleculen.

In Hoofdstukken 5 en 6 wordt de multivalente binding aan grensvlakken bediscussiëerd vanuit een kinetisch en thermodynamisch standpunt. Mono-, di- en trivalente fluorescente gastmoleculen zijn middels µCP gestempeld op een β-CD-printplaat. De kinetische stabiliteit is bestudeerd aan de hand van gepatroneerde SAMs met fluorescentie spectroscopie. In aanwezigheid van een oplossing van gastheermoleculen is de spreiding van de fluorescerende moleculen op het oppervlak

bestudeerd. Oppervlaktespreiding bleek een directioneel proces gedreven door de effectieve molariteit. Het effect van de thermodynamische evenwichtsconcentraties van de verschillende deeltjes werd gebruikt om potentiële spreidingsmechanismen te evalueren. Lijnpatronen van monovalente gasten lieten een spreidingssnelheid zien van 0.9 nm/s in de aanwezigheid van water, welke toenam naarmate de β-CD-gastheer-concentratie in de oplossing toenam. De monovalente gasten spreidden zich zowel in puur water als ook in β-CD-oplossingen door complete desorptie gevolgd door her adsorptie. Experimenten met de divalente gasten lieten een lagere spreidingssnelheid in water (0.02 nm/s) zien, in overeenstemming met hun hogere affiniteit voor het oppervlak, met een maximale spreidingssnelheid bij 0.8 mM β-CD in de oplossing. Verschillende spreidingsmechanismen domineren de spreiding van divalente gasten bij verschillende competitieve gastheer-concentraties in de oplossing. Spreiding kan optreden ten gevolge van "lopen" in puur water, ten gevolge van een "hinkstap"-mechanisme voor concentraties tussen 0 en 1.5 mM β-CD en ten gevolge van volledige desorptie en readsorptie bij hogere β-CD-concentraties. De afname van de levensduur van onverzadigde gastdeeltjes in de oplossing veroorzaakt een afnemende gemiddelde verplaatsing en een lagere fractie van succesvolle dissociatie-associatie-bindingscycli in de richting van andere lege gastheerholtes die zijn gebonden aan het oppervlak. Dit verklaart de waargenomen maximale spreidingssnelheid in het "hinkstap"-mechanisme. Trivalente moleculen volgden spreidingsmechanismen die gelijkenis vertonen met het divalente systeem. In het algemeen waren de spreidingssnelheden significant lager dankzij de hogere affiniteit voor het oppervlak.

De vorming van monolagen van verschillende zwavel-gemodificeerde α-CD-derivaten op goud is beschreven in Hoofdstuk 7. De resultaten van contacthoek-goniometrie, electrochemie, Röntgen-fotoelectron-spectroscopie en atomaire kracht-microscopie-metingen lieten zien dat de adsorbaten uniforme en stabiele SAMs op goud vormen. Electrochemische capaciteitsmetingen zijn gebruikt om de bindingssterktes aan deze SAMs te bepalen voor alifatische carboxylaten met vier, zes en acht koolstofatomen. De ongemethyleerde α-CD's lieten an oppervlakken hogere bindingsconstanten noteren dan in oplossing. Het gemethyleerde α-CD-derivaat liet geen bindingsaffiniteit zien, waarschijnlijk omdat de waterstofbrug-motieven zijn verbroken tussen de naburige glucose-eenheden, hetgeen kan leiden tot verlies van de moleculaire herkenningseigenschappen van de holte.

De resultaten die zijn gepresenteerd in dit proefschrift tonen de complexiteit en enige belangrijke overheersende principes van multivalente moleculaire interacties op oppervlakken. De adequate affiniteitskeuze van de inkt in relatie met het oppervlak en de simultane binding van meerdere functionaliteiten zijn beide bruikbare parameters om betrouwbaar structuren van nanogrootte over te dragen op oppervlakken. Een oplossing voor het fenomeen van inktspreiding in µCP is gegeven door gebruik te maken van hoogmoleculaire inkten of inkten met moleculaire herkenning. Hierdoor is "soft lithography" een krachtigere nanofabricagetechniek geworden. Het fundamentele begrip van de kinetiek van multivalente moleculaire zelf-assemblage op oppervlakken speelt een sleutelrol in het ontwerp van meer geavanceerde nanofabricagestrategieën.

Acknowledgements

About the author

András Perl was born on the 7th of November 1977 in Marghita, Romania. He graduated in chemistry at "Babeş-Bolyai" University, Cluj-Napoca, Romania, Faculty of Chemistry and Chemical Engineering, defending his master thesis in applied electrochemistry in 2001 under the supervision of prof. dr. Ionel C. Popescu and prof. dr. ir. Petru Ilea. From January 2002 he worked at Research Institute for Technical Physics and Material Science of the Hungarian Academy of Sciences, Laboratory for Nanostructure Research, Budapest, Hungary. In September 2002 he started his second master at University of Twente, working on his thesis in the Chemical Analysis group, supervised by prof. dr. Uwe Karst. From 2004 to 2008 he was a PhD candidate in the Molecular Nanofabrication and Supramolecular Chemistry and Technology groups under the supervision of prof. dr. ir. Jurriaan Huskens and prof. dr. ir. David N. Reinhoudt. The results of his research work from this period are described in this thesis. Since October 2008 he is employed by Aquamarijn Research B. V., The Netherlands.